UNIVERSITY OF LONDON THESIS

Degree PhD Year 2006 Name of Author KRAKOW
Elma Karsten

Imaging of epileptic activity using EEG-correlated functional MRI

by

Karsten Krakow

Department of Clinical and Experimental Epilepsy

INSTITUTE OF NEUROLOGY

Thesis for examination of

Doctor of Philosophy

UNIVERSITY OF LONDON

2005

ProQuest LLC
789 East Eisenhower Parkway
P.O. Box 1346
Ann Arbor, MI 48106-1346

Für Natascha

Preface

This thesis describes the results of two and a half years work as a full-time Research Fellow at the Department of Clinical Neurology, Institute of Neurology, University College London between August 1997 and February 2000. The research project resulting in this thesis comprised the technical development of EEG-correlated functional magnetic resonance imaging (fMRI) and its application to patients with epilepsy in a clinical setting. When I commenced my work on the project in August 1997 at the MRI-Unit of the National Society for Epilepsy in Chalfont St. Peter, I found an already elaborated system for recording EEG-recording inside a MRI scanner. This in-house built EEG-system was the result of more than two years of technical development work, mainly carried out by Philip Allen, Department of Clinical Neurophysiology, National Hospital for Neurology and Neurosurgery. At that time, no commercial system for recording EEG inside the MR scanner was available and there were only about three to four centres world-wide working with this technique. With the paper of Warach and co-workers, published in 1996, only one report on the clinical application of EEG-correlated fMRI in patients with epilepsy was published at that time. The EEG-system that was at my disposal was the only one for which safety issues had been systematically studied, a work which was carried out mainly by Dr. Louis Lemieux and which was published in 1997. Due to these preparatory works, I was in the lucky position to make immediately use of the EEG/fMRI system to study patients with epilepsy in August 1997. This enabled me to perform for the first time a larger scale clinical EEG/fMRI study. Beside this, I was involved in the further development of the EEG-system, particularly as co-investigator in the development of the the world-wide first method of pulse-artifact subtraction and as principle investigator of the first systematic study on MR image quality during concurrent EEG-recording. At the end of my involvement in the project, EEG-correlated fMRI had evolved into a technique used

by dozens of laboratories around the world for various scientific applications, including epilepsy, sleep research and cognitive neuroscience. At that time, commercial EEG recording systems exclusively developed for intra-MR use were distributed by several manufacturers and methods of image artifact subtration made continuous und simultaneous EEG-correlated fMRI possible, which gradually replaced the technique of EEG-triggered fMRI. Many of these advances were made possible or accelerated by the work presented in this thesis.

In total, 15 original publications (seven as first author, eight as co-author) resulted from the research project. The publications included in this thesis are listed in the introduction.

The project was funded as being part of a Co-operative Group Component Grant from the Medical Research Council, UK, held by Professor David Fish and Dr. Louis Lemieux of the Epilepsy Research Group of the Institute of Neurology, Queen Square, London. Their foresight enabled me to undertake this project in the best possible scientific environment. Professor Fish and Dr. Lemieux were also supervisors for this thesis. I am deeply indebted to them for their continuous support and inspiration.

The development and clinical application of a novel method combining modalities with a different technical background like functional MRI and EEG was very much a team effort.

The experimental work was mainly carried out at the MRI Unit of the National Society for Epilepsy, Chalfont St. Peter, Buckinghamshire. At the MRI Unit I have had the privilege to work together with the highly qualified MR physicists Dr Mark Symms, Dr Samantha Free, Dr Gareth Barker, and Dr Mary McLean. I am also grateful to the radiographers Phillipa Barlett, Kim Birnie, Elaine Williams and Jane Burdett for their support and patience during the lengthy EEG/fMRI experiments.

Mr. Philip Allen developed a novel system for EEG recordings inside the MR scanner

including EEG-artifact subtraction methods, which was the technical foundation of this research project.

Professor Simon Shorvon, Professor John Duncan, Professor Ley Sander, Dr Sheelagh Smith and Dr Sanjay Sisodiya of the National Hospital for Neurology and Neurosurgery generously referred patients for the studies.

I am also grateful to Catherine Scott, Department of Clinical Neurophysiology, National Hospital for Neurology and Neurosurgery, who supported the identification of suitable patients for the studies and performed the 64 channel EEG recordings which were part of one study.

I received valuable support from other Research Fellows who cooperated with parts of my project: Dr. Giovanni Polizzi, Dr Udo Wieshmann, Dr Friedrich Woermann (Epilepsy Research Group), Dr Chiara Maria Portas (Wellcome Department of Cognitive Neurology, University College London), and Dr Demetrio Messina (Visiting Research Fellow from the University of Catanzaro, Italy).

I would like to thank Dr Afraim Salek-Haddadi, my successor in this project, for keeping me updated with the progress in EEG-correlated fMRI while I was writing up the thesis.

From Dr Oliver Josephs and Professor Robert Turner (Wellcome Department of Cognitive Neurology) I received support to the fMRI acquisition and data analysis.

I am also grateful to Professor Bernd Pohlmann-Eden, Clinical Director of the Bethel Epilepsy Centre, Germany, who encouraged me to apply for the position as a Clinical Research Fellow at the Epilepsy Research Group in London, thus paving my way to this project.

My greatest debt is to the patients of the epilepsy clinics at the National Hospital for Neurology, Queen Square, London and the National Society for Epilepsy, Chalfont St. Peter. To work with these patients and trying to understand the nature of their disorder

was the most important motivation of my project. Their contribution was the most important of all.

Abstract

This thesis describes the method of EEG-correlated fMRI and its application to patients with epilepsy. First, an introduction on MRI and functional imaging methods in the field of epilepsy is provided. Then, the present and future role of EEG-correlated fMRI in the investigation of the epilepsies is discussed. The fourth chapter reviews the important practicalities of EEG-correlated fMRI that were addressed in this project. These included patient safety, EEG quality and MRI artifacts during EEG-correlated fMRI. Technical solutions to enable safe, good quality EEG recordings inside the MR scanner are presented, including optimisation of the EEG recording techniques and algorithms for the on-line subtraction of pulse and image artifact. In chapter five, a study applying spike-triggered fMRI to patients with focal epilepsy (n = 24) is presented. Using statistical parametric mapping (SPM), cortical Blood Oxygen Level-Dependent (BOLD) activations corresponding to the presumed generators of the interictal epileptiform discharges (IED) were identified in twelve patients. The results were reproducible in repeated experiments in eight patients. In the remaining patients no significant activation (n = 10) was present or the activation did not correspond to the presumed epileptic focus (n = 2). The clinical implications of this finding are discussed. In a second study it was demonstrated that in selected patients, individual (as opposed to averaged) IED could also be associated with hemodynamic changes detectable with fMRI. Chapter six gives examples of combination of EEG-correlated fMRI with other modalities to obtain complementary information on interictal epileptiform activity and epileptic foci. One study compared spike-triggered fMRI activation maps with EEG source analysis based on 64-channel scalp EEG recordings of interictal spikes using co-registration of both modalities. In all but one patient, source analysis solutions were anatomically concordant with the BOLD activation. Further, the combination of spike-triggered fMRI with diffusion tensor and chemical shift imaging is demonstrated in a

patient with localisation-related epilepsy.

In chapter seven, applications of EEG-correlated fMRI in different areas of neuroscience are discussed. Finally, the initial imaging findings with the novel technique for the simultaneous and continuous acquisition of fMRI and EEG data are presented as an outlook to future applications of EEG-correlated fMRI.

In conclusion, the technical problems of both EEG-triggered fMRI and simultaneous EEG-correlated fMRI are now largely solved. The method has proved useful to provide new insights into the generation of epileptiform activity and other pathological and physiological brain activity. Currently, its utility in clinical epileptology remains unknown.

Table of Contents

Glossary

ADC	Apparent diffusion coefficient
BEM	Boundary-element conduction model
AVM	Arteriovenous malformation
BOLD	Blood oxygen level dependent
CSI	Chemical shift imaging
DWI	Diffusion-weighted imaging
ECD	^{99m}Tc-ethyl cysteinate dimmer
ECoG	Electrocorticography
EEG	Electroencephalography
EMF	Electromotive force
EMG	Electromyography
EOG	Electrooculography
EPI	Echo-planar imaging
EV	Explained variance
FDG	^{18}fluoro-2-deoxyglucose
FOS	fixation-off sensitivity
FWHM	full width half maximum
HMPAO	^{99m}Tc-hexamethyl-propyleneamineoxime
HRF	Hemodynamic response function
HS	Hippocampal sclerosis
IED	Interictal epileptiform discharges
FMRI	Functional magnetic resonance imaging
MEG	Magnetoencephalography
MCD	Malformation of cortical development
MDM	Multiple unconstrained moving dipoles model

MRI	Magnetic resonance imaging
MRS	Magnetic resonance spectroscopy
PET	Positron emission tomography
RF	Radio frequency
SISCOM	Subtraction ictal SPECT co-registered to MRI
SPECT	Single photon emission computed tomography
SPM	Statistical Parametric Mapping
STSM	Spatio-temporal source modelling

Chapter 1

Introduction

This thesis describes the technique of recording electroencephalography (EEG) inside a magnetic resonance (MR) scanner and how this technique can be used to correlate spontaneous EEG phenomena with functional magnetic resonance imaging (fMRI) signal changes. The main objectives of the studies included in this thesis are (1) to describe a method of recording EEG in combination with fMRI (EEG-correlated fMRI); (2) to study systematically safety aspects, EEG quality, and fMRI quality in EEG-correlated fMRI; (3) to explore the feasibility of applying of EEG-correlated fMRI to patients with epilepsy; (4) to investigate the reproducibility of fMRI activation due to interictal epileptiform discharges (IED) in patients focal epilepsy; (5) to correlate the fMRI activation with epilepsy-related clinical information; and (5) to explore further clinical applications of EEG-correlated fMRI, in particular in the context of multimodal functional imaging.

Chapters four to seven are based on peer-review publications on the topic of EEG-correlated fMRI, which were published between 1999 and 2001. Here, a list of the publications included in this thesis and the corresponding chapters is given:

Chapter 2 provides an overview on the role of structural and functional MRI and other functional imaging techniques used in epilepsy.

Chapter 3 compares the established functional imaging techniques in epilepsy with EEG-correlated fMRI and explains the rationale for using this technique in the filed of epilepsy.

Chapter 4 describes the major technical problems of EEG-correlated fMRI, which fall

under three categories: patient safety, effects of EEG on MRI acquisition, and effects of EEG on MRI acquisition.

Krakow K, Allen PJ, Lemieux L, Fish DR: Methodology: EEG-correlated fMRI. Advances in Neurology 2000; 83: 187-201.

Krakow K, Allen PJ, Symms MR, Lemieux L, Josephs O, Fish DR: EEG recording during fMRI experiments: image quality. Human Brain Mapping 2000; 10: 10-15.

Principal investigator of the section on safety issues was L. Lemieux. P.J. Allen was principal investigator of the section on EEG quality and artifacts.

Chapter 5 illustrates the main study of this thesis, the application of EEG-triggered fMRI to study interictal epileptiform activity in patients with refractory focal epilepsy.

Krakow K, Woermann FG, Symms MR, Allen PJ, Lemieux L, Barker GJ, Duncan JS, Fish DR: EEG-triggered functional MRI of interictal epileptiform activity in patients with partial seizures. Brain 1999; 122: 1679-1688.

Krakow K, Lemieux L, Messina D, Scott CA, Symms MR, Duncan JS, Fish DR: Spatio-temporal imaging of focal interictal epileptiform activity using EEG-triggered functional MRI. Epileptic Disord 2001; 3: 67-74.

Krakow K, Messina D, Lemieux L, Duncan JS, Fish DR: Functional MRI activation of individual interictal spikes. Neuroimage 2001; 13: 502-505.

Chapter 6 deals with the combination of EEG-correlated fMRI with other imaging methods like MR spectroscopy, diffusion tensor imaging or EEG source analysis.

Krakow K, Wieshmann UC, Woermann FG, Symms MR, McLean MA, Allen PJ, Barker GJ, Fish DR, Duncan JS: Multimodal MR imaging: functional, diffusion tensor, and chemical shift imaging in a patient with localization-related epilepsy. Epilepsia 1999; 40: 1459-1462.

Wieshmann UC, Krakow K, Symms MR, Parker GJ, Clark CA, Barker GJ, Shorvon SD: Combined functional magnetic resonance imaging and diffusion tensor imaging demonstrate widespread modified organisation in malformation of cortical development. J Neurol Neurosurg Psychiatry 2001; 70: 521-523.

Krakow K, Baxendale SA, Maguire EA, Krishnamoorthy ES, Lemieux L, Scott CA, Smith SJ: Fixation-off sensitivity as a model of continuous epileptiform discharges: electroencephalographic, neuropsychological and functional MRI findings. Epilepsy Research 2000; 42: 1-6.

Lemieux L, Krakow K, Fish DR: Comparison of spike-triggered functional MRI BOLD activation and EEG dipole model localization. Neuroimage 2001; 14: 1097-1104.

Principal investigator of the section on EEG dipole modelling was L. Lemieux. U.C. Wieshmann was principal investigator of the section on diffusion tensor imaging.

Chapter 7 reviews further applications of EEG-correlated fMRI in cognitive neurosciences and introduces the technique of continuous and simultaneous EEG-

correlated fMRI.

Portas CM, Krakow K, Allen P, Josephs O, Armony JL, Frith CD: Auditory processing across the sleep-wake cycle: simultaneous EEG and fMRI monitoring in humans. Neuron 2000; 28: 991-999.

Lemieux L, Salek-Haddadi A, Josephs O, Allen P, Toms N, Scott C, Krakow K, Turner R, Fish DR: Event-related fMRI with simultaneous and continuous EEG: description of the method and initial case report. Neuroimage 2001; 14: 780-787.

Principal investigator of the section on simultaneous and continuous EEG-correlated fMRI was L. Lemieux. C. M. Portas was principal investigator of the sleep study.

Chapter 2

Background

In this chapter the applications of structural and functional magnetic resonance imaging (MRI) in clinical epileptology are briefly reviewed. Further, the principals of positron emission tomography (PET) and single-photon emission computed tomography (SPECT), which are the established functional imaging methods in the field of epilepsy, are summarised.

2.1. Structural MRI in epilepsy

Studies using MRI were first performed on humans in the late 1970s (Gadian, 1982). By the early 1980s, MRI had become available for routine clinical use and its role in evaluating epilepsy patients was becoming recognised (Oldendorf, 1984, Sostman et al., 1984). By the mid-1980s, it had become established that this imaging modality is more sensitive than CT in detecting lesions that cause epilepsy (Laster et al., 1985, Latack et al., 1986, Ormson et al., 1986, Schorner et al., 1987, Heinz et al., 1989). Since then, MRI has revolutionised the investigation and treatment of patients with epilepsy and the understanding of the basic mechanisms of epilepsy. The development of MRI can be considered to be the most important new diagnostic tool for the evaluation of the individual with epilepsy since the advent and application of EEG in the 1930s (Berger, 1929). MRI allows acquisition of multiplanar anatomic (and functional, see next section) data non-invasively without biologic toxicity (Kuzniecky and Jackson, 1995, Duncan, 1997). MRI may reveal the aetiology of the seizure disorder, the localisation of the epileptogenic structural abnormalities in patients with localisation-related epilepsy, and is of prognostic importance in patients undergoing epilepsy surgery (Bergen et al., 1989, Jackson et al., 1990, Berkovic et al., 1991, Cascino GD, 1994, Spencer, 1995, Duncan, 1997, Rosenow and Lüders, 2001).

Technique

Interpretation of MRI studies in patients with epilepsy begins with identification of the appropriate neuroimaging methodology. Due to the ability of MRI to generate many types of images, pulse sequences, slice orientation and thickness have to be adapted to the questions posed.

A combination of T1-weighted, T2-weighted and fluid attenuation inversion recovery (FLAIR) sequences forms the basic investigation in patients with epilepsy, as they are highly sensitive to various structural epileptogenic lesions. Volume T1-weighted acquisitions produce approximately cubic voxels without gap, allowing for reformatting in any orientation, subsequent measurement of hippocampal morphology and volumes, and for three-dimensional reconstruction and surface rendering of the brain (Duncan, 1997).

As hippocampal sclerosis (HS) is one of the most frequent underlying pathologies in refractory epilepsy (see below), thin, coronal T2-weighted and FLAIR images, which are the most sensitive for this condition, need to be included in an MRI protocol for the evaluation of patients with epilepsy. If mesial temporal sclerosis is suspected but not clearly visible, 1 to 2 mm thick T1-weighted coronal volume acquisition images allow volumetry of the hippocampus and the amygdala, which is more sensitive than visual inspection alone in the hands of experienced investigators (Kuzniecky et al., 1997, Watson et al., 1997, Cheon et al., 1998).

The range of structural cerebral abnormalities underlying epilepsy and identified with MRI

Hippocampal sclerosis (HS)

Nearly 80% of patients with partial epilepsy have temporal lobe seizures. Approximately 90% of patients with non-lesional temporal lobe epilepsy have

localisation of the ictal onset zone in the amygdala or hippocampus (Spencer et al., 1993). The majority of patients with mesial temporal lobe epilepsy have HS identified in the surgically excised epileptic brain tissue (Cascino et al., 1991). HS can be found in 21% of epileptic patients attending a tertiary epilepsy centre (Semah et al., 1998), compared to 3% in a population of newly diagnosed epilepsy (Annegers et al., 1996). Prior to the introduction of MRI, HS could be diagnosed only during pathologic examination. The MR-imaging alterations associated with HS are hippocampal atrophy, demonstrated with coronal T1-weighted images, increased signal intensity within the hippocampus on T2-weighted images, decreased T1-weighted signal intensity, and disruption of the internal structure of the hippocampus (Jackson et al., 1990, Duncan, 1997).

The assessment of hippocampal atrophy can be improved by measuring the volumes of hippocampi, i.e. MRI-based hippocampal volumetry (Jack et al., 1990, Sisodiya et al., 1995a, Van Paesschen et al., 1995, Van Paesschen et al., 1997). The ability of volumetry to detect abnormalities relies on volume asymmetry and brain-volume-adjusted normal data derived from a control group at the same institution (Jack et al., 1992, Chee et al., 1997, Kuzniecky et al., 1997). Initial studies performed by Jack and colleagues indicated that volumetric analyses might reliably identify the temporal lobe of seizure origin in patients with non-lesional focal epilepsy (Jack et al., 1990). Subsequently, it was demonstrated that the volume of the epileptic hippocampus correlated with the severity of the neuronal loss in certain hippocampal subfields (Cascino et al., 1991, Lencz et al., 1992).

Quantitative T2-relaxometry has been performed to analyse the presence of a signal intensity alteration objectively in the mesial temporal lobe (Jackson et al., 1994b). A combination of volumetry and quantitative measurements of T2 relaxation time can increase the sensitivity of MRI for unilateral or bilateral hippocampal atrophy

(Woermann et al., 1998). Currently, volumetry is an important research tool that permits the quantification of the degree of hippocampal asymmetry, but its direct impact on patient management is limited (Rosenow and Lüders, 2001).

Brain tumours and vascular malformations

The sensitivity of MRI approaches 100% in patients with tumours and vascular malformations. T2-weighted images are most sensitive in revealing foreign-tissue lesions (Bergen et al., 1989). Variably, there may be gadolinium enhancement (Cascino et al., 1989). Gadolinium-enhanced MRI scans may be useful to differentiate oedema from tumour (Cascino et al., 1989).

There are four types of congenital cerebral vascular malformations that can be identified in patients with symptomatic focal epilepsy using MRI: arteriovenous malformations (AVM), cavernous haemangioma, venous angiomas, and telangiectases (Dodick et al., 1994, Kuzniecky et al., 1993). The most common vascular malformations underlying focal epilepsy are the cavernous haemangioma and the AVM (including the angiographically occult lesions) (Dodick et al., 1994 Kuzniecky et al., 1993). Arteriovenous malformations may be associated with a flow signal on MRI. The cavernous haemangioma have a characteristic MRI "target" appearance on the T2-weighted scans with a region of increased T2 signal intensity surrounded by an area of decreased signal produced by haemorrhage associated with methemoglobin deposition in macrophages (Dodick et al., 1994, Kuzniecky et al., 1993).

Malformations of cortical development

Malformations of cortical development (MCD) are commonly identified as causes of epilepsy and neurodevelopmental deficits. With the use of structural MRI these abnormalities are increasingly being recognised in patients with epilepsy that were

previously regarded as being cryptogenic. The range of MCD identified with MRI include schizencephaly, agyria, diffuse and focal macrogyria, focal polymicrogyria, minor gyral abnormalities, subependymal grey matter heterotopias, bilateral subcortical laminar heterotopia, tuberous sclerosis, focal cortical dysplasia and dysembryoplastic neuroepithelial tumours (Duncan, 1997, Sisodiya, 2000).

MCD may not be detected by the sequences used for the basic investigation. FLAIR and T2-weighted inversion recovery sequences are currently considered most sensitive in this respect, the latter being especially useful to detect blurring of the grey-white matter junction (Chan et al., 1998, Lee et al., 1998). However, discrete MCD might be difficult to detect using the basic MRI sequences described previously. Therefore, three-dimensional brain volume reconstruction can be helpful, particularly in visualising the exact location of abnormalities of gyration (Sisodiya et al., 1995b, Sisodiya et al., 1996). However, there is a great variability of the normal gyral architecture (Falk et al., 1991, Maudgil et al., 1998). Several attempts have been made to overcome these problems, e.g. by identification of reproducibly identifiable landmarks around the cortical surface in normal subjects (Maudgil et al., 1998). Curvilinear reformatting was reported to be helpful in detecting subtle dysplastic lesions in otherwise MRI-negative cases (Bastos et al., 1999). Automated segmentation and quantification of cerebral grey matter can identify subtle structural changes not otherwise detected in patients with cortical dysgenesis or hippocampal sclerosis, and even in those with generalised epilepsies (Richardson et al., 1997, Woermann et al., 1999).

Selection of Patients for Epilepsy Surgery

In light of what has been discussed above, it is not surprising that MRI has an important impact on epilepsy surgery in general. In particular, it has significantly altered the selection of candidates for epilepsy surgery. MRI has been shown to affect the operative

strategy in these patients and to be of prognostic importance (Cascino 1994, Spencer, 1995, Zentner et al., 1995). A MRI-identified abnormality is crucial for patient identification for surgery and impacts directly on the preoperative evaluation, and can alter the operative strategy in patients with medically refractory seizures undergoing surgical treatment (Lüders, 1992).

Pathologies underlying the epileptogenic zone that are predictive of a favourable operative outcome include HS, low-grade neoplasm, and occult AVM. Patients with a MRI-identified structural abnormality may be triaged to epilepsy surgery early in the course of treatment if it is clear that the initial response to antiepileptic drug therapy is disappointing (Rosenow and Lüders, 2001). MRI, therefore, should be an integral part of the diagnostic evaluation of patients with presumed symptomatic focal epilepsy. Notably, structural brain imaging studies alone should not be used to determine surgical candidacy or operative strategy. A comprehensive presurgical evaluation is required in selecting patients for surgical treatment (Rosenow and Lüders, 2001), which must include an electro-clinical correlation to establish the localisation of the ictal onset zone and probable epileptogenic zone.

2.2. Diffusion and spectroscopic MR in epilepsy

Diffusion-weighted imaging

Diffusion-weighted imaging (DWI) is a form of MRI that achieves contrast by measurement of variation in rates of water molecule diffusion among various brain regions and tissue compartments. It achieved great practical importance for clinical neurology with the discovery in 1990 that it is a very sensitive and early indicator of brain ischemia. DWI can detect brain infarction within minutes of its onset (Neumann-Haefelin et al., 2000) and has therefore the potential to be used as a clinical tool in the diagnosis of acute stroke.

In epilepsy, prolonged ictal activity in animal models (Zhong et al., 1993) and humans has shown to be associated with changes of the apparent diffusion coefficient (ADC). Wieshmann et al. (1997) published a case report of a 51-year-old woman with chronic epilepsy and recurrent episodes of focal status epilepticus in the right leg. DWI obtained during status epilepticus showed increased signal intensity in the leg area of the left motor cortex. Following cessation of clinical seizure activity, the imaging abnormalities resolved. So far, no reproducible changes of the ADC associated with single (non-prolonged) seizures or interictal epileptiform discharges have been reported.

A major conceptual development in DWI was appreciation and measurement of diffusion anisotropy, i. e. variation of ADC values according to the direction in which the diffusion-weighted gradient is applied along than across myelated fibre tracts (Basser, 1995). As a result, ADC values measured parallel to myelinated axons are greater than those measured perpendicular to them. Hence, it can be used to identity organisation of brain tissue and neuronal pathways in patients with epilepsy (Krakow et al., 1999, Wieshmann et al., 2001).

Magnetic resonance spectroscopy

The physical principles underlying magnetic resonance spectroscopy (MRS) are the same as those for MRI. However, in MRS positional information is traded off for resonance frequency information providing chemical information, which may be displayed as a spectrum of signal intensity against frequency. The following nuclei can be imaged using MRS: ^{1}H (proton), ^{31}P, ^{13}C, and ^{23}Na. The most naturally abundant isotopes, ^{1}H and ^{31}P (99.98% and 100%) are present in compounds of interest in sufficient concentration to be detectable in vivo. The MR sensitivity to ^{31}P is only 7% that of ^{1}H so it is necessary to use larger volumes of tissue for ^{31}P than for ^{1}H-MRS, with a consequence loss of spatial resolution. The volume of brain from which MR

spectra are obtained may be defined in two main ways: (1) single voxel techniques in which spectra are acquired from a single volume of interest, and (2) chemical shift imaging (CSI) in which a large region is excited before the metabolite signals are spatially encoded using phase encoding gradients, as is done in MRI (Duncan, 1997). The application of MRS to patients with epilepsy has focused on three areas: (1) to identify the seizure focus, (2) to study the pathophysiology of the disease, and (3) to investigate the effects of medication (Constantinidis, 2000). Of these, the most common application has been the identification of seizure foci. The majority of MRS studies have been carried out in patients with temporal lobe epilepsy who are candidates for surgical treatment (Gadian et al., 1994, Conelly et al., 1994, Cendes et al., 1997). Most of the studies were proton based, although some ^{31}P studies also have been performed (Kuzniecky et al., 1992, Garcia et al., 1994, Chu et al., 1996, van der Grond et al., 1998). There are fewer studies using MRS for the investigation of patients with seizures of extratemporal origin (Garcia et al., 1995, Kuzniecky et al., 1997, Stanley et al., 1998, Li et al., 1998, Woermann et al., 2001).

In general, MRS studies show a reduction in the signal intensity of N-acetyl aspartate (NAA) and increases in signal intensities of choline and creatine in the lobe of the proposed seizure focus, resulting in a decrease of the NAA over choline and creatine ratio. This implies a loss or dysfunction of neurons and possibly gliosis in these regions (Duncan, 1997).

2.3. SPECT and PET in epilepsy

Functional MRI is a relatively new technique and there is so far only little experience in its application to patients with epilepsy. Therefore, before fMRI is described in the next section, first the two established functional imaging techniques in the field of epilepsy, Positron Emission Tomography (PET) and Single Photon Emission Computed

Tomography (SPECT), are briefly reviewed. As these techniques provide important information on cerebral perfusion and metabolism associated with epileptic activity, they represent an important background to interpret the results of fMRI.

Single Photon Emission Computed Tomography (SPECT)

SPECT is based on the detection and localisation of an internal source of gamma radiation emitted from a radiopharpharmaceutical that has been administered to the patient. SPECT images are acquired and reconstructed by gamma cameras. The basic images acquired by a gamma camera when it is stationary in one position are termed planar images. The SPECT technique uses a computer aided mathematical reconstruction of multiple planar images taken at different rotation angles to produce a series of cross sectional two-dimensional images of the brain.

The main use of SPECT in epilepsy is to image the distribution of relative cerebral blood flow to localise the seizure focus. SPECT also can be used to measure a variety of neurotransmitter systems, but these are not in widespread use and will not be mentioned here.

The radioligands currently used in SPECT are ^{99m}Tc-hexamethyl-propyleneamineoxime (HMPAO) and ^{99m}Tc-ethyl cysteinate dimer (ECD). HMPAO has been studied most extensively and is useful for interictal and peri-ictal studies. The spatial resolution of SPECT depends on the imaging equipment used with a range from 7 to 14 mm (Duncan, 1997).

The major strength of SPECT is in the ability to perform not only interictal, but also peri-ictal (ictal or early postictal) studies, making it complementary to PET. Peri-ictal studies of epilepsy with SPECT exploit the fact that focal seizures are associated with a transient focal increase in blood flow. Sir Victor Horsley first described focal ictal hyperperfusion over 100 years ago, by direct observation of the brain during seizures

(Horsley, 1892). It was only with the development of SPECT that this feature of seizure physiology was harnessed to provide a novel and valuable diagnostic test for the localisation of refractory focal seizures (Berkovic and Newton, 1998).

Interictal SPECT in temporal lobe epilepsy

It has been established for more than a decade that the marker of an epileptic focus studied interictally with SPECT is a region of reduced cerebral blood flow. In temporal lobe epilepsy, interictal hypoperfusion can be striking and, when extensive and clear cut, is likely to be of lateralising value. However, only about 50% of patients with temporal lobe epilepsy have hypoperfusion on the correct side, but 10% show incorrect lateralisation (Stefan et al., 1990, Jack et al., 1994, Theodore, 1996). This makes interictal SPECT with HMPAO in temporal lobe epilepsy neither a sensitive nor a specific marker of the side of the ictal focus. Moreover, temporal hypoperfusion can be observed in patients with extratemporal localization-related epilepsies leading to the possibility of misdiagnosis and incorrect localisation. Rarely, hyperperfusion may be seen in the region of the focus (Berkovic et al., 1993, Duncan et al., 1990, Henkes et al., 1991).

The failure of interictal SPECT with HMPAO or other cerebral blood flow ligands to match the sensitivity of interictal glucose PET appears to be a neurobiological phenomenon, rather than a technical problem related to the inferior resolution of SPECT, because determination of interictal cerebral blood flow with PET is similarly disappointing (Leiderman et al., 1992, Theodore, 1996).

Ictal SPECT in temporal lobe epilepsy

Ictal studies in patients with typical mesial temporal lobe epilepsy show a characteristic pattern of unilateral global temporal hyperperfusion, with relative decreased perfusion

in other cortical areas both ipsilaterally and contralaterally (Biersack et al., 1985). Hyperperfusion involves the medial, lateral, and inferior aspects of the temporal lobe. The relative change from the interictal state is often more striking in the lateral temporal cortex than the medial temporal region. In temporal lobe epilepsy arising from the lateral temporal regions there is usually hyperperfusion in the region of the focus with or without bilateral anteromesial temporal hyperperfusion (Ho et al., 1996, Valenti et al., 2002, Shin et al., 2002).

Ictal SPECT findings are very reliable in lateralising complex focal seizures in temporal lobe epilepsy. In ictal SPECT up to 95% of cases are correctly localised (Lee et al., 1988, Stefan et al., 1990, Duncan et al., 1993, Markland et al., 1994) and thus seem to be very reliable in temporal lobe seizures of proven unilateral temporal lobe origin. In order to obtain such good results, the ligand must be injected during or within 30 seconds of termination of the complex focal seizure. Results from simple focal seizures or secondarily generalised seizures are not as good (Lee et al., 1987, Newton et al., 1995).

Intracranial ictal EEG studies show that mesial temporal lobe seizures frequently spread to the contralateral temporal lobe. The usual lack of marked contralateral hyperperfusion appears to be related to some special characteristic of the focus that generates more relative hyperperfusion than do other regions with similar ictal involvement as judged by ictal EEG (Berkovic and Newton, 1998).

Postictal SPECT in temporal lobe epilepsy

The characteristic pattern of postictal blood flow consists of a focal area of relatively increased perfusion, usually in the mesial and anterior parts of the temporal lobe, with decreased perfusion in the adjacent lateral temporal cortex. This pattern represents a significant change from the ictal state (Newton et al., 1992). The pattern is typically

seen in early (1- to 5-minute) postictal scans. Later, only the lateral hypoperfusion remains, with the scan returning to the interictal state within about 20 minutes after seizure termination (Rowe et al., 1991, Newton and Berkovic, 1996). Postictal studies show correct lateralisation in 70% of cases of unilateral temporal lobe epilepsy (Rowe et al., 1991, Newton et al., 1994).

Interictal and ictal SPECT in extratemporal focal epilepsy

Interictal SPECT is of little localising value in extratemporal focal seizures. In cases where there is a large structural lesion, the observation of corresponding hypoperfusions adds little to seizure localisation. In the absence of a structural lesion, it is unusual to observe definitive interictal hypoperfusion in the epileptogenic area in seizures arising from the frontal, parietal, or occipital regions (Marks et al., 1992, Newton et al., 1995). However, interictal studies can be crucial in interpreting ictal studies. The sensitivity of ictal SPECT (in temporal and extratemporal epilepsy) can be improved by a subtraction of ictal from interictal SPECT images and coregistration with the structural MRI of the patients (subtraction ictal SPECT coregistered to MRI; SISCOM) (O'Bien et al., 1998, O'Bien et al., 1999, Kaiboriboon et al., 2002).

When ictal SPECT can be obtained, it provides valuable localising information, both lobar and intralobar. In some studies a correct localisation can be achieved in 60-90% of cases (Ho et al., 1994, Newton et al., 1995, Chinvarum et al., 1996, O'Brien et al., 2000). In contrast to complex focal seizures of temporal lobe origin, where diagnostic ictal changes are seen up to 30 seconds after seizure termination, in extratemporal epilepsies there is little or no persistence of ictal hyperperfusion into the postictal period. Therefore, injections must be given during the seizure itself. Another difference is that ictal SPECT in extratemporal cases may highlight regions of spread, and the region of seizure initiation may be less prominent. Thus, late ictal injections can be

difficult to interpret because there may be a number of hyperperfused regions (Berkovic and Newton, 1998).

Positron emission tomography (PET)

PET can be used to map regional cerebral blood flow (using ^{15}O-labelled water), metabolic rates, and receptor densities. Compared to SPECT, the technique produces quantitative data with a superior spatial resolution (Henry and Chugani, 1998).

Most clinical studies to date have used ^{18}fluoro-2-deoxyglucose (^{18}FDG) to image glucose metabolism, but investigations with specific ligands (e.g. [^{11}C]flumazenil to the central benzodiazepine-$GABA_A$ receptor complex or [^{11}C]diprenorphine to opiate receptors) become more and more important to study the neurochemical abnormalities associated with the epilepsies. This includes both static interictal derangements and dynamic changes in ligand-receptor interaction that may occur at the time of seizures (Duncan, 1997).

The clinical role of ^{18}FDG-PET requires re-evaluation in the light of the advances in structural imaging with MRI. In a comparative study in patients with temporal lobe epilepsy, ^{18}FDG-PET data did not provide clinically useful data if the MRI findings were definitive, but had some additional sensitivity (Gaillard et al., 1995). With increased knowledge of the sensitivity and specificity of MRI in particular clinical situations, interictal ^{18}FDG-PET will be probably reserved for those cases in which MRI is non localising or in which MRI provides localisation discordant with ictal EEG and other routinely acquired data in refractory partial epilepsy. PET data should always be interpreted in the light of high quality anatomical MRI, to provide a structural-functional correlation. Coregistration of PET scans with MR images also helps to clarify partial volume effects (if a structure is smaller than the detection threshold permitted by a system's spatial and contrast resolution, its functional activity will be averaged with

the activities of adjacent structures) (Mazziota et al., 1981, Mazziotta et al., 1991, Phelps, 1992, Frey, 1994, Knowlton et al., 2001).

Both in normal and epileptic subjects, PET is usually performed in the waking, resting state. Epilepsy patients are usually in their interictal state. In interictal PET studies of both temporal and extratemporal focal epilepsy, the hallmark of an epileptogenic focus is an area of reduced glucose metabolism and reduced blood flow that is usually considerably larger than the pathological abnormality (Duncan, 1997). The most likely reason for the large region of reduced blood flow and metabolism is inhibition or deafferentation of neurons around an epileptogenic focus. Comparisons of ^{18}FDG-PET scans with [^{11}C]flumazenil scans indicate that the neuronal loss is confined to a more restricted area than the region of reduced metabolism.

Ictal PET scanning is difficult to obtain, given the relatively short half-life and expense of PET radiopharmaceuticals. Further, the mathematical model underlying PET quantitation requires steady-state metabolism to accurately quantify regional metabolism (Phelps, 1979). Therefore, quantification of ictal metabolism would be impossible because ictal metabolism is not in steady state during the ^{18}FDG uptake and phosphorylation period. Further, the temporal resolution of static ^{18}FDG-PET is such that single seizures occurring at or shortly after ^{18}FDG injection will produce mixed interictal-ictal-postictal scans, with unpredictable effects. Ictal ^{18}FDG images may reveal areas of qualitatively apparent increases and decreases in relative metabolism (Engel et al., 1982, Engel et al., 1983). One such peri-ictal scan had qualitatively normal metabolism of the temporal lobe of probable ictal onset, whereas an interictal FDG scan of this patient revealed hypometabolism of that temporal lobe (Henry et al., 1993). For "purely" ictal FDG scanning prolonged seizures like epilepsia partialis continua would be required (Hajek et al., 1991).

Interictally spiking cortex takes up 2-deoxy[C14]glucose at greater rates than does non-

spiking cortex in bicuculline-treated rats (Handforth et al., 1994), suggesting that interictal spiking EEG may be a determinant of regional ^{18}FDG activity in human PET studies. Therefore, continuous EEG monitoring should be performed during PET scanning to exclude unintentional ictal scanning that could lead to misinterpretation of PET data (Henry et al., 1993).

PET in temporal lobe epilepsy

Several studies of ^{18}FDG-PET in patients with temporal lobe epilepsy have found a 60-90% incidence of hypometabolism in the temporal lobe (Kuhl et al., 1980, Theodore, 1983, Gaillard, 1995). The area of hypometabolism often extends beyond the temporal lobe, e.g. involving the thalamus, the basal ganglia, and the frontal lobe (Sperling et al., 1990, Henry et al., 1993). A recent study found ipsilateral insular glucose hypometabolism and benzodiazepine receptor loss (Bouilleret et al., 2002). In patients with mesial temporal lobe epilepsy and hippocampal sclerosis, the hypometabolism has frequently been found to be more pronounced in lateral neocortex, and also neocortical changes of central benzodiazepine binding were found, suggesting more widespread abnormalities are present in hippocampal sclerosis (Hammers et al., 2001).

In general, ^{18}FDG-PET studies are considered to be less reliable for identifying the precise localisation of seizure onset than for answering the question of lateralisation (Duncan, 1997). Patients with hippocampal sclerosis have the lowest glucose metabolism in the whole temporal lobe. However, temporal hypometabolism is not related to severity of hippocampal damage as measured by quantitative magnetic resonance imaging or histopathological analysis (Lamusuo et al., 2001).

In some studies, additional hypermetabolic areas were found in patients with (cryptogenic) temporal lobe epilepsy. Possible explanations for this finding are increased neuronal activity due to ongoing focal interictal epileptiform activity or

increased neuronal numbers, as may occur in a focal malformation of cortical development with a thickening of the neocortical ribbon (Franceschi et al., 1995, Richardson et al., 1996a).

Cerebral blood flow PET imaging during cognitive performance demonstrates disseminated bihemispheric sites of activation in temporal lobe epilepsy, which differ from activation patterns of normal subjects. The degree of left hemisphere hypometabolism has been correlated with impairment of verbal IQ, and lateral left temporal lobe hypometabolism with impairment of verbal memory (Rausch et al., 1994).

The binding of [^{11}C]flumazenil to central benzodiazepine receptors in epileptogenic foci was found to be reduced by an average of 30% (Savic et al., 1988). Using statistical parametric mapping (SPM) applied to parametric images of cerebral [^{11}C]flumazenil binding, it was found, in patients with unilateral hippocampus sclerosis, that reduction of benzodiazepine receptors was confined to the sclerotic hippocampus with no significant abnormalities elsewhere (Koepp et al., 1996).

The degree and extent of temporal lobe hypometabolism has been strongly correlated with the seizure outcome following temporal lobectomy. Greater severity of preoperative hypometabolism of the resected temporal lobe is associated with significantly better postoperative seizure control (Manno et al., 1994, Radtke et al., 1993, Theodore et al., 1992, Dupont et al., 2000). The high correlation of temporal hypometabolism and seizure outcome is independent of the pathologic diagnosis. Qualitatively evident extratemporal hypometabolism was found to be associated with a higher incidence of postoperative seizures (Swartz et al., 1992). After selective amygdalo-hippocampectomy, there was an increase of regional cerebral glucose metabolism in the ipsilateral and also the contralateral hemisphere in patients with mesiobasal temporal lobe epilepsy and hippocampal sclerosis (Hajek et al., 1994),

similar results were found for benzodiazepine receptors (Savic et al., 1998). It can be concluded, that not only brain metabolism, but also regional reductions in benzodiazepine receptor density may be dynamic and related to seizures.

PET in extratemporal focal epilepsy

^{18}FDG-PET shows hypometabolism in about 60% of patients with frontal lobe epilepsy. In 90% of those with a hypometabolic area, structural imaging shows a relevant underlying abnormality. In common with temporal lobe epilepsy, the area of reduced metabolism in frontal lobe epilepsy may be much larger than the pathological abnormality. However, normal metabolism and discrete focal areas of hypometabolism are also frequently seen (Swartz et al., 1989, Sperling et al., 1990, Swartz et al., 1990, Henry et al., 1991, Henry et al., 1992, Swartz et al., 1992, Theodore et al., 1992, Hayek et al., 1993, Henry et al., 1993, Hayek et al., 1994, Radkte et al., 1994). Diffuse regional hypometabolism often includes mesial temporal, thalamic, and basal ganglial hypometabolism ipsilateral to the neocortical hypometabolism. The degree of hypometabolism usually varies across a region of diffuse hypometabolism. The zone of most severe hypometabolism, excluding the site of a foreign-tissue lesion, usually contains the electrophysiologically defined ictal onset zone (Henry et al, 1993). The mean surface extent of [^{11}C]flumazenil-PET abnormalities in lesional epilepsy was significantly smaller than areas of glucose hypometabolism, but still significantly larger than the corresponding structural lesion (Juhasz et al., 2000). In patients with MCD, glucose hypometabolism concurred with MRI findings of abnormal cortex. However, ^{18}FDG-PET did not identify abnormalities that were not evident on MRI, although in some cases the area of hypometabolism was more extensive than the MRI lesion (Lee et al., 1994). In the quantitative analysis of [^{11}C]flumazenil PET data, flumazenil binding was decreased in some MCDs with increased grey matter volume and increased in some

adjacent or overlying areas of normal-appearing cortex, also suggesting functional abnormalities beyond MRI-detectable structural changes (Hammers et al., 2001). However, in the absence of a lesion detectable with MRI interictal PET is usually normal in the neocortical focal epilepsies (Henry et al., 1991, Radtke et al., 1994, Kim et al., 2001). Therefore, it does not appear to provide additional clinically useful information in the majority of patients with this condition.

PET in primary generalised epilepsy

In idiopathic generalised epilepsy, interictal ^{18}FDG-PET scans usually are normal (Engel et al., 1985, Engel et al., 1990, Ochs et al., 1987, Theodore et al., 1985). Studies carried out when frequent absences were occurring have shown a diffuse increase in cerebral glucose metabolism of 30-300%. Absence status, however, was associated with a reduction in cerebral glucose metabolism. There were no focal abnormalities and the rate of metabolism did not correlate with the amount of spike-wave activity (Engel et al., 1985, Theodore et al., 1985, Ochs et al., 1987). For these studies, the poor temporal resolution of ^{18}FDG-PET studies has to be considered, resulting in an amalgam of pre-ictal, ictal and postictal periods contributing to a scan.

Savic et al. (1990) reported a slight reduction in cortical binding of [^{11}C]flumazenil to central benzodiazepine receptors of patients with generalised seizures, compared with the "nonfocus" areas of patients with focal seizures. Subsequently the same authors reported that, compared with normal subjects, patients with primary generalised tonic-clonic seizures had an increased benzodiazepine receptor density in the cerebellar nuclei and a decreased density in the thalamus (Savic et al., 1994). However, these results have not been replicated. Prevett et al. (1995) found no significant difference in [^{11}C]flumazenil binding in the cerebral cortex, thalamus or cerebellum between patients with absence epilepsy and control subjects. In patients taking valproate, however, the

benzodiazepine receptor density was decreased suggesting that this drug may result in reduced number of available benzodiazepine receptors. In general, it is currently not certain whether the alterations found in patients with generalised epilepsy are a result of an increased number of neurons or a functional change in available receptors (Duncan, 1997). Correlative neuropathological studies are required to answer this question. There was no significant difference in [^{11}C]diprenorphine binding between control subjects and patients with absence epilepsy, suggesting there is no overall abnormality of opioid receptors in this condition (Prevett et al., 1994). In a dynamic study, however, it was found that serial absences were associated with an acute 15-41% reduction in [^{11}C]diprenorphine binding to association areas of fronto-parieto-temporal association cortex. This result implied release of endogenous opioids in the neocortex that may have a role in the pathophysiology of typical absence seizures (Bartenstein et al., 1993).

2.4. Functional MRI in epilepsy

Although there are various MR techniques capable of identifying dynamic changes within the brain (e.g. MR spectroscopy, MR diffusion and perfusion imaging), this section concentrates on BOLD (blood oxygen level dependent)- fMRI, which is now the leading technique for mapping human brain activation and which is the method used in this work.

EPI data acquisition

BOLD-fMRI benefits greatly from high-speed imaging, both for the acquisition of temporal information as well as for the reduction of the effects of physiological noise and head movement. The common imaging methods for MRI involve acquiring data in the two- or three-dimensional Fourier transform space of the object, commonly known as k-space. The goal of any rapid imaging method is to sample the k-space information

as quickly as possible with a minimum of image artifacts. The image acquisition method used in most fMRI applications is echo-planar imaging (EPI). It was first proposed by Mansfield et al. in 1977 and further developed more recently following the advent of high-power gradient-coils. The technique uses rapidly alternating gradients and can acquire an entire image within a single excitation. EPI is still a technologically challenging method and vulnerable to system imperfections such as timing mismatch, gradient waveform asymmetry and field inhomogeneity. This can result in severe geometric distortion and image ghosting (Allen et al., 2000).

Data pre-processing

The term pre-processing refers to operations performed on fMRI prior to their statistical analysis. The most prevalent procedures involve realignment of image volumes to correct for rigid body motions of the subject's head while in the scanner, "warping" or "deformation" of an individual subject's MRI brain volume to a template, reference brain volume, and smoothing.

Image registration can be performed within or between modality. The most common application of within modality coregistration is in motion correction of series of images. This is of particular importance in fMRI, as the signal changes due to any hemodynamic response can be small compared to apparent signal changes that can result from subject movement. Motion correction increases the sensitivity of the test to true activations. Furthermore, without suitable image registration, artifacts arising from subject movement correlated with the paradigm may appear as activations. Image registration is performed by determining a rigid body transformation for each of the images that registers them to the first of the series. This can be achieved through optimisation of the motion parameters by minimising the residual sum of squares (Ashburner and Friston, 2000).

An example of between modality registration is the registration of a structural image to a functional image series. Again, this is a rigid body registration, but because the structural image is acquired in a different modality, the registration cannot simply be performed by minimising the residual sum of squares. Between-modality registration can be performed by first partitioning the images into grey and white matter and then simultaneously registering the partitions together (Ashburner and Friston, 1997).

Images from several subjects can be analysed together by first registering them into a common space; this registration process is called spatial normalisation. Spatial normalisation allows for a wide range of voxel-based analyses and facilitates the comparison of different subjects and databases. Using spatially normalised images, activation sites can be reported according to a standard coordinate system. The most commonly adopted standard space is that described by Talairach and Tournoux (1988). Spatial normalisation usually begins by matching the brains to a template image (defined within the standard space) of the same modality using a 12-parameter affine transformation. This transformation corrects for the variations in position, orientation and size of the brain. More subtle differences are then corrected by a subsequent non-linear registration. Matching is only possible on a coarse scale, since there is not necessarily a one-to-one mapping of the cortical structures between different brains. Because of this, the images are smoothed prior to the statistical analysis in a multi-subject study, so that corresponding sites of an activation from different brains are superimposed (Ashburner and Friston, 2000).

Smoothing is a process by which data points are averaged with their neighbouring points in a series, such as a time series or an image. There are different methods of smoothing. The method applied in the SPM software package, which was used for the studies of this thesis, is smoothing with a Gaussian kernel. The kernel for smoothing defines the shape of the function that is used to take the average of the neighbouring

points. Thus, a Gaussian kernel is a kernel with the shape of a normal distribution curve. The Gaussian used for smoothing is usually described with the width of the Gaussian with another related measure, the Full Width at Half Maximum. Spatial smoothing has three objectives: (1) it increases the signal to noise ratio; (2) it conditions the data so that they conform more closely to a Gaussian field model, which is important if Gaussian field theory is used to make statistical interferences about regionally specific effects; and (3) it ensures that effects between different subjects are assessed on a reasonable spatial scale with respect to functional anatomy (Ashburner and Friston, 2000). *Figure 1* provides a flow chart of the SPM image processing including the steps mentioned above.

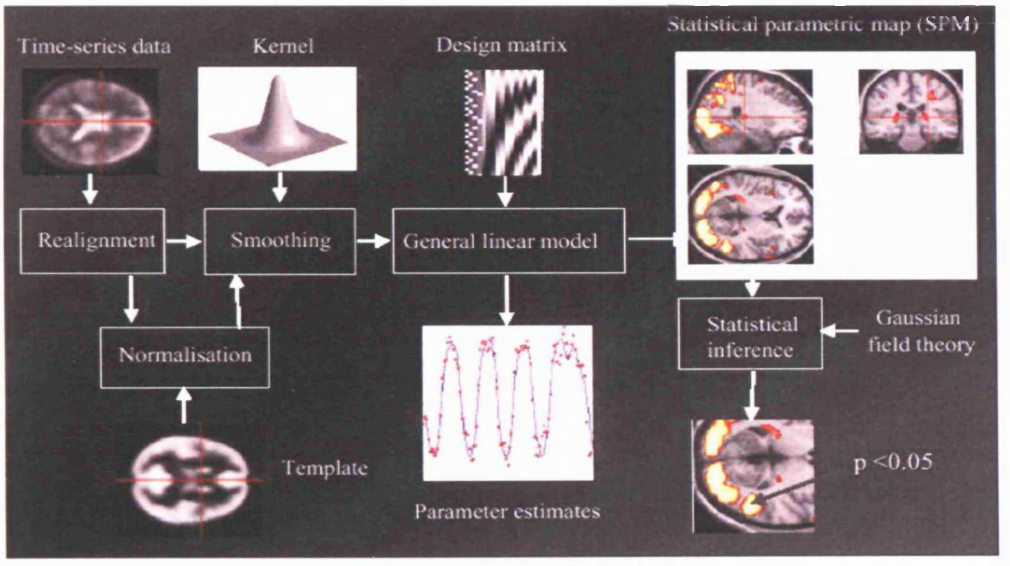

Figure 1: *The SPM approach is voxel based: Images are spatially normalised into a standard space and smoothed. Parametric statistical models are assumed at each voxel, using the General Linear Model to describe the variability in the data. Hypotheses expressed in terms of the model parameters are assessed at each voxel with univariate*

statistics. This results in an image whose voxel values are statistics, a Statistical Parametric Map. Temporal convolution of the General Linear Model enables the application of results from serially correlated regression, permitting the construction of statistic images from fMRI time series. The multiple comparisons problem of simultaneously assessing all the voxel statistics is addressed using the theory of continuous random fields, assuming the statistic image to be a good lattice representation of an underlying continuous stationary random field. This results in corrected p-values for each voxel hypothesis.

Experimental Design for fMRI

Functional MRI relies on contrasts between images acquired in different brain states. From the different experimental designs possible in fMRI, the one should be chosen which provide maximum sensitivity for the effect to be detected.

The prototypical fMRI experimental design is the boxcar approach in which two conditions alternate over the course of the acquisition of serial scans. The periods of this "block design" consist usually of blocks of several trials. The "experimental blocks" are designed to evoke a particular response and alternate with "control blocks" that are designed to evoke all the processes present in the experimental block except for the response of interest. The strength of blocked designs is their high statistical power. The fundamental frequency of the boxcar can be positioned so that variance is maximally passed by the hemodynamic response function but avoids the elevated noise range at low frequencies (Aguirre and D'Esposito, 2000). However, blocked fMRI designs as a subtractive method rely upon the assumption of "pure insertion". This means the idea that a (e.g. cognitive) process can be added to a pre-existing set of (cognitive) processes without affecting them. This assumption is difficult to prove because one would need an independent measure of the pre-existing process in the absence and presence of the new

process. If pure insertion fails as an assumption, a difference in neuroimaging signals between two conditions might result of an interaction between the added component and pre-existing components rather than the evocation of the process of interest (Zarahn et al., 1997).

Parametric designs offer the opportunity to obviate the assumption of pure insertion. In a parametric design, the experimenter presents a range of different levels of stimulation, and seeks to identify relationships between imaging signal and the values that the parameter assumes. In parametric designs, only the magnitude of the process of interest is altered. This approach is able to avoid the questionable experimental assumptions of blocked designs mentioned above, but it should be noted that it has a reduced sensitivity compared to a two-condition design that only uses the extreme stimulation levels. The most frequently used parametric statistical procedure in fMRI employs the general linear model (Cohen et al., 1997).

Continuously varying parametric or *event-related designs* attempt to model signal changes associated with individual trials as opposed to a larger unit of time comprised of a block of trials. Each individual trial may be composed on one event (e.g. a behavioural event or an EEG event) or several events. Even-related designs have the advantages (1) to allow the analysis of events with variable or random presentation sequences (Josephs et al., 1997) or even spontaneous and unpredictable occurrence, (2) to test for functional changes between different characteristics of a trial, and (3) to avoid the possibility of confounds that are the result of blocking events together.

BOLD-fMRI

BOLD imaging uses deoxyhemoglobin as an endogenous MRI contrast agent. Local cerebral blood flow is increased during cortical activity, even though oxygen consumption is little changed (Raichle, 1991). Under these circumstances, the delivery

of oxygen to the capillary bed is increased, but much of it passes through to the venous system, resulting in a relative increase in venous PO_2. The ferrous iron of deoxyhemoglobin is paramagnetic, but diamagnetic in oxyhemoglobin. When erythrocytes containing deoxyhemoglobin are exposed to the scanner's main magnetic field, local field perturbations arise due to the difference in the magnetic susceptibility relative to the surrounding tissue. This susceptibility induced field shift is the source of BOLD contrast in T2* sensitised acquisitions: A reduced susceptibility of the venous blood then causes an increase in T2* (less T2* relaxation) and an increased MR signal. One important question for functional brain mapping using fMRI is how well the BOLD response is correlated with neuronal activation. There is a bulk of literature both in humans and animals demonstrating a consistency of the activation locations between BOLD functional maps and other modalities or anatomical landmarks (Chen and Ogawa, 2000, Logothetis et al., 2001).

The feasibility of using BOLD-fMRI for mapping neuronal activation was first demonstrated in the human brain during simple visual perception (Kwong et al., 1992, Ogawa et al., 1992) and motor tasks (Bandettini et al., 1992). In the following decade, numerous studies have applied fMRI to study physiologic brain function.

BOLD-fMRI activation studies in epilepsy

Only in the last years has fMRI been applied also to neurological patients, with perhaps the greatest impact in preoperative evaluation of patients with intractable epilepsy. Through the determination of functionally viable brain tissue (eloquent cortex), fMRI may predict deficit in cognitive, motor, and sensory perceptual functions that might arise from surgical intervention and influence surgical decisions.

There is reason to be optimistic that cognitive procedures used with fMRI will offer an alternative to the Wada test (intracarotid amobarbital test) in the future, which is the

current "gold standard" for determination of language and memory lateralisation in the preoperative evaluation of epileptic patients. A number of investigators have now demonstrated that fMRI has potential to assist in the determination of lateralisation of language functions (McCarthy et al., 1993, Binder et al., 1995, 1997, Hertz-Pannier et al., 1997, Lehericy et al., 2000). The problem of identifying memory function with fMRI is the difficulty of developing tasks that can reliably activate mesial temporal structures thought to be critical to forming new explicit memories, i.e. the hippocampal formation and adjacent cortices. Such tasks are now being refined and show promise for exploring memory lateralisation capability in fMRI (Bookheimer et al., 1996, Stern et al., 1996, Peterson et al., 1997). However, results in epileptic patients are preliminary (Bellgowan et al., 1998, Jokeit et al., 2001). FMRI can also be used to predict functional deficits in other domains such as primary sensory and motor functions and thus help to identify boundaries of functional tissue before surgical intervention.

Further, fMRI is also capable of providing evidence for the direct localisation of the epileptic focus by identifying ictal or interictal epileptic activity, as described in the next section.

2.4.1. Ictal and interictal fMRI in epilepsy

Ictal fMRI

The first attempt to use fMRI for localisation of epileptic activity was reported in 1994 by Jackson et al. This case report dealt with a 4-year old patient with the diagnosis of Rasmussen's encephalitis. The authors had performed a standard MRI of the patient's brain that showed evidence for widespread right hemispheric atrophy primarily over the more dorsal lateral frontal region and inferior Rolandic area. The patient was prone to frequent and prolonged focal motor seizures that involved the left arm, hand, and face. These bouts of epilepsia partialis continua were then targeted for investigation using a

perfusion MRI scan. This study demonstrated a seizure-related perfusion defect over the right inferior motor cortex, corresponding to the area of maximum atrophy seen on the conventional MRI and to the region of maximum abnormality as identified with an ictal single photon emission tomography (SPECT) study using TC^{99} (Jackson et al., 1994a). A similar case was reported by Warach et al. (1994). This patient had prolonged focal status epilepticus and demonstrated a perfusion MRI abnormality over the left parieto-frontal region using a susceptibility-weighted sequence and dynamic enhancement with gadolinium. This abnormal region was in keeping with the localisation of the spike focus of scalp EEG and the hyperperfusion defect detected with ictal SPECT. The EEG, perfusion-based MRI abnormality, and SPECT findings normalised after more aggressive medical management. Further case reports were published by Detre et al., 1995 and 1996, Krings et al., 2000 and Salek-Haddadi et al., 2002. These studies have demonstrated that fMRI was capable of imaging reversible perfusion or BOLD abnormalities associated with epileptic seizures, with the abnormality localised closely to the site of maximum electric abnormality. However, ictal fMRI is not routinely feasible for a number of reasons: Most ictal events are associated with head and body movement and impairment of consciousness usually to a degree that the required level of cooperation for an MRI scan cannot be achieved. Furthermore, BOLD-fMRI is not sensitive to detecting low frequency state-related changes due to large intersessional effects and scanner noise characteristics. Together with the slow HRF, this limits detection power to a narrow frequency band and will tend to necessitate capturing both seizure onset and termination. Seizures, however, are usually short lasting and unpredictable. It is impracticable for a patient, even with frequent seizures, to lie for hours in a MR scanner awaiting the onset of one or several seizures. FMRI studies with concurrent EEG recording are complicated further by the extra time involved in attaching electrodes and equipment set up (Salek-Haddadi et al., 2002). For these

practical reasons, the investigation of ictal activity will be limited to highly selected patients who have (1) seizures without gross head movement, and (2) seizure series, status epilepticus, epilepsia partialis continua or other predictable seizures, e.g. reflex epilepsy.

Interictal fMRI

Compared with ictal fMRI, mapping of interictal activity has several advantages: (1) IED are a common phenomenon in patients with epilepsy; (2) IED are usually not associated with stimulus-correlated motion; and (3) fMRI activation associated with single IED are less likely to be confounded with propagation effects compared with ongoing ictal activity. As IED are by definition a sub-clinical phenomenon, a second modality is necessary to identify these events. Hence, this approach was only made possible by recording EEG inside the MR scanner (EEG-correlated fMRI). With this technique, single sub-clinical epileptiform discharges can be detected during a scanning session and can be used to trigger fMRI acquisitions. The rationale for using EEG-correlated fMRI in epilepsy, and the methodology and clinical application of EEG-correlated fMRI are described in detail in chapter two and the following sections.

Chapter 3

Rationale for using EEG-correlated fMRI to study epileptic activity

This thesis deals mainly with EEG-*correlated* functional MRI (EEG/fMRI), which is the general term that refers to fMRI experiments with recording of EEG inside the MR scanner. The term EEG-*triggered* fMRI is used for EEG/fMRI experiments in which fMRI acquisitions are triggered after spontaneous EEG events, and the term *simultaneous* EEG/fMRI designates for experiments in which fMRI is acquired periodically or continuously during concomitant EEG recording.

3.1. Using EEG-correlated fMRI to localise epileptic activity

Epilepsy is a disorder of brain function characterised by clearly defined, transient behavioural and electrophysiological disturbances, with or without clinically detectable structural lesions (Engel, 2000). Even when structural abnormalities are identified, functional tests are necessary to demonstrate that they are epileptogenic. Investigations of epileptic foci in humans have been hitherto limited by either the low spatial or temporal resolution of the available diagnostic tools. Due to their restricted spatial sampling and the insoluble „inverse problem" of working back from scalp potentials to derive the likely sites of their generators, neither EEG nor MEG can directly localise the source of epileptic activity. Furthermore, as described in chapter 1, functional imaging studies using PET and SPECT have shown an increased blood flow and metabolism in the region of the seizure focus during ictal events (Engel et al., 1983, Lee et al., 1986) and, in contrast, a decreased blood flow and metabolism during the interictal state (Engel et al., 1982). Due to their low temporal resolution, however, these methods sample activity continuously over a prolonged period of time, and hence cannot investigate the changes in blood flow and oxygenation related to brief epileptic activity such as IED.

The main diagnostic question in patients with focal epilepsy, particularly in presurgical evaluation, is to localise the area of brain necessary to generate seizures, the „epileptogenic zone" (Lüders et al., 1993). Functional MRI correlated with IED localises brain areas involved in generating these particular EEG events. The area of cortex that generates interictal spikes is labelled as the „irritative zone". This is not necessarily identical with the cortical area that initiates seizures, the „ictal onset zone", but has typically a close spatial relation (Ebersole and Wade, 1991; Lüders et al., 1993). Knowledge of the generators of IED would provide crucial information for :

(1) interpreting the findings of routine EEG studies. The detection of interictal epileptiform discharges in the scalp EEG has been the mainstay for the diagnosis and classification of epilepsy for more than fifty years. However, the EEG interpretation is still limited by the impossibility to identify directly the underlying generators of EEG events. This is due to the restricted spatial sampling and the insolubility of the „inverse problem". The distribution of fMRI-derived cortical activation could be used to constrain generator modelling of the scalp-recorded epileptiform discharges and thereby may be helpful in addressing the inverse problem, which limits the interpretation of scalp EEG;

(2) understanding the underlying pathophysiological mechanisms of epilepsy, e.g. the neuro-vascular coupling of epileptic activity or the propagation of epileptic activity;

(3) relating the anatomical site of the underlying structural abnormalities to the sites of functional disturbance (e.g. in malformations of cortical development, vascular malformations or brain tumours);

(4) planning the appropriate extent of surgical resection in respect of different lesional pathologies in pharmaco-resistant patients undergoing epilepsy surgery. Experimental work has indicated that there are likely to be different mechanisms of epileptogenesis, and outcome of epilepsy surgery appears to be crucially related to pathology.

3.2. EEG-correlated fMRI beyond localising epileptic activity

As mentioned above, EEG-correlated fMRI, like other functional neuroimaging techniques, can be used for identification of localised interictal (or ictal) abnormalities in patients with epilepsy. However, accurate localisation of the epileptogenic region is only of direct clinical importance when patients are candidates for surgical treatment. At present, therefore, functional neuroimaging does not play much a role in clinical epilepsy diagnosis apart from considerations for surgical treatment.

According to (Engel, 2000) in addition to improving the localisation of the epileptogenic region for surgical treatment, future applications for EEG-correlated fMRI in epilepsy, in combination with other functional imaging modalities, therefore might derive from the potential to (1) assess the degree of epileptogenicity; (2) provide differential diagnosis among various epileptic seizures, syndromes, and diseases, (3) offer insights into basic mechanisms of epilepsy and epilepsy-related disturbances, and (4) provide information on the mechanisms of actions of antiepileptic pharmacotherapy and alternative therapies. So far, as it will be discussed later, EEG-correlated fMRI has demonstrated that it can contribute to localise the epileptogenic region, but it provides no reliable information about its extent. Interictal spikes recorded during electrocorticography commonly occur beyond the area that needs to be removed in order to eliminate habitual seizures (Lüders et al., 1993). This has given rise to the concept of "red spikes" and "green spikes". It would be a major advantage if "red spikes", which indicate the epileptogenic region, could be distinguished from "green spikes", which do not. EEG-correlated fMRI might have the potential to distinguish specific characteristics of interictal spikes directly related to the generation of seizures from spikes that represent propagation. There is experimental evidence in animals and humans that interictal spikes arising from the primary epileptogenic region contain very fast (250-500 Hz) oscillations that are not associated with interictal spikes occurring

elsewhere (Bragin et al., 1999). If this is the case, and fMRI imaging of interictal spike generators can be used to identify a distinctive physiologic correlate, fMRI may be capable of accurately mapping the extent of the epileptogenic region, particularly in patients with no structural lesion visible on anatomical MRI and in patients with diffuse or multiple structural abnormalities. Furthermore, should this succeed in identifying interictal disturbances unique to the epileptogenic region, ictal recordings may not be necessary. (Video EEG telemetry monitoring is the most expensive part of the presurgical evaluation, and eliminating it would greatly reduce the cost of surgical treatment).

The development of a functional imaging technique that could reliably identify epileptogenic potential interictally could have other major clinical applications. Such a test could be used to distinguish between epileptic disorders and other conditions that mimic epilepsy. If the test could be used to predict whether lesions are likely to give rise to spontaneous seizures (e.g. following head trauma or stroke), it might lead to the development of preventive measures. If the test could be used to determine in patients who already have epilepsy whether the underlying substrate is progressive, or whether secondary epileptogenic regions are likely to appear, more aggressive treatment, such as epilepsy surgery, might be recommended earlier than currently.

Further, there is a need for a means of determining whether an antiepileptic drug will be effective in a given patient without waiting for seizures to occur. If fMRI could be used to measure the epileptogenic potential, it might be possible to test efficacy of specific drugs in individual patients, and even adjust dose regimens, without the need for the tedious trial-and-error assessment currently in use. Such a test would have a major impact on clinical trails of antiepileptic drugs, on drug development in experimental animal models. Furthermore, such a test could be able to determine when it is safe to taper and discontinue antiepileptic drugs after a period of freedom from seizures.

Chapter 4

Methodology

All studies presented in chapters 4 to 7 were approved by the ethics committee of the National Hospital for Neurology and Neurosurgery. All patients and probands gave informed consent.

4.1. Patient safety issues in EEG-correlated fMRI

General considerations

The potential health hazards in EEG/fMRI experiments can be classified into two categories: first, the risks associated with the interactions between the patient, the EEG leads and the MRI scanner's electromagnetic fields; second, the risks associated with the handling of patients and the EEG recording equipment in the MR environment. This section will concentrate mainly on the former; a discussion of the issues related to patient and equipment handling can be found in standard textbooks on MRI (Shellock and Kanal, 1996). The only explicit recommendations regarding this issue are that all EEG equipment introduced in the vicinity of the MR scanner should be tested for MR-compatibility (Holshouser et al., 1993, von Smekal et al., 1995) and that a specific EEG/fMRI patient and equipment handling protocol be devised.

The main steps to study potential hazards from the interactions between the patient, the EEG leads and the scanner's fields can be summarised as follows: (1) identify the mechanisms which may lead to harm to the patient; (2) identify existing relevant safety guidelines; (3) derive theoretical estimates of the effects based on the basic physical laws; (4) adapt those estimates to the specific context of MRI; (5) identify the mechanisms that represent the largest potential risk factors; (6) perform measurements to confirm estimates when the uncertainty is too large; and (7) make recommendations on measures to satisfy guidelines (Lemieux et al., 1997).

The physical principles of the interactions between patient, EEG equipment and MRI scanner

There are three types of electromagnetic fields used in a MR imager which can lead to potential safety hazards due to the induction of currents in the EEG electrodes and leads: the main static magnetic field, the time-varying magnetic gradient fields, which have different orientations and operate at ~ 1 kHz; and the radio-frequency (RF) pulsed field generated by the head coil which is homogeneous in the central region of the head coil and operates at 42.6 MHz/T. The RF field has two components: magnetic and electric. MR head coils are designed to maximise the RF energy, which is transmitted to the body via the magnetic field and minimise the electric contribution (Hayes et al., 1985, Chen and Hoult, 1889,). Nonetheless, the electric component can be a potential health hazard when wires are placed in the vicinity of the RF transmitting coil (Hofman et al., 1996, Konings et al., 1998). This is due to a resonant antenna effect occurring if the length of the wire is of the same order as the wavelength of the RF field, and is strongly dependent on the position of the wire in the coil, the immediate environment of the wire (e.g. air or tissue) and the type of coil (body or head, field polarisation). For the set-up described here, this effect was not found to be a significant potential hazard (Lemieux et al., 1997).

Conducting loops and other mechanisms

Low-impedance conduction through the patient represents a potential hazard as currents may be induced in the presence of the electromagnetic fields used in MRI due to the presence of a loop in the time-varying gradients and RF fields and the loop movement in the static field due to body movements. In EEG/fMRI, conducting loops will inevitably be present in order to measure electrical potentials on the head. Although these normally have a high impedance (due to the EEG amplifiers) low-impedance

loops may form as follows: exposed lead wire in contact with patient; two leads in direct electrical contact; a single wire bending on itself and current being able to flow through the insulation at RF frequencies; and failure of the EEG pre-amplifier circuit. Most of the above represent single-fault conditions. However, pre-amplification circuits that have a low-pass filter at the "front end" could also provide relatively low-impedance in the RF bandwidth. Similarly, a conducting loop could be formed due to the capacitance between parallel leads, with the induced current flowing through the patient. Currents in the leads may cause excessive heating of current-limiting resistors, and must therefore be investigated. Heating due to eddy currents induced within the electrodes and other conducting media in contact with the patient must also be assessed (Duckwiler et al., 1990, Lufkin et al., 1988, Roth et al., 1992). The results of Lemieux et al. (1997) for standard electrodes and gel revealed negligible heating, even when using sequences with high RF output.

Specific health risks and relevant safety guidelines

Conducting loops provide a concentration of current in metallic components and therefore a high current density in the adjacent tissue. Currents induced in the body through conducting materials or within conductors in contact with the body in the presence of time-varying electric or magnetic fields, such as described above, are referred to as "contact currents" and represent a well documented health risk (National Radiological Protection Board, 1995). These hazards are: ulcers due to electrolysis from DC currents (Smallwood et al., 1983); electric shock or stimulation below 100 kHz; and heating above 100 kHz from currents flowing through the patient or in objects in contact with the patient (National Radiological Protection Board, 1991, Schaefer et al., 1993).

To date, there are no specific official safety guidelines for EEG/fMRI. However,

relevant general guidelines for physiological monitoring (mainly derived from experience with ECG monitoring inside MR scanners) have been published (Shellok and Slimp, 1989, Brown et al., 1993, von Smekal et al., 1995). For ECG/MRI, the main risk is that of RF burns at the points of contact between the ECG leads and the patient (Shellok and Slimp, 1989, Brown et al., 1993). Therefore, it is recommended to minimise loops, avoid wires from crossing each other and limit currents by using higher-resistance leads. As the amplitude of EEG signal is approximately two orders of magnitude lower than ECG, such leads are likely to give significant degradation of the EEG signal.

Safety guidelines and investigative work in other areas which address the same basic physical interactions as described above can be used to establish safety limits: (1) recommendations on maximum contact currents resulting from exposure to time-varying electromagnetic fields by the National Radiological Protection Board, UK (1995); (2) safety guidelines on the use of electrical equipment from the International Electrotechnical Committee's "Medical electrical equipment: specification for general safety requirements" (*IEC601:1*) (1998); (3) published research on RF-burn hazard in animals (Brown et al., 1977).

In the study of Lemieux et al. (1997) the above limits have been interpreted as representing root-mean square (RMS) continuous-wave values and the lowest value across all standards and guidelines were chosen: 0.01 mA in the normal operating mode (NOM) and 0.05 mA for the single-fault condition (SFC) for DC; 0.1 mA (NOM) and 0.5 mA (SFC) at low frequency (~1 kHz;); and 10 mA (NOM and SFC) for RF. For RF the value for normal operating mode as low-impedance loops can exist during normal operation was selected; at lower frequencies this mechanism does not apply and the single-fault condition values must be used. In the case of potential heating of objects in (sustained) contact with a subject, the relevant safety guideline specifies a maximum

allowable temperature of 41°C (Lorrain and Corson, 1970).

Estimates of induced voltages

Here a summary of the derivation of formulas for the calculation of the induced voltages due to the switching gradients, RF pulses and loop movement in the static field is presented. These are derived from the application of Faraday's induction law (Lorrain and Corson, 1970). Then the current-limiting resistor values for each of these for a specific scanner are calculated.

Gradient switching

It is assumed that all gradients can be simultaneously switched at the maximum rate and that the loop is lying in a plane perpendicular to the direction of the main field, Z, i.e. the worst case, at a distance z from the gradient coil isocentre. Then, the peak voltage induced by the switching gradients, V_G, is given by:

$$|V_{Gz,\max}| = \sqrt{3}\, s_{\max} A z$$

where A is the loop area and s_{max} is the maximum gradient slew rate.

$$V_{rms} = \omega_0 A K H(w) \sqrt{SAR_{avg}}$$

RF pulses

A circularly polarised magnetic field, B_1, rotating in the axial plane at the Larmor frequency ω_0 (=2πx42.*58*MHz/T) and a conducting loop of area A placed in a plane placed perpendicular to B_1 is considered. Consideration of the effects of loop position, field inhomogeneity and time averaging, gives the following equation for the time-

averaged induced voltage, V_{rms} (Lemieux et al., 1997):

$$V_{rms} = \omega_0 A K H(w) \sqrt{\mathrm{SAR}_{avg}}$$

where K is a geometric gain factor to take into account the loop position in the head coil and RF B_1-field inhomogeneity, $H(w)$ is an empirical function of the subject's body weight, SAR_{avg} is the average whole-body Specific Absorption Rate in Watt/kg. Note that this equation has been derived for a specific scanner (Lemieux et al., 1997).

Movement in B_0 field

Movement of a loop relative to B_0 may result in an induced voltage, V_{mov}, given by:

$$|V_{mov}| = B_0 \frac{dS}{dt}$$

where dS/dt is the rate of change of loop area normal to the field.

Current-limiting R value for a GE Signa MRI scanner and worst case low impedance loop

The concept of a worst-case low impedance loop with an area of 400 cm^2 was used. This is based on a head diameter of 20 cm and electrodes positioned around the head. For our GE Signa 1.5 T Echospeed (GE Medical Systems, Milwaukee, USA), the relevant parameter values are: s_{max} = 120 T m^{-1} s^{-1}; length of the head coil is 0.4 m. The loading function of the body weight $H(w)$ was obtained from the scanner's manufacturer (Lemieux et al., 1997).

For the gradients, assuming that the induced waveform (the *time derivative* of the gradient waveform) is a continuous square-wave of the same amplitude, application of the first equation gives a worst case RMS value of 1.66 V; This is a pessimistic estimate, because for the MR system used, the gradient waveform is a trapezoid and therefore there is a non-zero time gap between successive periods where dB/dt is non-zero. Taking a maximum allowable current at 1 kHz of 0.5 mA RMS, a current-limiting resistance of 3.3 kΩ is obtained.

For RF, the measurements have shown that K~1 (Lemieux et al., 1997). In order to assess a worst case, the example of a fast spin-echo sequence with magnetisation transfer contrast is used, with a SAR_{avg} value of 0.06 W/kg[1], which is near the allowed maximum. From the second equation a V_{rms} of 52.7 V is obtained. Given a maximum allowable current of 10 mA, a current-limiting resistance of 5.3 kΩ is obtained.
If a loop is moved from a position parallel to static field to one normal to the field in 0.25 second, i.e. a brisk movement of the head, with a constant rate of change of area, V_{mov} will be 0.24 V. Assuming that the threshold of sensation is 1 mA (Smallwood et al., 1983) this indicates that a resistance of 240 Ω is required to protect against this risk.

Heating in current-limiting resistors and other components

The current-limiting values calculated above do not take into account the heating of the resistor that may arise when the maximum allowed current flows through it. Heat dissipation in resistors generally obeys the relationship:

$$\Delta T = R_{th}\frac{V_{rms}^{2}}{R}.$$

where ΔT is the temperature increase (°C), R_{th} is the thermal resistance (°C/Watt) and V_{rms}^2/R is the RMS power (Watt). As indicated previously, ΔT must be less than 20°C,

$$R > \frac{R_{th}}{20} V^{2}_{rms}$$

and therefore:

Taking a specific type of resistor (½-Watt carbon-composition resistor, type 101-4, Vitrohm GmbH, Germany), R_{th} is 85. For the gradient-induced currents, $V_{rms} < 1.66$V and therefore the inequality gives: $R > 11.7$ Ω. For the RF-induced currents, $V_{rms} < 53$

[1]This is the whole-body value when using the headcoil.

V, and therefore $R > 11.9$ kΩ. For loop movement-induced currents, $V_{rms} < 0.2$ V, and therefore $R > 0.17$ Ω.

Therefore, the minimum value of resistance that ensures that both the maximum allowable current at any given frequency and the resistor temperature increase are not exceeded is 11.9kΩ.

General comments on higher field strengths

The equations given above can be used to obtain theoretical estimates of the induced voltages for a range of main and gradient field slew rates. However, factors like RF coil transmission homogeneity and the gradient switching waveform should be considered when trying to implement EEG/fMRI in a different scanner. In certain cases it may be possible to adapt the above equations to the specific parameters of the new scanner, for example in the case of a different gradient switching waveform, whereas in other cases new experimental work may be required. Regarding the calculation of the RF-induced voltages, the general form of the second equation should apply to any scanner, however the exact form of the factors K and $H(w)$ may vary.

Summary of patient safety issues

The study of Lemieux et al. (1997) remains the main source of guidance in this field. In summary, it was found that the main source of potential hazards is the RF field. It was therefore recommend placing a resistor at each EEG lead, as close as possible to the electrode, with a minimum value of 11.9 kΩ.

4.2. EEG quality

Interactions between the patient, EEG electrodes leads and the magnetic fields in the scanner can result in artifacts, which make recognition of EEG events difficult. These

artifacts are generated as a result of two physical principles: a change in the magnetic flux through a loop will induce an electromotive force (emf) in the loop (Faraday's induction law), and movement of blood (a conductor) normal to a magnetic field leads to induced potentials (Tenforde et al., 1983). These principles may lead to EEG artifacts of varying significance for a number of reasons.

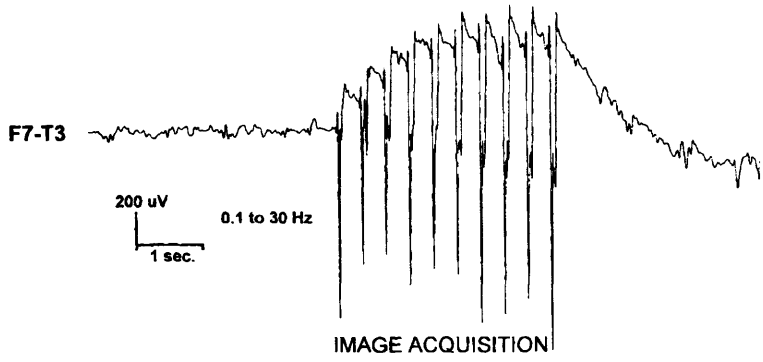

Figure 2: *EEG artifact due to the changing magnetic fields applied during image acquisition. This artifact is clearly much larger than the EEG activity.*

Image acquisition artifact

The changing magnetic fields applied during image acquisition may induce emfs in the electrode leads and the subject's head. These emfs can be of large amplitude *(figure 2)* and are generated by the gradient fields, which may contain activity in the EEG frequency range, and the RF pulses which, although of much higher frequency, can also generate EEG artifact due to the demodulating effect of non-linearities in electrodes and EEG amplifiers. The significance of this artifact depends on the EEG/fMRI experiment paradigm. For EEG-triggered fMRI, providing the images are acquired in a brief period

(less than the peak hemodynamic response time), this artifact does not present a significant problem as it occurs after the EEG event has been identified and any additional EEG events masked by the artifact should not contribute to the fMRI response. For simultaneous EEG/fMRI, this artifact is more significant. A method for removing the image acquisition artifact from EEG recordings is presented in chapter 7.2. Although low-pass filtering before the amplifier front-end can reduce effectively the contribution due to RF interference and amplifier non-linearity (Laudon et al., 1998), overlap of the EEG and gradient interference spectra suggests that linear filtering alone will not remove this artifact without significant distortion of the EEG waveform. Laudon et al. (1998) have reported a method for minimising this artifact in ECG recordings, by subtracting the induced signal detected by an external loop aligned with a pair of ECG electrodes. Although this method achieved an 80% reduction in artifact amplitude, the method has not been evaluated in vivo or for echo-planar imaging (EPI), and would be difficult to apply to multi-channel EEG recordings. Kreger and Giordano (1992) have described an adaptive filtering technique for removing this artifact from ECG signals. This technique correlates noise reference signals derived from the gradient field currents (modified to model the frequency characteristics of the ECG recording equipment), and subtracts the correlated signals from the noisy ECG signal. However, no quantitative results were provided and the method has not been evaluated for EEG recordings.

Pulse artifact

Movement of the subject's head and electrode leads may alter the area normal to the static field of a loop between electrode leads, resulting in an induced emf in the leads. Tilting of the subject's head may change the area of scalp normal to B_0, inducing an emf on the scalp. Artifacts due to these factors both result from patient movement. Large

movements such as swallowing, talking or head turning cause gross artifacts *(figure 3).*

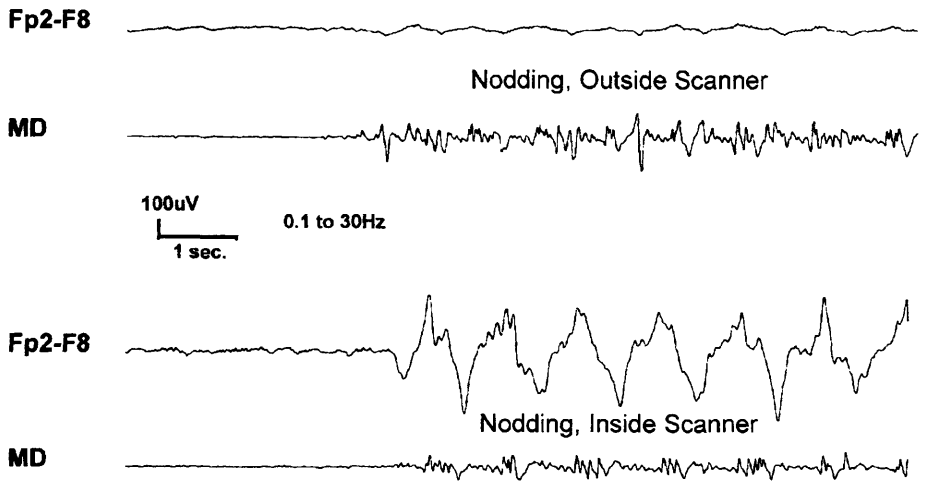

Figure 3: *Low amplitude movement artifact in the EEG recorded outside the scanner due to the subject nodding his head. The MD channel is a movement detector, which gives a broad indication of the amount of head movement. Inside the MR scanner, the movement detector indicates a similar amplitude of the head movement, but the movement artifact is now much larger.*

These may mimic epileptiform activity, although recording from a movement detector can assist in differentiating these (Hill et al., 1995). In contrast, small body movements due to pulse and the blood flow effect may produce pulse artifact which is a more significant problem as this may be widespread on the scalp, have a large amplitude peak followed by a complex waveform throughout the inter-pulse period, and persist throughout a recording *(figure 4)*. This appears to be a universal problem as there are many reports of this artifact from different centres, using different EEG recording equipment (Ives et al., 1993, Hill et al., 1995, Huang-Hellinger et al., 1995, Felblinger et al., 1997).

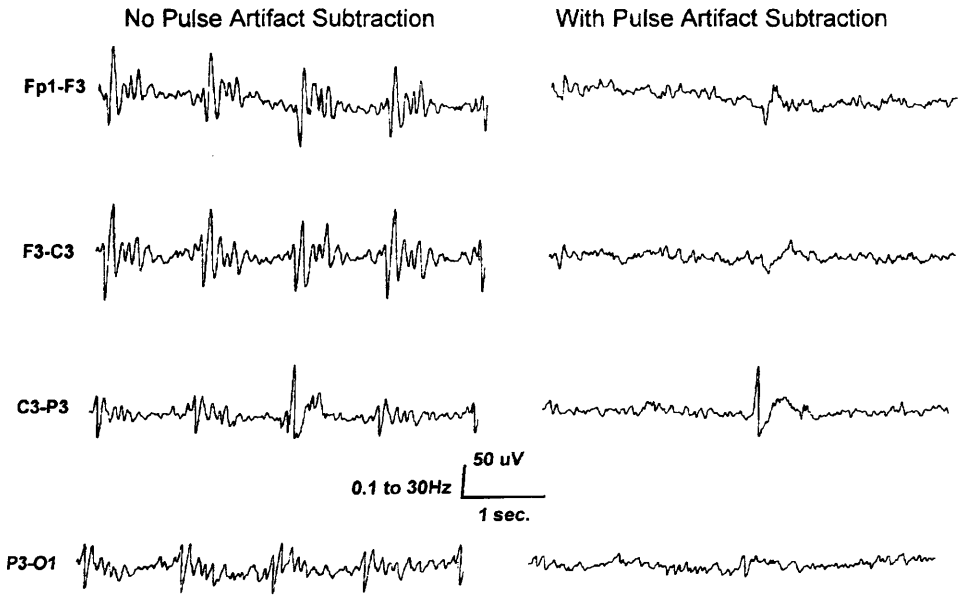

Figure 4: *A section of EEG recorded from a normal subject inside the scanner, with and without pulse artifact subtraction. An epileptiform discharge (spike) has been added to this record. Without pulse artifact subtraction, the EEG is obscured by large amplitude widespread pulse artifact and the spike is difficult to identify. After applying pulse artifact subtraction, the spike is clearly visible.*

To quantify the extent of this problem, Allen et al. (1998) measured the amplitude of pulse artifact for bipolar derivations in 6 subjects in a 1.5 tesla scanner and found that pulse artifact was largest in channels with frontal-polar or fronto-central electrodes and showed large intra- and inter-individual variations in amplitude. Using bundles of electrodes with leads twisted together to minimise the inter-electrode lead loops (for example the 5 electrodes for an anterior-posterior chain) gave 37% less artifact than if loops were not minimised, but the artifact was still greater than 50 μV in at least one channel in 5/6 of these recordings. As the amplitude of most scalp EEG events is normally between 10 and 150 μV, this artifact is clearly a significant problem. Interestingly, the experience of our research group (>70 EEG/fMRI recordings) indicates that pulse artifact is normally larger in males than females although the explanation for this is unclear.

Although the relative contributions to this artifact of head movement and blood flow effect are unclear, rejecting either is difficult as setting electrodes distant from scalp arteries and preventing small pulse-related head movements for the duration of an EEG/fMRI study (typically > one hour) are both impractical. In addition, the amplitude of pulse artifact is directly related to B_0 and hence pulse artifact for scanners with higher B_0 will present a greater problem. Hence, with the exception of large amplitude (>200 μV) frontal EEG events or lower amplitude events in the posterior/temporal regions, reliable EEG event detection is difficult in many subjects unless a method for removing the pulse artifact is used.

Allen et al. (1998) developed a pulse artifact removal method that subtracts an on-going average of the artifact waveform for each EEG channel *(figure 5)*. ECG peaks (QRS complexes) in the previous 10 seconds are automatically identified by pattern recognition, then the average pulse artifact waveform is identified for the period ± half the R-R interval, time-locked to these ECG peaks, is calculated for each EEG channel.

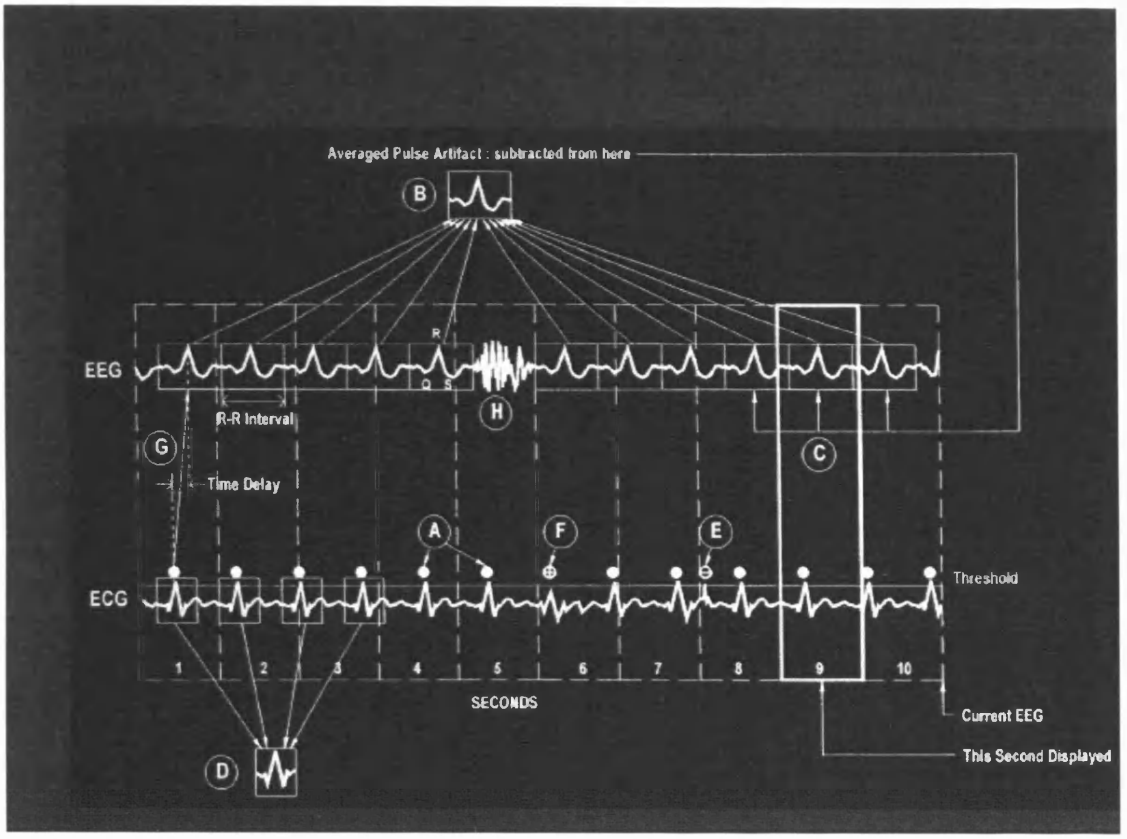

Figure 5: *A schematic of the pulse artifact subtraction method used for all EEG/fMRI studies presented here. This method processes EEG on a second-by-second basis and requires the previous 10 seconds of EEG and ECG signals. (A) An ECG peak corresponding to a QRS complex is identified by detection of a turning point following an amplitude threshold crossing. (B) PA waveforms in the EEG channels, time-locked to the ECG peaks (for example at points A and F) are averaged. (C) The averaged PA signal for each channel is subtracted from the EEG signals at times corresponding to the ECG peaks (plus the time interval described in part G below) in the last 3 seconds. This ensures all PA waveforms affecting the penultimate second of EEG are subtracted: this second of EEG is then displayed. (D) To confirm that an ECG peak detection corresponds to a QRS complex, an averaged QRS waveform is calculated from the first four ECG peak detections with temporal characteristics which indicate a high probability of being QRS complexes. (E) ECG peaks corresponding to noise in the ECG*

signal are rejected due to a low value of cross-correlation with the averaged QRS waveform calculated in D. (F) QRS complexes which are not detected by threshold crossing are identified by detecting an "R-R" interval between successive ECG peaks which is an integer number of the mean R-R interval and extra ECG peaks are added accordingly. (G) The sections of EEG (duration ± half the mean R-R interval) occurring a short time interval after the ECG peaks are averaged. A time interval is necessary as the peak of the PA in an EEG channel normally occurs a short time after the QRS complex. (H) If the section of EEG time locked to an ECG peak contains other artifacts, the section is excluded from the average PA waveform.

This average waveform is then subtracted from the current section of the EEG channel. A 10 second averaging period is sufficiently short to allow changes in the pulse artifact waveform to be identified, but is long enough to separate the pulse artifact and underlying EEG by averaging out cerebrally generated components. This method was evaluated in 6 subjects using spectral analysis (Allen et al., 1998). The frequency spectra for EEG recorded inside the scanner with no pulse artifact subtraction showed a large increase in activity relative to that recorded outside the scanner, across the frequency range of most EEG activity, with the largest median increase (307%) present in the 4 to 8 Hz range. The pulse artifact subtraction method reduced this increase significantly across the whole frequency range analysed. To validate the method for identification of EEG events, lateralised IED were added to recordings from inside and outside the scanner: the method increased significantly the proportion of correctly identified spikes (from 35% to 73%) and decreased the rate of false spike detection (from 15.7 to 8.7 per hour). Artifact subtraction is performed on-line, and introduces a 1-second delay in the display of the corrected EEG. This method of pulse artifact subtraction was implemented on the intra-MRI EEG recordings system and used in all

EEG/fMRI experiments described in the following chapters.

Other artifacts

Outside the magnet bore, the static field is non-uniform and hence movement of a loop formed between electrode leads may cause the loop to experience a relatively large change in magnetic flux resulting in an induced emf. However, by twisting electrode leads together from the subject's head to the amplifier inputs (to minimise inter-electrode lead loops) and fixing the leads securely to a stationary surface (to minimise lead movement), this artifact can be reduced effectively.

As has been stated previously, a current-limiting resistor is recommended in each electrode lead for patient safety (for the equipment described here). EEG from a subject inside the scanner both with and without these resistors (amplifier input impedance >20 MOhm) was recorded. No visually identifiable difference in background noise was apparent in the EEG, suggesting that this value of resistance can be used without compromising EEG quality. Indeed, the electromagnetic shielding of the scanner room can help reduce mains 50 Hz artifact in the EEG to an amplitude lower than is present with the subject outside the bore.

Summary of EEG quality

EEG of sufficient quality to allow reliable identification of most EEG events can be recorded while scanning is not ongoing providing careful arrangements of electrode leads and pulse artifact subtraction are used allowing event identification for the purpose of EEG-triggered fMRI.

4.3. MR image quality

EEG recording inside the MR scanner can decrease MR image quality, especially when

echo-planar imaging (EPI) is used, which is more sensitive to artifacts than conventional imaging sequences. While the issue of image artifacts caused by biomedical implants and devices has been investigated extensively, the specific effects of EEG-recording on the EP image quality have been addressed only by a few studies (Ives et al., 1993, Huang-Hellinger et al., 1995, Krakow et al., 2000). Nonetheless, these studies have identified two main mechanisms of the EEG recording, which can compromise the MR image quality:

(1) Local signal drop-outs and geometric distortions due to EEG electrode assemblies attached or close to the head due to their magnetic susceptibility and the possible existence of eddy currents in the conductive components of these assemblies.

(2) Degrading of the image signal-to-noise-ratio due to electromagnetic noise emitted by the EEG recording equipment.

In this section, the results of a detailed study of the above effects are described (Krakow et al., 2000a). The main purpose of this study was to evaluate the above effects on a representative sample of EEG recording components in order to identify the most appropriate components for the EEG/fMRI experiments performed in our laboratory, and to provide a general framework that can be useful to other researchers interested in evaluating their own equipment for EEG recording inside a MR scanner.

Material and methods

All imaging was performed on a 1.5 tesla Horizon EchoSpeed MRI scanner (General Electric, Milwaukee, USA) unless stated otherwise.

1. Measurement of the scalp-cortex distance: T1-weighted inversion-recovery prepared volume acquisitions (Fast IRSPGR: TI/TR/TE/flip = 450/15/4.2/20; 124 1.5 mm thick coronal slices; 256x192 matrix, 24x18 cm FOV) of 10 healthy volunteers were acquired (4 males, median age 36.0, range 17-50 years). The distance between the surface of the

scalp and the cortex was measured at locations corresponding to the position of the FP1, F3, F7, C3, T3, P3, T5 electrodes of the 10/20 system, using the image display and analysis software *MRreg* (Moran et al.,1999).

The three following experiments were carried out using a gradient-echo EPI sequence similar to the one which has been used in fMRI experiments: TR/TE = 3000/40, bandwidth 100 kHz, 24 cm FOV, flip angle 90, acquisition matrix 96x96, reconstruction matrix 128x128. Fat saturation was explicitly selected to prevent the scanner from using the spectral spatial pulse. Twenty contiguous 5 mm-thick slices were acquired in an interleaved fashion.

2. Quantification of the local signal drop out and geometric distortions on a phantom: The EEG electrode assembly is the part of the EEG recording equipment, which is in close contact to the subject's head. It consists of the following components, which all were assessed in this study: EEG electrodes, conductive electrode gel and paste, electrode adhesive, current-limiting resistors, insulating sleeve enclosing the resistor, and wire. Details of the origin and composition of the components are given in table 1. Each component was attached individually on the surface of a 10 cm glass sphere filled with distilled water. Electrodes, resistors and wires were tested both with their long axis parallel (placed on top of the phantom, axial sections) and perpendicular (frontal side of phantom, coronal sections) to the B_0 magnetic field. Adhesive and gel were only tested on top of the phantom for practical reasons. All objects were scanned twice in each position on different occasions. Measurements were also made with the whole electrode assembly attached to the phantom. The maximum perpendicular depth of artifacts was measured in the images using *MRreg*.

3. Quantification of artifacts *in vivo* for the components with acceptable artifacts as measured in the phantom experiments: Electrode assemblies (consisting of an electrode, resistor, resistor insulation, wire and 0.1 ml of electrode adhesive and gel) made of the

components which gave acceptable results in the first experiment where placed on the right side of the scalp of a volunteer at the 10/20 electrode positions used in clinical studies (FP2, F8, T4, T6, O2) (Krakow et al., 1999b). These were compared to electrode assemblies made up of non-optimised components, which had been used previously for intra-MR EEG recordings (Ag/AgCl electrode, carbon current-limiting resistor, silicone-insulated lead) (Krakow et al., 1998). These were placed at the equivalent positions on the left side of the head. The experiment was repeated using a high resolution EPI (sequence parameters as above, except matrix size: 256x256). The depth of the artifact was measured using *MRreg*.

4. Quantification of the image noise caused by the electromagnetic fields generated by the EEG recording equipment: The EEG recording system consisted of electrode assemblies, placed in the head coil beneath the phantom and connected to a non-ferrous headbox (developed in-house) located at the entrance to the bore of the magnet (head coil - headbox distance = 125 cm). The headbox was connected to an unscreened battery-powered Neurolink Patient Module (Physiometrix, MA, USA), placed at the side of the MR scanner (distance to the bore of the magnet: 130 cm). This digitises and transmits the EEG signal out of the scanner room via a fibre optic cable to the Neurolink Monitor Module, which reconstructs the analogue EEG signals. Phantom images were acquired with (a) the unshielded Patient Module switched off, (b) the unshielded Patient Module switched on and (c) the Patient Module switched on, shielded with a double-walled aluminium/plastic box and a RF-filter in-line with all wires connecting to this box.

To measure the noise transmitted by the EEG equipment, the EPI sequence above was used with flip angle = 0 to ensure that no RF was transmitted into the phantom. The mean and peak intensities over the whole image were measured using *Dispimage* (Plummer, 1992). As image noise due to electromagnetic fields may be a function of the

scanner RF frequency, this experiment was repeated in a 2 T scanner (MAGNETOM Vision, Siemens, Erlangen, Germany) using the same EEG recording equipment.

Results

1. Scalp-cortex distance: The mean distance between surface of the scalp and the cortex measured was 13.8 mm (SD 3.5). The smallest individual scalp-cortex distance, measured over the position T5, was 7.5 mm.

2. Local signal drop out and geometric distortions on a phantom: The pattern of signal drop out and geometric distortion of the phantom image caused by the tested objects was dependent on their spatial orientation with respect to the B_0 magnetic field. The figures given in *table 1* represent the maximal depth of the artifact caused by the components placed on top of the phantom and orientated parallel to the B_0 vector. Artifacts were slightly more pronounced (<20% increase in depth) if the long axis of objects was at right angle to the main magnetic field. The image artifacts caused by carbon, plastic covered silver and gold electrodes were within acceptable range (smaller than the minimum scalp-cortex distance in normal controls). Ag/AgCl electrodes caused slightly larger artifacts *(table 1)*.

The different types of resistor showed significant differences. Carbon resistors caused an artifact intruding almost 20 mm into the phantom. Two planar cermet resistors gave satisfactory results with artifacts less than 2 and 6 mm in depth, respectively *(figure 6)*. All leads tested resulted in negligible artifacts (< 2mm).

While the tested collodion adhesive caused an artifact intruding less than 4 mm, even minute amounts of conductive electrode gel (0.1 ml) led to artifacts of almost 10 mm depth. The size of the artifact appeared to be proportional to the amount of gel.

From the materials commonly used to insulate the resistor and improve the mechanical strength of the electrode assembly, epoxy putty gave the largest artifact (10 mm depth).

When single components were combined to form electrode assemblies, the extent of the artifact was comparable to that of the worst single component.

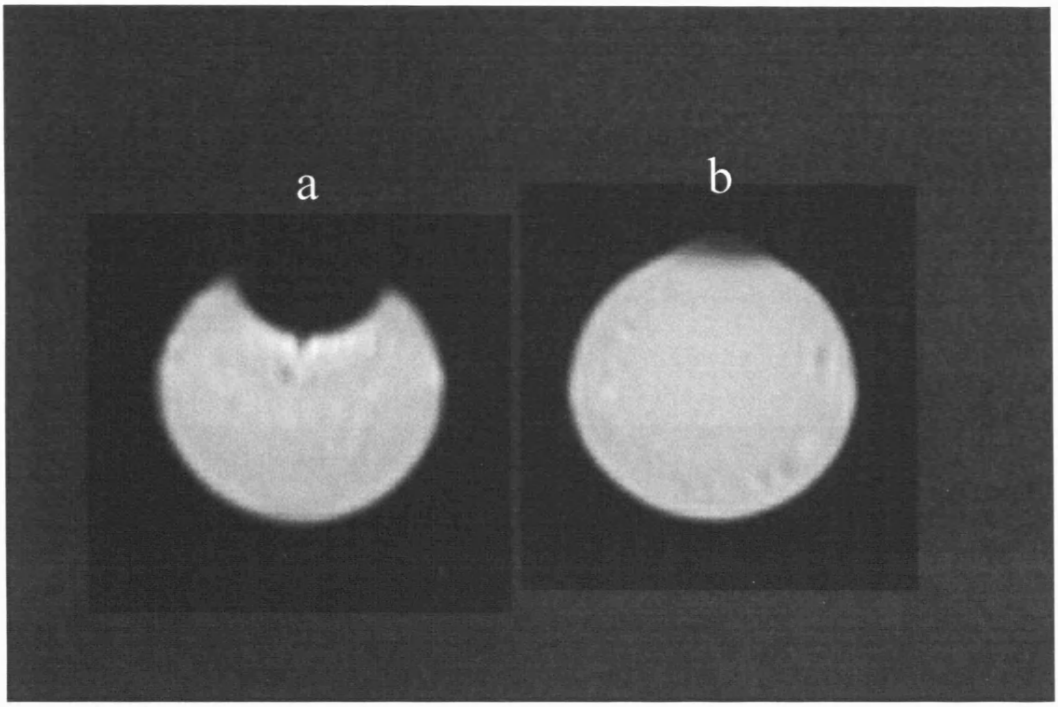

Figure 6: *Examples of image artifacts caused by current-limiting resistors as used in electrode assemblies. The images show the signal drop out/geometric distortion caused by the carbon composition resistor (a), and by the cermet film resistor (b), placed on the top of the phantom (diameter 10 cm).*

3. Artifacts *in vivo* for the components with the smallest artifact as measured in the phantom experiments: EP-images of a volunteer with the optimised electrode assemblies demonstrated artifacts in superficial scalp tissue only (maximal depth < 5 mm), while non-optimised electrode assemblies showed artifacts intruding the cortex (maximal depth > 15 mm) *(figure 7)*.

4. Image noise caused by the electromagnetic fields generated by the EEG recording equipment: With the EEG equipment switched off (baseline) no image artifact was

visible. The mean background noise was 10.5 (SD 7.3) with a maximum intensity of 55.0. When the EEG digitiser (Patient Module) was switched on without shielding, the images were compromised by coherent noise. Approximately 0.3% of pixels had an intensity above background noise, forming a chequered design. The mean signal was 15.2 (SD 18.6), the maximum signal, measured in the brightest pixels, was 538.0. When the shielding was applied to the Patient Module, no noise was detectable and the signal was in the range of the baseline-measurements (mean 10.1 (SD 7.2), maximum 60.0). Similar results were obtained at 2 tesla.

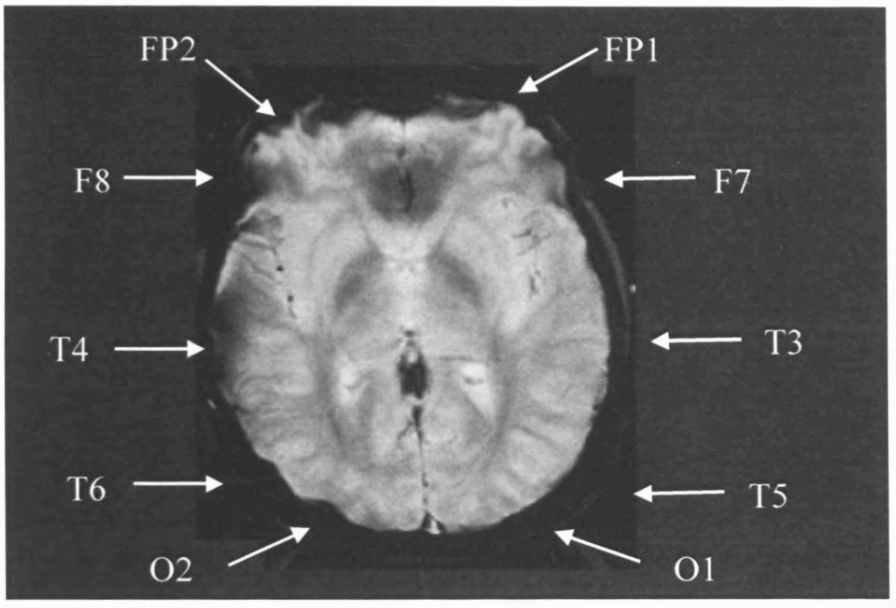

Figure 7: *High resolution EPI of a subject with two EEG electrode assemblies applied on the scalp. On the right side of the head (electrode positions FP2, F8, T4, T6, O2), non-optimised electrode assemblies (silver/silver chloride electrodes, carbon composition resistor) caused artifacts intruding into the cortex. Optimised electrode assemblies (gold electrodes, cermet film resistors) used on equivalent positions on the left side of the head did not compromise the cortical signal.*

Discussion

All components of the electrode assemblies tested caused some signal drop out and geometric distortions. In some cases these exceed the minimum scalp-cortex distance as measured in a population of normal subjects (7.5 mm), thus potentially degrading the fMRI results. Large differences in the artifact depth were found between components, indicating the need to test carefully all objects intended to be used in electrode assemblies.

Most types of electrodes gave image artifacts less than 7.5 mm. Although the smallest artifact was found in carbon and plastic electrodes, there are practical difficulties associated with constructing electrode assemblies from these as they cannot be soldered (for example to connect the electrode to the current-limiting resistor). Gold electrodes were found to give the optimum combination of small artifact and ease of use.

There were large differences in artifacts for different resistor types. Many resistors use iron end caps (ferromagnetic) or nickel (paramagnetic) to attach the wire to the resistive material. These resistors were not included in this study as they would necessarily lead to unacceptable artifacts. It is worth noting that the carbon composition resistor tested, despite being composed mainly of carbon, gave unacceptably large artifacts.

Some means of insulation of the resistors and wires from the patient is required and it was shown that a specific heat shrink sleeving could be used without causing a significant artifact. However, injecting epoxy into the sleeving around the resistor leads (to improve the mechanical strength of the lead-to-resistor joints) gave large artifacts and should be avoided. On the other hand, the wires tested caused only small artifacts and this suggests that carbon leads do not offer a significant advantage over metallic wire, but have two disadvantages: poor mechanical strength and difficulty in connecting to other parts of the electrode assembly.

Conductive gel gave large image artifacts and as the depth of the signal drop-out and

geometric distortion was roughly proportional to the amount of gel tested, only the minimum amount of gel necessary to give acceptable electrode impedance should be used.

A phantom was used for these measurements to facilitate quantification of the image artifacts and a comparison between the various components of EEG electrode assemblies. However, it was found that the magnitude of the image artifacts in vivo were of similar depth to those on the phantom. Optimised electrode assemblies led to artifacts clearly smaller than the minimum scalp-cortex distance. It can therefore be concluded that EEG can be recorded inside a MR scanner without compromising the cortex signal by local artifacts.

With regard to electromagnetic noise radiated from the EEG equipment, significant coherent noise was found in the images if no shielding was used. This is presumably due to broadband signals generated by fast switching signals in the EEG digitising circuit in the frequency range detected by the receiver chain of the MRI scanner. This noise is likely to be dependent on the type of the EEG equipment, its location in respect to the headcoil, and the scanner Larmor frequency (i.e. field strength). However, it was found that the image noise levels measured in the 1.5 tesla and 2 tesla scanners were similar. By using an appropriate shielding device (aluminium box and RF filter) the noise could be removed completely.

Although a representative range of MR compatible components was tested, it has to be emphasised that subtle changes in their manufacture process (e.g. modification of composition) or differences between manufacturers can cause significant changes of the MR-related material properties. The same applies for the EEG-recording module as a source of electromagnetic noise. The results of this study should therefore be seen only as a primary guideline for the selection of EEG recording equipment and a framework for an individual testing of components. The methods described and the results of this

study should be useful to other researchers as a framework for testing of their own equipment and for the selection of appropriate equipment for EEG recording inside a MR scanner.

Summary of MR image quality

Concurrent EEG and fMRI can be carried out without compromising the image quality significantly if appropriate materials are chosen and precautions to shield electromagnetic noise are taken.

Table 1: *Ag: silver, AgCl: silverchloride, Au: gold. Dimensions of components: length/width/height, d: diameter. The two values in the third column represent the results of the two measurements.*

Table 1: *Artifact measurements in phantom*

Component description	**Material/design**	**Artifact size (mm)**
Electrodes		
Ag/AgCl: SLE UK; 131/9/TP	cast pure Ag coated in AgCl; d: 9mm	8/8
Au: Grass USA; E5GH	cast pure Ag with heavy Au coating; d: 10mm	6/4
Plastic Ag/AgCl: Meditec Italy; 1183 AGCL	plastic coated in Ag/AgCl; d: 10mm	4/4
Carbon: Telefactor USA; carbon electrodes	carbon electrodes with carbon wire; d: 10mm	2/4
Resistors		
Carbon composition: Vitrohm Germany; series BT, 104-0	carbon black, phenol resin, bakelite; length: 9.9mm, d: 3.5mm	19/19
Planar thick film cermet, BI Technology, BPCE	Ruthenium oxide on aliminia substrate; 25.4/10.2/2.5 mm	6/4
Cermet film: Meggitt CGS; HB01	cermet film on ceramic substrate with epoxy coating; 26.5/10.5/3.0 mm	2/2
Resistor insulation		
Epoxy	rapid setting two part epoxy; 0.1ml	8/8
Epoxy putty	0.1ml	13/13
Heatshrink, black	Irradiated polyolefin tubing; d: 9.5mm	2/2
Leads		
Copper wire 1	annealed copper stranded wire, silicone rubber insulation; 128/0.05	2/2
Copper wire 2	silver plated copper stranded wire, PTFE insulation; 7/0.12	2/2
Carbon wire		0/0
Electrode adhesives/gels		
Collodion Adhesive: SLE UK	0.1ml	4/4
Electrode gel: Dracard ECG Gel, Crown Graphic UK	0.1ml	9/9
Elefix electrode paste: Nihon Kohden	combined adhesive/gel 0.1ml	8/6

4.4. EEG-triggered fMRI methodology

The EEG and fMRI acquisition processes can be combined in different ways. Here the experimental concept of fMRI triggered by real-time review of EEG recorded in the MR scanner is considered. Until it became possible to remove or prevent image acquisition artifact in the EEG (see chapter 7.2), these two modalities had to be acquired in an interleaved manner. This type of acquisition is here described in detail, but also the potential advantages of simultaneous EEG/fMRI acquisition are considered.

EEG-triggered fMRI acquisition

EEG-triggered fMRI is made feasible in event-related paradigms by the time lag associated with the Hemodynamic Response Function (HRF). Assuming that the response to a brief EEG event (IED) is similar to the brain's response to other stimuli, then an IED can be approximated as a delta function stimulus (Lassen and Kanno, 1997), and the associated fMRI signal change is expected to peak between approximately 4 and 6 seconds after the spike (Aguirre et al., 1998). As an initial approach aimed at detecting and localising the BOLD correlates of EEG events, the fMRI acquisition should thus be triggered to sample this period optimally. Control images can also be taken, the event in this case is a period of predefined duration (10 seconds in the studies presented here) of EEG activity without a spike. A voxel-by-voxel statistical test between these two sets of data will then establish areas of significant difference and so localise areas of change of blood oxygenation that correlate with the changes observed by the EEG. The optimal resolution, both temporal and spatial, of this data is that of fMRI, but the changes observed can be correlated with the EEG data, providing direct information about neuronal activity and a superior temporal resolution.

By acquiring fMRI at several time points following a spike, spatial coverage can be

traded for greater temporal sampling. This allows the measurement of the HRF of the area associated with the epileptiform activity, which provides the possibility of characterising the neurovascular coupling of these areas.

Experimental design considerations in EEG-triggered fMRI

Following the above considerations, the delay between the IED detected in the EEG recording and the start of the fMRI acquisition should be set carefully. If the delay is less than 3 or more than 5 seconds, then the EP images could sample the HRF outside the peak response resulting in a loss of sensitivity. EEG-triggered fMRI is limited by image acquisition artifacts which obscure the EEG. However, provided the EPI acquisition is shorter than three seconds, the lag associated with the HRF ensures that EEG events obscured during the image acquisition will have little effect on the measured response (*figure 8*).

Spikes and rest states do not occur on demand, so following an acquisition, it is necessary to allow the NMR spins to return to equilibrium, which means a typical wait of 15 seconds. Data collection efficiency is thus less than 10% (3/30 seconds) for EEG-triggered fMRI. Even with favourable EEG activity a study requiring 50 spike and 50 control epochs can take up to two hours raising patient compliance considerations and giving larger variations in the fMRI data than normally occurs in functional paradigms with periodic stimulus. Large head motion due to subject discomfort in long sessions places unusual demands on the registration software used for motion-correction, and the bright CSF may cause large partial volume and interpolation effects when the data is resliced. Global changes in image intensity may increase the overall variation in spike and rest states and reduce the significance of differences between them, unless some form of de-trending is performed.

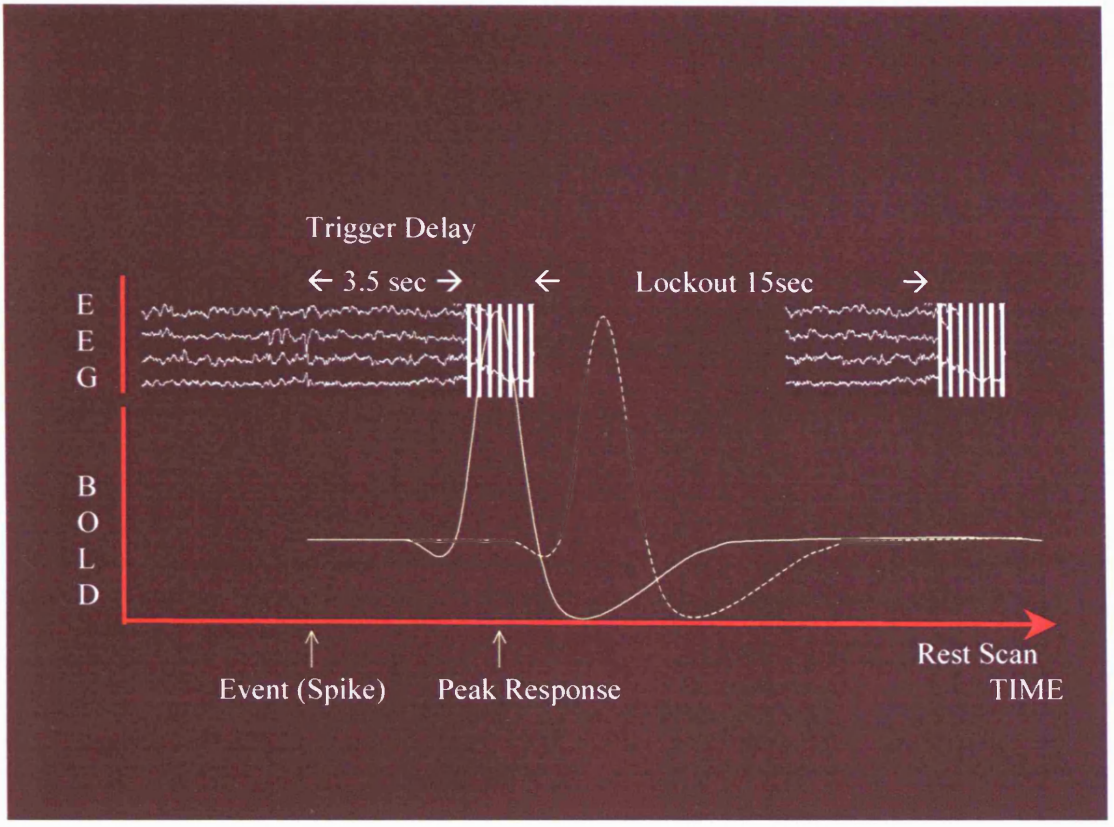

Figure 8: *A schematic of the experimental set- up of spike-triggered fMRI experiments. The EEG is observed on-line. When an IED is detected on the EEG, a fMRI acquisition is triggered manually with a delay of approximately 3.5 seconds. This delay enables the fMRI acquisition to cover the peak of the spike-related BOLD response. Control images are acquired after periods of at least 10 seconds of background EEG activity without IED. An interval of at least 15 seconds is kept between successive acquisitions to ensure the same T1 weighting for each acquisition. Due to the large image acquisition artifact it is not possible to identify EEG events during image acquisition. The dashed line represents the BOLD response of an IED occurring during fMRI acquisition, which remains undetected. Image acquisitions are performed non-periodically with activation and control images interleaved, depending on the sequence of the EEG events.*

Illustrative example

To illustrate the preceding discussion, the application of EEG-triggered fMRI to a patient with localisation-related epilepsy and frequent IED is described.

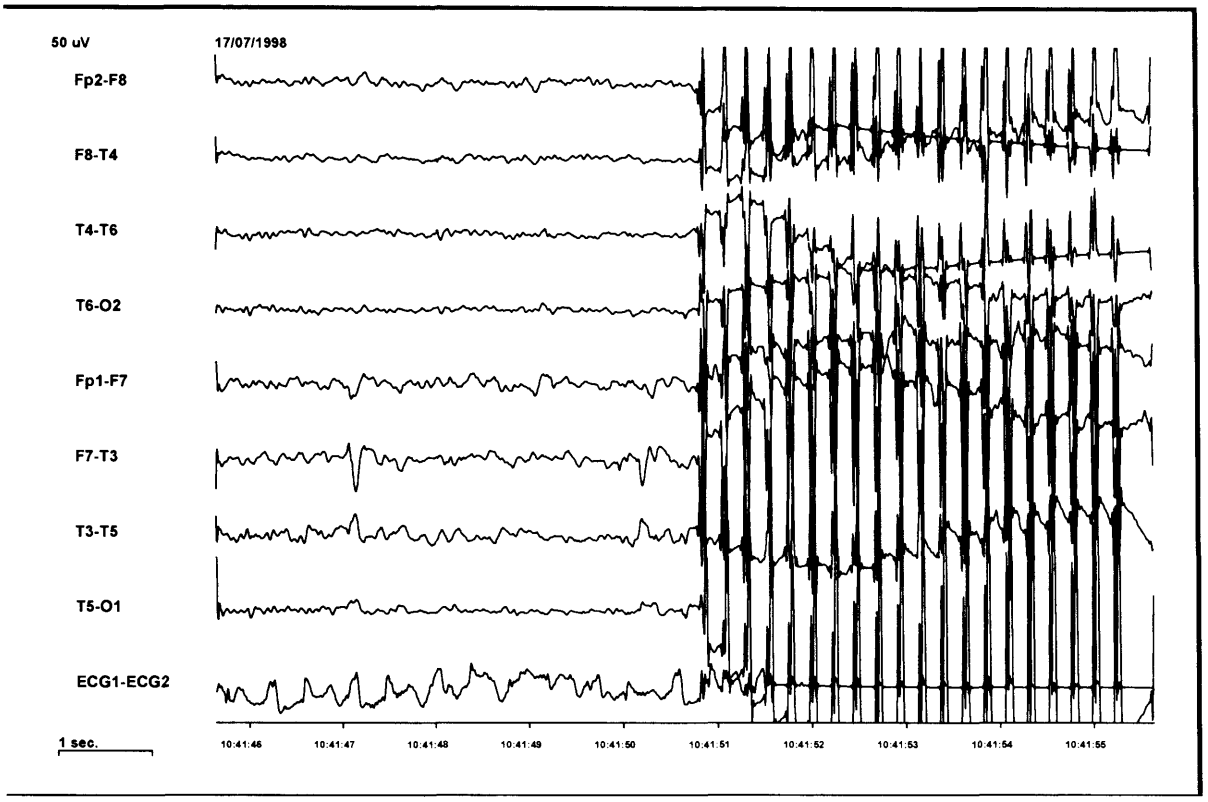

Figure 9: *EEG recording inside the MR scanner during a spike-triggered fMRI experiment. Displayed is a bipolar montage of a temporal electrode chain according to the 10/20 system. A typical left temporal spike of patient 1 (table2) with phase reversal over electrode position T3 occurs at 10:41:47. This spike was observed on-line and led to the image acquisition at 10:41:51, which is clearly detectable by the image acquisition artifact. In the delay period between the spike and the image acquisition another spike occurs at 10:41:50.*

EEG recording

EEG was recorded in the MR scanner using the following system: the electrode assemblies were connected to a non-ferrous headbox (developed in-house) placed at the entrance to the bore of the magnet. The headbox was connected to a Neurolink Patient Module which digitises and transmits the EEG signal out of the scanner room via a fibre optic cable to a Neurolink Monitor Module which reconstructs the analogue EEG signals. These were then recorded using a digital EEG recording system (sample rate 200 Hz, bandwidth: 0.12-50 Hz). Twelve electrodes were applied to the scalp positions FP1/FP2, F7/F8, T3/T4, T5/T6, O1/O2, Fz and Pz according to the 10/20 system. In addition, two precordial ECG channels were recorded to facilitate pulse artifact subtraction (75 kOhm current limiting resistors were fitted to each ECG-electrode) (Allen et al., 1998). EEG spikes and rest periods were detected by visual inspection, and fMRI acquisitions were triggered manually. The activation state was defined as a stereotyped IED (spike or spike wave) and the control state was defined as at least 10 seconds without a spike. *Figure 9* gives an example of an IED recorded in the EEG during the fMRI experiment.

fMRI acquisition and processing

Functional MRI was performed on a 1.5 tesla Horizon EchoSpeed MRI scanner using snapshot gradient-echo EPI (TE=40ms, 24cm field-of-view, 64x64 matrix). Twenty contiguous 5 mm slices were acquired in 4.5 seconds in an oblique axial orientation, with an average delay of 3.5 seconds between the EEG spike and the start of EPI acquisition, and a subsequent delay of 15 seconds to permit NMR spin equilibration. Forty-eight control and activation states were acquired, evenly distributed across the examination period.

The time-course of the fMRI response was measured in a separate study. Six images

(slice thickness = 7mm, flip angle 60 degrees, other parameters as before) covering the activated region of the first study were taken at one second intervals, starting 3 seconds after the spike.

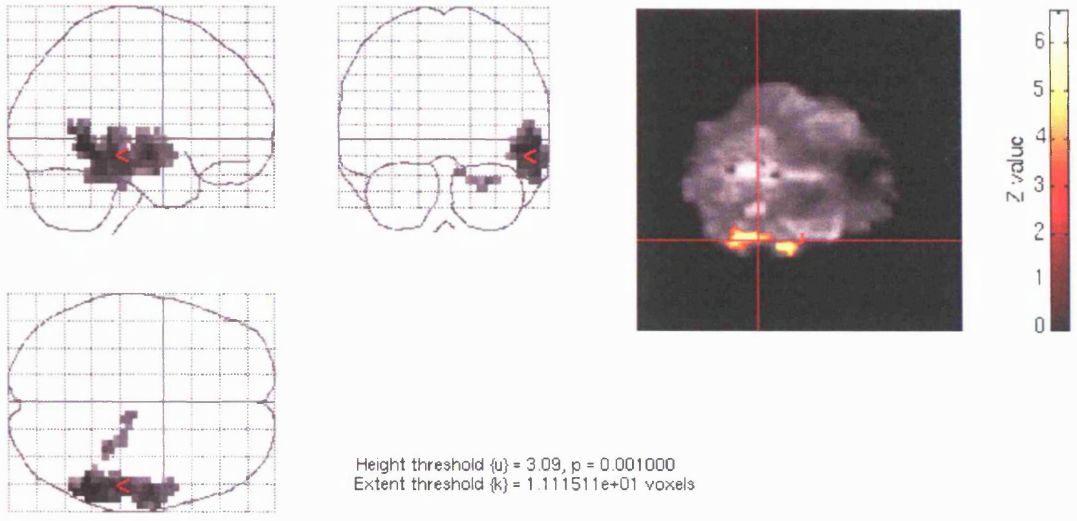

Figure 10: *SPM activation map results showing activation in the left temporal lobe (this activation map is not spatially normalised, so the left side of the brain appears on the right side of the images).*

The choice of packages for processing was partly determined by familiarity, and it is likely that other fMRI processing/registration packages meeting the above requirements would perform equally well. *Figure 10* shows the SPM-activation map of the experiment. The SPM98 package was used to perform spatial realignment, SPM96 was used for statistical analysis. Spatial smoothing and temporal high-pass filtering was applied, and the significance threshold was set to $p<0.001$. Activation was observed in the left temporal lobe, and this area was consistent with the source of the EEG spikes as indicated by previous electrocorticography. The same area was localised in the time

course study, and *figure 11* shows a graph of the number of significant pixels in that region activated at each time point. The response is strongly suggestive of the typical HRF, with a peak around 4 seconds.

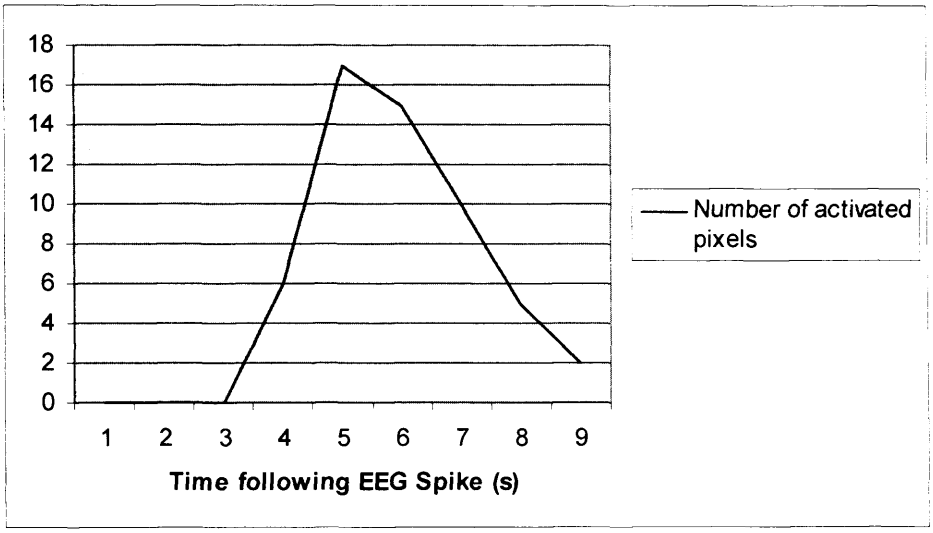

Figure 11: *Time course of the number of significantly activated pixels in the left temporal lobe following a spike.*

Summary of the EEG-correlated fMRI methodology

Using EEG-triggered fMRI, it is possible to identify epileptiform activity with the specific characterisation of EEG and the accurate localisation of fMRI. Furthermore, it is also possible to examine the HRF of epileptogenic areas. However, the acquisition efficiency of interleaved EEG/fMRI is sub-optimal as it fails to sample a significant proportion of the spikes during the scanning period. The advent of image acquisition artifact suppression on the EEG recording will enable simultaneous EEG/fMRI acquisition (see chapter 6.2). The resulting increase in sensitivity should allow more complex studies such as the comparison of different EEG events and time-course studies of the whole brain.

Chapter 5

EEG-triggered fMRI of interictal epileptiform activity

5.1. EEG-triggered fMRI of interictal epileptiform activity in patients with focal seizures

Interictal scalp EEG remains a principal diagnostic tool in epilepsy. It provides real-time information about physiological and pathological neural activity and can be recorded in any clinical setting. IED (spikes) are the most common EEG feature in patients with epilepsy and are the mainstay for classifying the type of epilepsy. Their localisation has an important role in presurgical evaluation of drug resistant patients (Gilliam et al., 1997). The knowledge of the underlying generators of these EEG events, however, is still limited. Due to their restricted spatial sampling and the limitations of the „inverse problem", neither EEG nor MEG (magnetoencephalography) can directly identify these generators with certainty (Ebersole, 1998). Conventional visual inspection of spikes on scalp EEG provides only limited information about the location of the focus. The possibility of characterising and localising the source of interictal epileptiform activity based on scalp EEG would therefore advance its diagnostic value. When combined with scalp EEG, functional imaging techniques could provide this information about the EEG source. However, the low temporal resolution of functional imaging techniques like PET and SPECT prevents an investigation of brain activation linked to brief IED.

During the last decade, the possibility of monitoring EEG inside an MR scanner (Ives et al., 1993, Huang-Hellinger et al., 1995, Lemieux et al., 1997, Allen et al., 1998) and to correlate the EEG with ultra-fast blood oxygen level dependent functional MRI (BOLD-fMRI) (Warach et al., 1996, Krakow et al., 1999b) has been described. In select patients with localisation-related epilepsy EEG-triggered fMRI could reproducibly identify brain

areas involved in the generation of interictal spikes (Krakow et al., 1999). Compared to EEG source modelling, EEG-triggered fMRI is based on a direct biological measurement and takes advantage of the higher spatial resolution of MRI. Conversely, it can only identify neural activity indirectly through BOLD signal changes: Neural activation results in increased local blood delivery and hence reduced local deoxyhemoglobin concentrations, to which the BOLD signal is sensitive (Kwong et al., 1992). The cerebral hemodynamic response takes several seconds to develop and decay and therefore acts as an endogenous filter which smoothes and delays the signal. The specific shape of the response function is of importance to the design and analysis of fMRI experiments used to detect brief event-related responses (Rosen et al., 1998). Although there is evidence for significant variability in the shape of hemodynamic responses across subjects in physiological stimulation paradigms (Aguirre et al., 1998), there is only anecdotal information on the responses to epileptic activity in humans (Krakow et al., 1999c).

The purpose of the study presented here was to evaluate the capabilities of EEG-triggered fMRI in localising interictal EEG foci in a heterogeneous group of patients with refractory localisation-related epilepsy and frequent IED. The site of the fMRI activation was compared to the focus of previous interictal scalp EEG recordings, and, if available, invasive and ictal EEG recordings. All patients were studied at least twice on different occasions in order to investigate the reproducibility of the fMRI results. Furthermore, the temporal evolution (time course) of the hemodynamic response function to spikes was studied.

Patients

24 consecutive patients (14 male, 10 female, median age 27.5 years, range 16-63 years) were studied. All patients had a confirmed diagnosis of medically intractable

localisation-related epilepsy with frequent stereotyped spikes on previous routine 20-channel scalp EEG recordings (at least one spike per minute on average). In all patients repeat EEG studies revealed a consistent spiking pattern. Patients with generalised or multifocal spikes were excluded. All patients had structural MRI prior to the study. Fifteen patients had structural abnormalities, the remaining 9 patients were classified as having cryptogenic focal epilepsy. The most common structural abnormalities were malformations of cortical development (MCD) (n= 6), hippocampal sclerosis (n = 3), glioma (n = 2), and dysplastic neuroepithelial tumour (DNT) (n = 2). One patient had an anterior temporal lobe resection, and another had unilateral cerebral atrophy due to chronic encephalitis. All patients were receiving antiepileptic drug treatment at the time of the study.

Initially, all patients underwent between one to four fMRI experiments in order to identify possible areas of brain activation associated with their habitual spikes. In these experiments, the data acquisition is designed based on the assumption that the peak BOLD response occurs roughly 5.5 seconds following each event (spike), as has been observed in normal brain function (Aguirre et al., 1998). In four patients with positive fMRI activations, additional BOLD-signal time course experiments were performed mainly to assess the actual time to peak of the BOLD response and compare it with the assumed value.

EEG recording during fMRI experiments

Details about patient safety (Lemieux et al., 1997), EEG- (Allen et al., 1998) and image- (Krakow et al., 2000a) quality aspects of EEG recording inside the MR scanner are given in chapter 4. In summary, 12 standard gold disk electrodes were applied to scalp positions according to the 10/20 system (FP1/FP2, F7/F8, T3/T4, T5/T6, O1/O2, Fz and Pz) using collodium. These had 15 kOhm current limiting carbon resistors fitted

adjacent to each electrode (Lemieux et al., 1997). The electrodes were connected to a non-ferrous headbox (developed in-house) placed at the entrance to the bore of the magnet. The headbox was connected to a Neurolink Patient Module (Physiometrix, MA, USA) which digitises and transmits the EEG signal out of the scanner room via a fibre optic cable to the Neurolink Monitor Module which reconstructs the analogue EEG signals. These were then recorded using a digital EEG recording system (sample rate 200 Hz, bandwidth: 0.12-50 Hz). In addition, two precordial ECG channels (75 kOhm current limiting resistors were fitted to each ECG-electrode) were recorded to enable digital pulse artifact subtraction, which was employed in all experiments to improve EEG quality (Allen et al., 1998). EEG data was digitally remontaged and displayed to show bitemporal chains.

EEG-triggered fMRI

fMRI was performed on a 1.5 tesla Horizon EchoSpeed MR scanner (General Electric, Milwaukee, USA) using snapshot gradient-echo echo-planer imaging (EPI) (TE = 40 ms, 240 mm field of view, 64x64 matrix). The EEG was observed on-line (with a 1-second display delay due to the pulse artifact subtraction software) and 20 contiguous 5 mm slices were acquired in 4.5 seconds in an oblique axial orientation. Image acquisition was manually triggered with a delay of approximately 3.5 seconds after an IED was observed ("trigger spike") on EEG ("activation state"), or after at least 10 seconds of background activity without spikes ("control state"). The delay of approximately 3.5 seconds between the observation of the IED and the image acquisition was applied because the peak blood oxygenation level change detected by fMRI occurs approximately 4 to 7 seconds after the onset of the brain activity (Hennig et al., 1995, Rosen et al., 1998).

Images were acquired randomly and non-periodically with activation and control states

evenly distributed throughout the experiment. A minimum delay of 15 seconds between the image acquisitions was implemented to permit NMR spin equilibration (identical T1-weighting for each acquisition).

Due to scanner hardware limitations a maximum of 98 acquisitions could be obtained per experiment. Acquisitions started earlier than 3 or later then 4 seconds after a spike and acquisitions that followed equivocal activation or control states were excluded from the statistical analysis (<7% of acquisitions in all studies). The typical total scanning time was 60 to 90 minutes, depending the frequency of EEG events.

Images were processed and analysed using Statistical Parametric Mapping (SPM96) (Friston et al., 1995a). The data was processed in the same fashion as data acquired using the conventional block-design fMRI approach, with the assumption that all voxels in a given image were acquired simultaneously, except for the fact that the sequence of activation and control images was random. All volumes were realigned (rotation and translation) to the first volume for motion correction. A mean image was created using realigned volumes. All images were spatially normalised (Talairach and Tournoux, 1988, Friston et al., 1995b) to an echo-planar image template in the same stereotactic space as the Montreal Neurological Institute template (Evans et al., 1993). The images were smoothed using a Gaussian kernel of 6 mm full-width half maximum. The aims of this processing step are to condition the data to conform more to a Gaussian Random Field (on which theory SPM cluster statistics is predicated), increase the signal-to-noise ratio and minimise the effect of inter-subject anatomical differences. An adaptive high-pass filter was added to the confound partition of the design matrix to account for low-frequency drifts, and the global means were normalised by proportional scaling. Voxel time-series were temporally smoothed with a Gaussian filter. Specific effects were tested with appropriate contrasts of the parameter estimates for each condition (activation vs. control state), resulting in a t-statistic for each voxel. These t-statistics

were transformed to standardised z-scores and constitute a statistical parametric map (SPM{Z}). The results were displayed using a height threshold of $p = 0.001$ and an extent threshold of $p = 0.05$. The resulting SPM{Z} was saved as an image volume for comparison with other findings. The amplitude of each trigger spike (in the channel where it was highest) and the delay between spike and the onset of acquisition (indicated by the image acquisition artifacts on EEG) were measured retrospectively on the EEG recorded inside the scanner.

EEG-triggered fMRI time-course

Additional experiments to study the time course of the hemodynamic response after interictal spikes were performed in four patients (patients 3, 4, 10, 17, see *table 2*). The EEG recording system described above was used to identify spikes and control states on-line. MR imaging was performed on a 2 tesla Siemens Vision (Siemens, Erlangen, Germany). A burst of nine EPI acquisitions with 20 axial 2 mm slices was acquired starting 1.5 seconds after either a spike or during a control period (TE = 40 ms, 192 mm field of view, 64x64 matrix). The volume acquisition time was 2.0 seconds, and each burst covered nine time points (ti ; i =1,2...,9) over a period of 18 seconds. A minimum gap of 15 seconds was employed between bursts. Imaging data was processed using SPM99b as described above for spatial realignment, normalisation and smoothing. Statistical parametric maps corresponding to contrasts between homologous time points in the spike and control conditions (t1,s vs t1,c, t2,s vs t2,c, ..., t9,s vs t9,c) were derived. The amplitude of the BOLD signal change at the voxel with the maximum Z-score was then plotted as a function of time.

Assessment of localisation concordance

The localisation of the EEG spike focus (as assessed on standard referential and bipolar scalp EEG recorded outside the scanner), MRI lesion (if present) and fMRI activation, was assessed on a lobar basis. The localisations were categorised into either frontal, temporal, parietal, or occipital, also left, right or bilateral. These categories were used to determine concordance between EEG focus, MRI lesion, and fMRI activation for each patient. Concordance was defined as being localised to the same lobe, and non-concordance as being located on different lobes. If the EEG and MRI findings involved more than one lobe, the main lobe affected was considered.

Results

EEG and MRI findings

15 patients had a unilateral temporal spike focus on scalp EEG, 3 patients a frontal focus (two unilateral, one bilateral), 3 patients a unilateral parietal focus, and 3 patients a bilateral occipital focus. In all patients with structural lesions (n=15), the lesions were concordant with the EEG foci, i.e. located in the same lobe.

EEG-triggered fMRI

In all 44 fMRI experiments the EEG data was sufficient to detect activation and control states reliably throughout the study and to trigger fMRI acquisitions after these events. A typical example of an IED used to trigger an fMRI acquisition is given in *figure 12*, with and without applied pulse artifact subtraction (patient 2 of table 2). The fMRI data was not compromised by the concurrent EEG recording. In some patients, the scalp EEG electrodes caused small signal drop outs in the echo-planar images, affecting the scalp and skull signal. However, these artifacts did not intrude into the cortex.

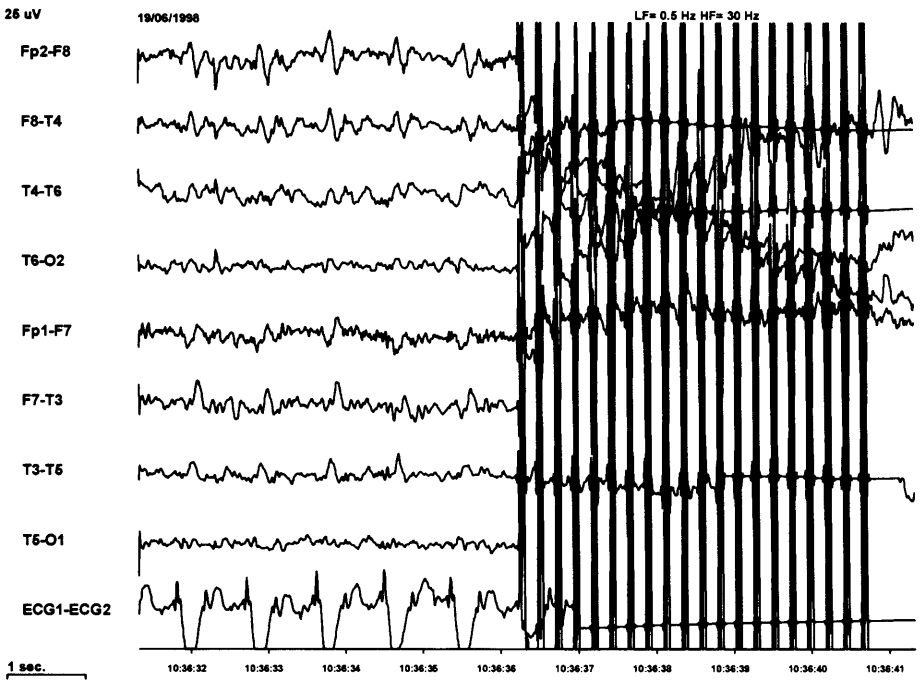

***Figure 12**: EEG recording inside the MR scanner (patient 2 of table2). The same EEG sequence with a low amplitude spike over the right hemisphere without (above) and with pulse artifact subtraction (below). The spike (indicated by an arrow) is clearly detectable only with applied pulse artifact subtraction. 3.5 seconds after the spike occurs the image acquisition artifact of a 20 slice EPI acquisition.*

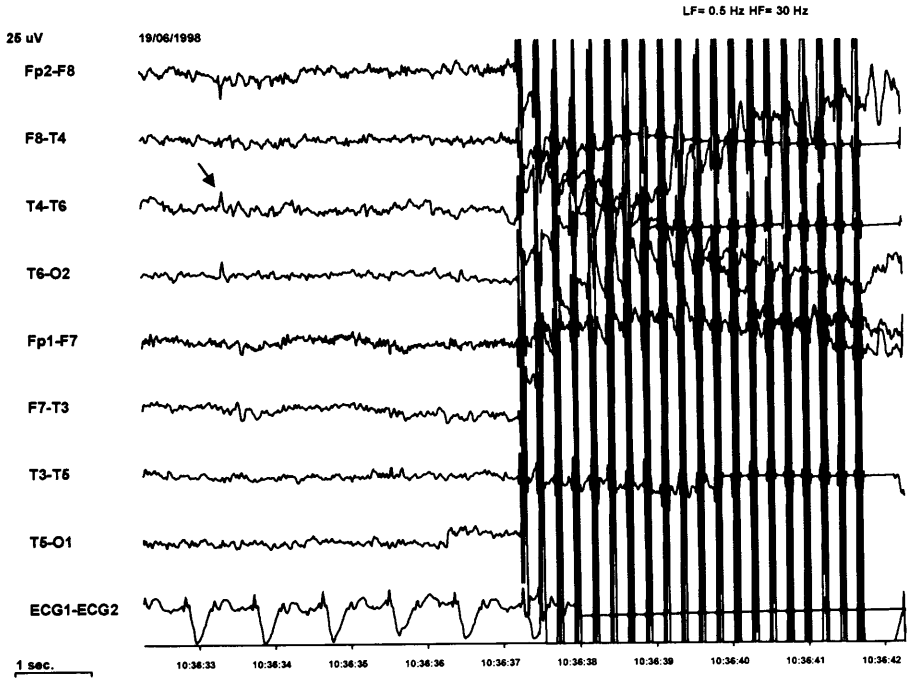

No clinical or electroencephalographic manifestations of ictal events occurred during the scanning procedure in any experiment. None of the patients reported discomfort due to the EEG recording. Between 12 to 50 fMRI trigger spikes were identified during scanning sessions that lasted between 35 and 95 minutes. The image acquisitions triggered after spikes and included in the statistical analysis were acquired 3.5 seconds (± 400ms) after the onset of the spike. The mean fMRI trigger spike amplitude was 116.8 μV (SD 43.9).

Of the 24 patients studied, 14 patients (58.3%) had a focal fMRI activation. In 12 patients (50.0%), the fMRI activation was concordant with the EEG focus and, where present, with the structural lesion. In all 7 fMRI positive patients with structural lesions (including MCD, post-operative glioma, and hippocampal sclerosis) the fMRI activation was within or overlapping the lesion. The mean cluster size of the activation was 720 voxels (SD 1631.0), the maximum Z-score being 4.9 (SD 1.2). There was a tendency for patients with a high mean spike amplitude to have larger and stronger fMRI activations. However, this tendency did not reach significance ($r = 0.51$; $p = 0.09$; Spearman rank correlation). The clinical details of the 12 patients with a concordant fMRI activation are summarised in *table 2*. *Figure 13* is an example of an SPM activation map. The activation of this patient is concordant with a right central spike focus on scalp EEG and the structural lesion, a large nodular heterotopia of the right central region. The fMRI activation is located within the central cleft of the heterotopia.

In two patients with an fMRI activation (8.3%), the activation was not concordant with the EEG focus. The first patient with left temporal spikes and confirmed left hippocampal sclerosis had a right temporal neocortical fMRI activation. The second patient with a left temporal EEG focus had two contradictory fMRI results: The first revealing a left temporal activation, which was replaced by a right parietal activation in

the second study. In all remaining fMRI positive patients with positive fMRI results in repeated experiments (n=8), the results were consistent.

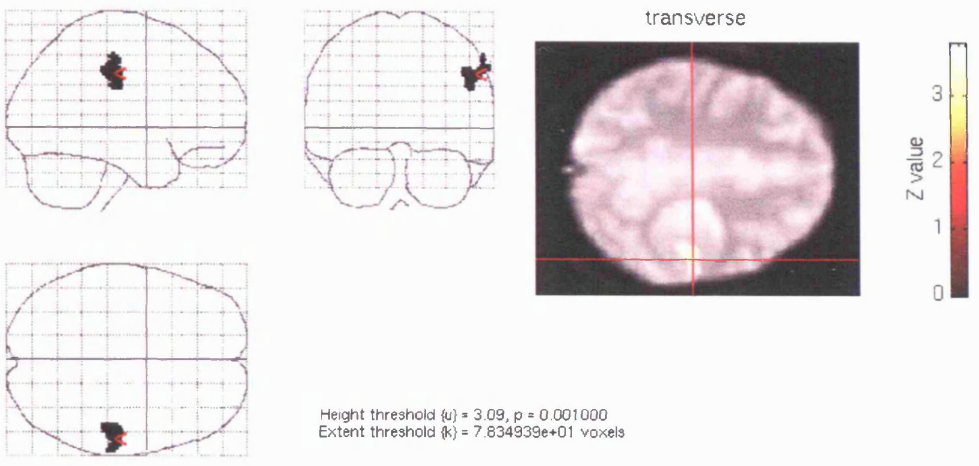

Figure 13: *fMRI result for patient 2 (table 2). The SPM BOLD-activation map shows an axial image with crosshair through the centre of the activation (overlaid in yellow), in the centre of the nodular heterotopia of the right hemisphere, adjacent to a cleft in the lateral part of the heterotopia. The image orientation follows the SPM convention for normalised images, in which the patient's right appears on the right.*

Ten of the 24 patients (41.7%) did not show a significant fMRI activation in any experiment. All 16 experiments with these patients failed to reveal a focal cortical activation even with a lowered significance threshold (from $p = 0.001$ to $p = 0.01$). Patients with positive fMRI activations had significantly higher spike amplitudes (136.0 μV (SD 43.0)) compared to those without (99.9 μV (SD 39.8)); ($p = 0.03$). There were no significant differences between the two groups for age, number of sampled spikes

per experiment, or delay from spike to start of acquisition. In both groups different underlying pathologies and patients with cryptogenic epilepsy were equally represented. However, three patients with MCDs or DNTs limited to a single temporal lobe gyrus had no fMRI activation, while all patients with larger or widespread MCDs had a positive result.

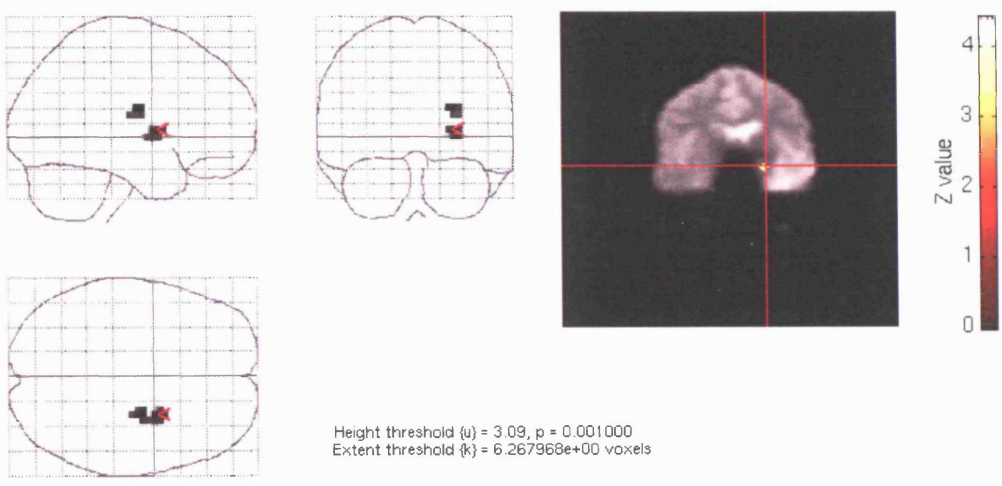

Figure 14: *FMRI result for patient 3 (table 2). The SPM BOLD-activation map shows an spike-associated activation of the left mesial temporal lobe (overlaid in yellow, not normalised).*

Table 2. *Summary of clinical data and fMRI results in the 12 patients with concordant fMRI and EEG results.*

Patient no.	Principal Pathology	EEG spike focus mean amplitude (μV SD)	FMRI activation cluster size (voxels) /Z-score
1	chronic encephalitis of left hemisphere	left temporal 184.2 (33.1)	left temporal 221/7.0
2	nodular heterotopia of right central region	right central 84.2 (15.4)	right central (in lesion) 166/3.8
3	hippocampal sclerosis	left temporal 168.1 (26.3)	left mesial temporal 57/4.0
4	low-grade astrocytoma of left middle frontal gyrus	left frontal 187.8 (26.3)	left precentral (in lesion) 44/4.4
10	cryptogenic	bilateral occipital left>right 127.2 (15.4)	bilateral occipital 340/5.2
11	cryptogenic	bilateral occipital 94.7 (38.7)	bilateral occipital 106/3.9
14	cryptogenic	right temporal 94.7 (38.6)	right temporal 55/4.1
15	MCD of left middle and inferior temporal gyrus	left temporal 82.2 (12.3)	left temporal (in lesion) 48/4.4
16	bilateral, mainly occipital subcortical heterotopia	bilateral occipital 193.3 (6.7)	bilateral occipital (in lesion) 5751/6.9
17	MCD of right hemisphere, max. posterior temporal and parietal	right temporal 102.1 (14.6)	right posterior temporal (in lesion) 217/4.9
20	cryptogenic	right temporal 95.8 (7.3)	right temporal 238/4.4
22	cryptogenic	left fronto-central 162.8 (32.0)	left fronto-temporo-parietal 1493/6.56

EEG-triggered fMRI BOLD time-course

In one of the four patients (patient 3, see *table 2*), fMRI image analysis failed due to gross movement artifact. In the remaining patients, a fMRI activation concordant with the initial experiment was identified and the maximally activated voxel was plotted against time. There was an initial percentage increase in the BOLD signal to a peak of 4.0 to 4.3 %, which was followed by signal decay. In two patients, the peak signal occurred between 1.5 and 5.5 seconds after the spike, and in one case the peak took place 5.5 to 7.5 seconds post spike. 10 seconds post spike a steady state was reached with no further signal change. There was no evidence for an undershoot after the initial signal increase.

Discussion

EEG-triggered EPI BOLD fMRI was found to be a practicable and robust method in the evaluation of epilepsy patients with frequent focal IED. In all experiments, a good quality EEG was obtained, spontaneous IED were detected on-line and EPI BOLD acquisitions were triggered after these events. The MR image quality was not significantly compromised by the EEG recording equipment.

Using EEG-triggered fMRI it was demonstrated that it is possible to identify brain areas involved in the generation of focal spikes in patients with localisation-related epilepsy. In a group of 24 consecutive patients with frequent interictal spikes, 58% of patients had a focal fMRI activation, usually concordant with the interictal scalp EEG spike focus. Additional electrocorticography was performed in one patient (no. 1) and confirmed the co-localisation between interictal epileptiform activity and fMRI activation. In all patients with fMRI activation and previous lateralising ictal EEG recordings (patients 1, 3, 4; *table 2*), the findings were concordant. MRI was useful in identifying the spike focus in patients both with underlying structural lesions and cryptogenic epilepsy. It

provided an opportunity to study the relationship between different structural abnormalities and the generation of epileptic activity. In all patients with structural lesions showing a fMRI activation, the activation was within or overlapping the lesion. Four of these patients had MCD. This adds to the evidence for grey matter having intrinsic epileptogenic properties within MCD (Palmini et al., 1995, Hannan et al., 1999). Studies with larger groups of patients are warranted to determine the spatial relation between different underlying pathologies and the generators of epileptic activity. This would be of particular interest in patients with vascular malformations and brain tumours, which were not present in our study. The epileptogenicity of these structural abnormalities is not well understood but thought to be due to effects on the adjacent cortex rather than being an intrinsic property (Awad et al., 1991, Haglaud et al., 1992, Pilcher et al., 1993). One patient (no. 4) with a low-grade glioma and an associated fMRI activation was studied only after surgery and radiotherapy and so failed to help with the above objective.

One patient with confirmed unilateral hippocampus sclerosis showed an fMRI activation of the mesial temporal lobe (*figure 14*). The activation of deep temporal structures is remarkable as it is correlated with epileptiform discharges recorded with scalp EEG. This requires propagation of the epileptiform activity to a larger superficial cortical area. An activation solely in deep structures might suggest that fMRI more readily identified the site of primary spike generation. The possibility that the site of the primary generator of epileptic activity could be associated with different metabolic and hemodynamic changes compared to brain areas involved in the propagation of this activity requires further studies given its potential clinical relevance.

The large inter-individual variability in the extent (i.e. the number of significantly activated voxels, see *table 2*) of the fMRI activations rendered a description of a quantitative relationship with structural abnormality difficult. Although a consistent

threshold was used in order to allow for inter-subject comparison and to study the effects of spike amplitude on activation, in some patients only a circumscribed cortical area was activated (< 50 voxels in patients 2, 3, 15; *figure 15*), whilst in others the activation covered more than one cerebral lobe (e.g. both occipital lobes in patient 16).

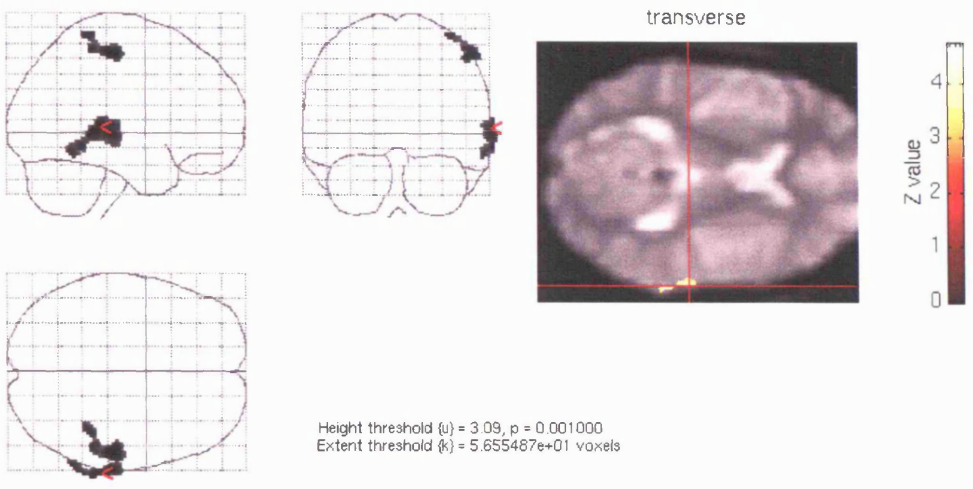

Figure 15: *fMRI result for patient 17 (table 2). The SPM BOLD-activation map shows an spike-associated activation of the of the right posterior temporal lobe and the right parietal lobe (normalised image, the right side of the brain appears on the right). The activated area shows co-localisation with a malformation of cortical development in this area.*

The reason for this variability remains unclear. No significant correlation was found between EEG spike amplitude or frequency and the activation cluster size. There are two likely explanations for this lack of correlation. Firstly, amplitudes of scalp EEG potentials do not necessarily reflect the extent of cortex involved in generating the events. For example, a small superficial source might generate a higher amplitude spike

than a larger deep focus. Secondly, only 12 EEG channels were recorded inside the MR scanner. The limited number of channels provide only restricted information for quantification of spike related electric fields.

Although the 10 patients with a negative fMRI result had significantly lower mean spike amplitudes, it was not possible to reliably predict a significant fMRI activation based on the EEG data. The physiological explanation of a negative fMRI result is most likely that a non-significant difference in the blood oxygenation exists between activation and control states. This might be due to there being only a modest cerebral hyperperfusion following a spike, or due to an absence of a true control state, e.g. such as ongoing epileptic activity not detected on scalp EEG. In both cases the relative signal change within the spike generator may not achieve significance.

The high percentage of negative results hinders the potential wider clinical application of EEG-correlated fMRI. To increase the clinical usefulness of this tool, further technical developments are necessary. Firstly, the use of higher strength magnets will increase further the signal to noise ratio and hence fMRI sensitivity. Multi-channel EEG has already been recorded in a 4 tesla MR scanner on humans (Ives et al., 1997) and in a 7 tesla MR scanner in animals (Sijbers et al., 1999). An improved signal to noise ratio may not only increase the proportion of fMRI-positive experiments, but may also reduce the number of sampled spikes necessary for a significant fMRI activation, thus rendering this method applicable to patients with less frequent interictal spikes.

Secondly, the data acquisition for EEG-correlated fMRI could be improved. As epileptiform spikes occur unpredictably, the fMRI acquisition sequences are run at variable intervals, thus introducing varying longitudinal T1-relaxation effects (Josephs et al., 1997). As spike-triggered fMRI relies on the reproducibility of the T1 effect, a temporal gap between acquisitions has to be introduced to allow full longitudinal relaxation (15 seconds in our experiments). In contrast, continuous image acquisition

with a fixed repeat time (TR) would allow more data to be collected in a shorter time as well as allowing more sophisticated modelling of the hemodynamic response. Continuous image acquisition has been limited by artifacts, which completely obscure the EEG once acquisition has commenced. Using recently proposed methods to remove the image acquisition artifact from the EEG (Sijbers et al., 1999, Allen et al., 2000), continuous acquisition is likely to improve the data-collection efficacy and sensitivity of this method (see also chapter 7.2). This will be of particular importance in BOLD signal time course studies. In the time course experiments performed in this study, the EEG was blinded to further events during the image acquisition time, for a period of 18 seconds following each spike. This method therefore depends on the assumption of an equal probability of spikes during all acquisitions. Despite this limitation, a clear temporal pattern for the BOLD hemodynamic response was established with a peak between 1.5 to 7.5 seconds post spike. A more precise description of the time-course was prevented by the restricted temporal resolution (2 seconds) of the scanning protocol. However, the temporal characteristics of this pathological (spike related) BOLD response resembled that of physiological brain activation. The time-to-peak of the BOLD response after stimulation of primary sensory or motor cortex is reported to be approximately five seconds with a significant inter-individual variability ranging from under three to over six seconds. For event-related fMRI designs, accurate estimation of the hemodynamic response function is crucial, as failure to accurately specify its shape results in loss of sensitivity. Given the inter-individual variability apparent in the data, and the proportion of subjects in which an activation was obtained, the use of subject-specific hemodynamic response functions could be important in optimising fMRI data analysis.

In contrast to EEG-derived localisation methods, EEG-triggered fMRI uses a direct biological measurement as opposed to relying on mathematical modelling techniques.

At present no explicit biological model exists for the spatio-temporal relationship between the generators of IED and the BOLD response. During the past decade, several techniques for scalp EEG source localisation have been proposed and applied to clinical and experimental data (Ebersole, 1998, Ebersole and Wade, 1991, Nakasato et al., 1994, Roth et al., 1994, Krings et al., 1998). Previously, intracranial EEG recordings have been used to assess the localisation accuracy of EEG source models (Nakasato et al., 1994, Roth et al., 1994). EEG-correlated fMRI could be used as a non-invasive alternative for validating EEG source models. Further investigations, using co-registration of functional and anatomical MR images may provide quantitative measures of the spatial relationship between the localisation obtained by fMRI and EEG source analysis. In some cases with equivocal information on localisation, a combination of EEG-correlated fMRI and EEG source analysis may provide complementary information. In patients with widespread fMRI activation for example, the EEG data can provide additional temporal information thereby helping to distinguish primary sources from areas of propagation (Seeck et al., 1998).

In conclusion, EEG-correlated fMRI can directly identify the generators of interictal epileptiform activity with high spatial resolution in select patients with frequent spikes. This is currently not possible with any other non-invasive means. Improvements in fMRI sensitivity, and further validation of the results are necessary before it can be routinely applied effectively to the presurgical evaluation of patients with epilepsy, but it may become a useful tool – including the possibility of generating additional hypotheses prior to test in patients requiring intracranial studies due to its high spatial resolution.

5.2. Functional MRI activation of individual interictal epileptiform discharges

In event-related fMRI events are usually averaged to improve the signal-to-noise ratio of the data. In all studies using EEG-triggered fMRI in patients with epilepsy reported up to now, between 17 and 49 spikes were averaged in experiments showing positive results (Warach et al., 1996, Seeck et al., 1998, Krakow et al., 2001). These figures represent the maximum number of spikes which could be recorded in individual patients during a tolerable scanning time. The number of spikes actually necessary to produce a significant fMRI activation has not yet been systematically investigated.

Single event-related fMRI of cognitive tasks were previously reported (Richter et al., 1997), but studies of individual spikes would be of particular interest as they allow the direct linkage of an individual electromagnetic EEG event with the associated hemodynamic-based fMRI activation. In this section a study is described which investigated whether individual spikes are associated with BOLD signal changes detectable with fMRI performed on a clinical 1.5 tesla MRI scanner.

Patient

The patient was a 47-year-old female with a seven-year history of epilepsy due to chronic encephalitis of the left hemisphere (patient 1 of *table 2*). She had simple partial seizures with motor symptoms mainly of the right side of her face and secondarily generalised tonic-clonic seizures. Neurological findings included mild right-sided facial weakness with intermittent myoclonic jerks and expressive dysphasia. Scalp EEG showed a widespread left hemisphere abnormality with a background rhythm dominated by theta activity and frequent spike and slow wave discharges over the left temporal region, maximum at electrode positions F7, T3 and T5 with equipotential voltages. Previous electrocorticography (ECoG) revealed epileptiform spikes distributed over the

pars opercularis of the superior temporal gyrus and the adjacent perisylvian regions. The structural MRI was normal.

EEG-triggered fMRI

The experimental set-up of the EEG/fMRI experiment is described in section 5.1. Images were processed and analysed using Statistical Parametric Mapping (SPM99b) (Friston et al., 1995). All volumes were realigned and all images were smoothed (full-width half maximum 6 mm). The two conditions were compared with a t-statistic (which was transformed to standardised z-scores) on a voxel-by-voxel basis. The data was analysed twice: firstly, all active states were compared to all control states; and secondly, each active state was compared individually to all control states. The results were displayed with the significance threshold set to $p < 0.001$ and the extent threshold to $p < 0.5$. The results of the second analysis were classified into two categories: (1) maximum activation within or adjacent to the activated area of analysis one; and (2) maximum activation outside activated area of analysis one, or no focal activation. The cluster size and the Z-score of the maximum activation were identified. In the EEG data, the channel with the maximum spike-amplitude was identified and the amplitude and duration of spikes were measured. The spatial extent of the spikes (number of EEG channels in which the spike was identified) and the delay between each spike and the start of the image acquisition (indicated by an EEG artifact, see *figure 2* and *figure 9*) was also measured. Mean values of the measured parameters were calculated and a t-test was performed to compare spikes associated and not associated with fMRI activations.

Results

The EEG quality inside the MRI scanner was sufficient to detect active and control states reliably throughout the study. The mean spike amplitude, occurring consistently at electrodes F7 or T3, was 159 μV (SD 41). 43 active and 46 control states were sampled during a scanning session of 55 minutes and included in the statistical analysis. The activation map derived from averaged active and control states is shown in *figure 16*. The activation covered a large area including the superior left temporal lobe and adjacent perisylvian regions. The Z-score of this activation was 7.1, and the cluster size was 2765 voxels. The activation was concordant with the spiking cortex identified with previous ECoG.

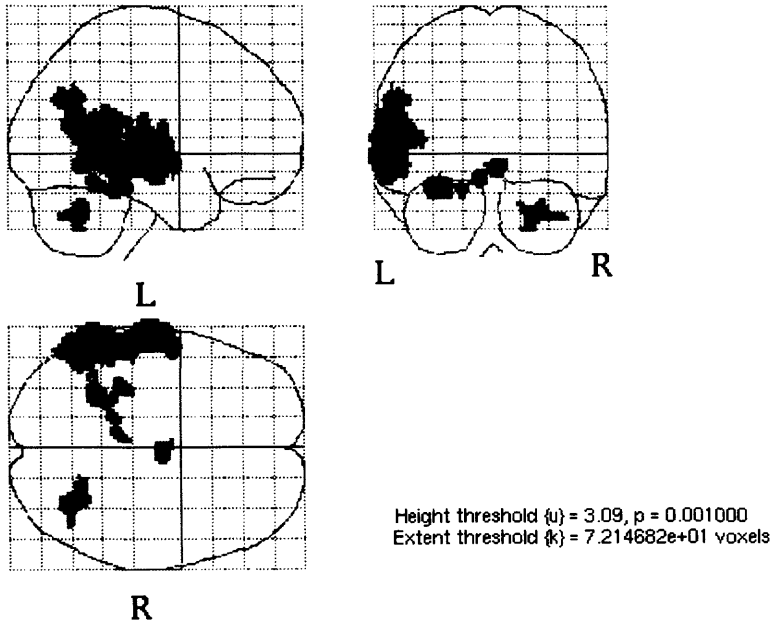

Figure 16: *SPM activation map of 43 averaged spikes showing an extended activation of the left superior temporal lobe and adjacent perisylvian areas (patient 1, table2).*

Individual analysis of the 43 spikes revealed that 15 (34.9%) of spikes were associated with a significant fMRI activation showing co-localisation with the result of the averaged data *(figure 17)*. The mean cluster size was 46.9 voxels (SD 38.7) and the

mean Z-score was 4.0 (SD 0.45). The remaining 28 spikes were associated with scattered activation without a focal cortical maximum (n = 16, 37.2%), or showed no activation above the significance threshold (n = 12, 27.9%). Spikes associated with fMRI activation had a tendency towards higher amplitude (mean amplitude 170.8 μV; SD 55.3) compared to spikes without activation (153.8 μV; SD 45.0), but the difference was not significant (p = 0.09). There was no significant difference in the duration of the spikes, the number of EEG channels showing the spike, and the delay between spike and image acquisition between the spikes with and without fMRI activation.

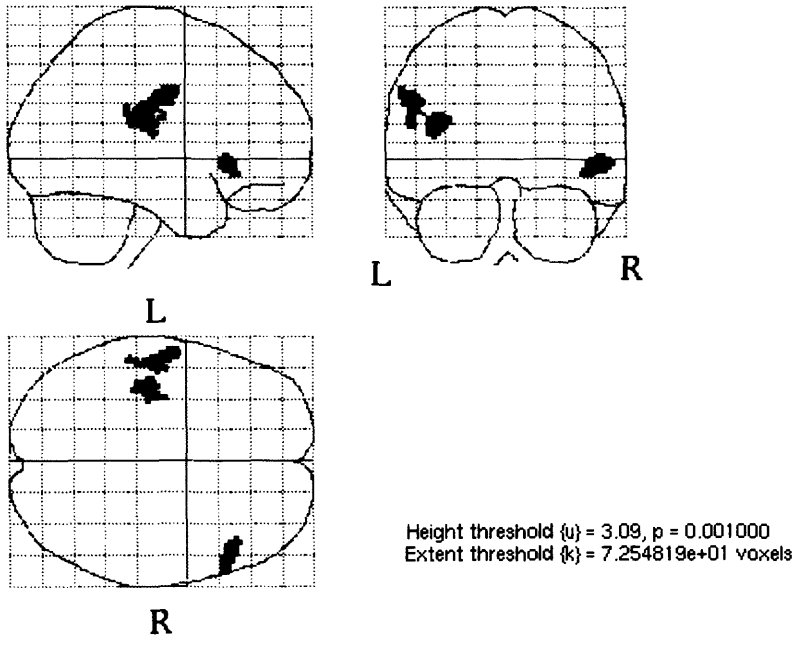

Figure 17: *SPM activation map based on an individual spike. The area of the maximum activation overlaps the activation of the averaged spikes. Most of the activation maps of individual spikes show additional smaller activations, in this example in the right frontal cortex. These activations had variable locations between the different spikes.*

Discussion

In this study it could be shown that single spikes as brief as 100 ms can be associated with focal changes of cerebral hemodynamics detectable with BOLD fMRI. fMRI of single events provides information complementary to averaged data. Averaging across trials allows for central tendencies in the hemodynamic response to be observed, whereas examination of individual hemodynamic responses provides information about the unique aspects of an isolated event. In spike-triggered fMRI the latter is of particular interest for several reasons. It allows study of the relation between the morphology of individual EEG events and the hemodynamic response provided by fMRI. Thus, the question whether characteristics like amplitude or waveform of individual spikes influence the fMRI activation can be addressed. In this study there was no significant correlation between spike amplitude and fMRI response. This might be due to the limitation of recording only 12 EEG channels, as a small number of channels provides only restricted information for the quantification of electrical fields resulting from spike activity.

A comparison between characteristics of EEG events and fMRI activation is also complicated by the high level of noise in non-sampled fMRI activation maps. In these images it is therefore difficult to distinguish between the variation of the spike-related activation and the effect of random noise.

Although it was shown that fMRI activations of individual spikes could be identified in this patient, it has to be emphasised that in previous studies using spike-triggered fMRI some patients did not show fMRI activations despite averaging as many as 50 spikes (Krakow et al., 2001c). Hence, fMRI of single spikes seems to be only possible in selected patients without further improvements of the image signal-to-noise ratio, e.g. by using a higher field strength MR scanner. The reason for the variability of fMRI sensitivity in different patients and between different spikes in an individual patient

remains unclear. Further prospective studies are necessary to reveal the relation of IED and fMRI activation and to predict which forms of epileptic activity are likely to be associated with fMRI activation.

In conclusion, EEG-triggered fMRI can localise neuronal activity associated with individual IED in selected patients with epilepsy.

Chapter 6

EEG-triggered fMRI in epilepsy and its combination with other methods

6.1. Co-registration of fMRI and EEG source analysis

During the past decade, several techniques for scalp EEG source localisation have been proposed and applied to clinical and experimental data (Ebersole, 1998). Through such models, an inverse solution can be calculated using the shape and magnitude of the scalp-recorded voltage fields, the three-dimensional location of the electrode arrays, and the conductivities of the brain, skull and scalp compartments. As is well known, there is no unique solution to the electromagnetic inverse problem: different source distributions can be found that result in the same field distribution. This fundamental difficulty can be addressed by imposing suitable constraints on the solution. For example, physiological and anatomical considerations have lead to the single (or multiple) point dipole model of generators of IED. In such circumstances, a unique solution can be found (Cohen et al., 1990). One of the main factors presently limiting the value of EEG source modelling is the question of the validity of such assumptions.

In contrast to EEG source modelling, BOLD EEG-correlated fMRI consists of a 3D measurement matrix with a spatial resolution of the order a few millimetres. However, the spatio-temporal relationship between the underlying neural activity and the resulting vascular changes remains to be elucidated (Kwong et al., 1992). Recent experiments with normal brain function in animal models have shown partial concordance between invasive electrophysiological measurements and fMRI activation maps (Disbrow et al., 2000). In epilepsy, a number of studies have already compared EEG source modelling with other functional and structural imaging results, as well as clinical data and some have now shown that source analysis can localise epileptic foci in a clinical setting

(Ebersole and Wade, 1991, Nakasato et al., 1994, Roth et al., 1997, Krings et al., 1998). However, the comparison of different generator models is still needed to establish a standard for wider clinical application. The comparison of scalp and invasive electrophysiological data acquired simultaneously has been extremely valuable in assessing the potential practical limitations of source localisation based on dipole modelling of scalp EEG, particularly for deep temporal sources (Alarcon et al., 1994, Merlet et al., 1998, Merlet and Gotman, 1999).

The combination of EEG and fMRI data has already been proposed as a way of improving the temporal resolution of fMRI (Liu et al., 1998, Seeck et al., 1998). For example, in patients with widespread fMRI activation, the EEG data may provide additional temporal information thereby helping to distinguish primary sources from areas of propagation.

The purpose of the study presented here was to take a step back from this idea and compare quantitatively spike-triggered fMRI results with EEG source modelling solutions obtained independently in a group of patients with frequent, stereotyped, focal IED and in whom spike-triggered fMRI revealed a BOLD activation consistent with clinical findings (Krakow et al., 1999b). Moving point dipoles modelling and spatio-temporal source modelling were used, chosen mainly for their relative simplicity and potential applicability to a wide range of data, reflecting the range of etiologies in the patient group. Patient-specific conduction models were derived from structural images. Automatic methods for the registration of the structural and functional images were used for visualisation of the combined data and distance measurements (Lemieux et al., 2001b).

Patients

Six patients (3 males, median age: 26 years, range: 22-48 years) were studied. These patients represented a subgroup of the patients described in section 5.1. Clinical summaries and EEG/fMRI findings are shown in *table 2*. Patients 1, 2 , 3, 10, 15, and 17 of the table were included in this study. All patients were subjected to an additional anatomical volumetric MRI scan, with the following parameters devised to obtain high-resolution and full coverage of the head: T1-weighted, fast, inversion recovery-prepared SPGR (TI/TR/TE: 450/17.4/4.2 ms, flip angle: 20°), 24×18 cm (or 28×21 cm) FOV, 256×192 matrix, 124 1.5 mm (or 1.8 mm) thick slices.

EEG-triggered fMRI

The intra-MR EEG-recording was performed as described in section 5.1., fMRI was carried out on a 1.5 tesla Horizon EchoSpeed MR scanner (General Electric, Milwaukee, USA) using snapshot gradient-echo echo-planer imaging (EPI) (TE = 40 ms, 240 mm field of view, 64x64 matrix, phase encode direction: A/P) as described in the same section.

EEG source analysis

64-channel EEG (sample rate: 200 Hz) was recorded in a routine setting (outside the scanner) using the Neuroscan QuickCap (Neuroscan, Sterling, Virginia, USA). EEG channels of poor quality were discarded (maximum: 5 per study); in some cases a notch filter was applied to remove interference. For each subject, between five and 20 epochs containing typical spikes were extracted from the recordings. Typical spikes were defined as stereotyped events similar to the events used to trigger the activation images in the EEG-fMRI experiment. Using the CURRY software (version 3.0, Neuroscan Labs, Sterling, VA, USA) the epochs were concatenated and the spikes were detected

using template matching based on the choice a representative segment, and cross-correlation and amplitude thresholds. Detected events were checked visually prior to averaging.

Source analysis was performed for the averaged spikes using CURRY and using a common average reference. A realistically-shaped boundary-element conduction model (BEM) was derived from the volumetric scan by automatic segmentation (Wagner et al., 1995; Fuchs et al., 1999). EEG electrode positions in relation to the scan and BEM were calculated based on the 10-20 system and four anatomical point landmarks identified on the skin as visualised on 3D rendering of the volumetric scan: nasion, inion and the two preauricular points (Wagner et al., 1996).

A signal-to-noise ratio normalisation was performed, followed by a principal components analysis to obtain the dominant spatio-temporal field patterns allowing us to determine the probable number of generators needed to model the data (Fuchs *et al.*, 1999). This was the number of components with a loading value, expressed in terms of SNR, greater than unity. Two different generator models were then used for source localisation: (1) multiple unconstrained moving dipoles model (MDM); (2) spatio-temporal source modelling (STSM) with three fixed point dipoles, following (Merlet and Gotman, 1999). The number of moving dipoles used was set initially to the PCA-derived value, and reduced to the smallest number for which the explained variance (EV) was greater than 90% when possible. Sources were derived for the negative (t_1) and positive (t_2) peaks of the averaged spikes. These were identified as the two peak values in the mean global field power, which is the mean square amplitude over all channels.

Assessment of agreement between dipole and BOLD localisation

The comparison of the 64-channel EEG source analysis solutions and BOLD activation(s) was performed as follows: the mean EPI fMRI volume obtained after realignment and spatial normalisation was co-registered with the subject's T1 volume using the coregistration module in SPM99, which consists of a 9-parameter (3 translation, 3 rotation, 3 scaling), rigid-body registration (Ashburner and Friston, 1997; Ashburner et al., 1997). In one case, this process failed to give a satisfactory solution (the edges of the brain were mis-registered by approximately 1 cm) and another, semi-automated, procedure was used successfully (Lemieux, 2000). The resulting transformation was then applied to the SPM{Z} volume. The resulting realigned BOLD map was then merged (this is purely a display operation) with the T1 volume using CURRY's image fusion tool. Following this, the BOLD, EEG and structural data were in the same space and distance measurements could be made. The distance between the structural abnormality(ies) (in patients 1, 2, 3, 15, and 17), BOLD and dipole(s) could then be measured by selecting a dipole from the list of active dipoles and mouse-clicking at the desired location in the fused BOLD-T1 image, giving the Cartesian distance between the dipole (centre of displayed arrow) and selected location in cm. The distance between the dipole with the largest amplitude and the centre of the nearest BOLD activation was used as the measure of agreement, *d*. In cases of multiple activations, the distance between each activation and the nearest dipole was measured and the results averaged. In one case (patient 1) the BOLD activation was large and a local maximum was used.

Results

For patients 1, 2, 3, 15, and 17, which all have an abnormality visible on structural (T1-weighted) MRI, the BOLD activation is entirely contained within the abnormality,

except for the two following cases: Patient 1, where the BOLD and abnormality overlap by approximately 80%, and there was slight, but noticeable mis-registration, resulting in the margin of the BOLD activation outside the brain (see *figure 18*); and patient 15, where the smallest edge-to-edge distance is 1.4 cm and the abnormality centre to BOLD peak distance is 1.7 cm.

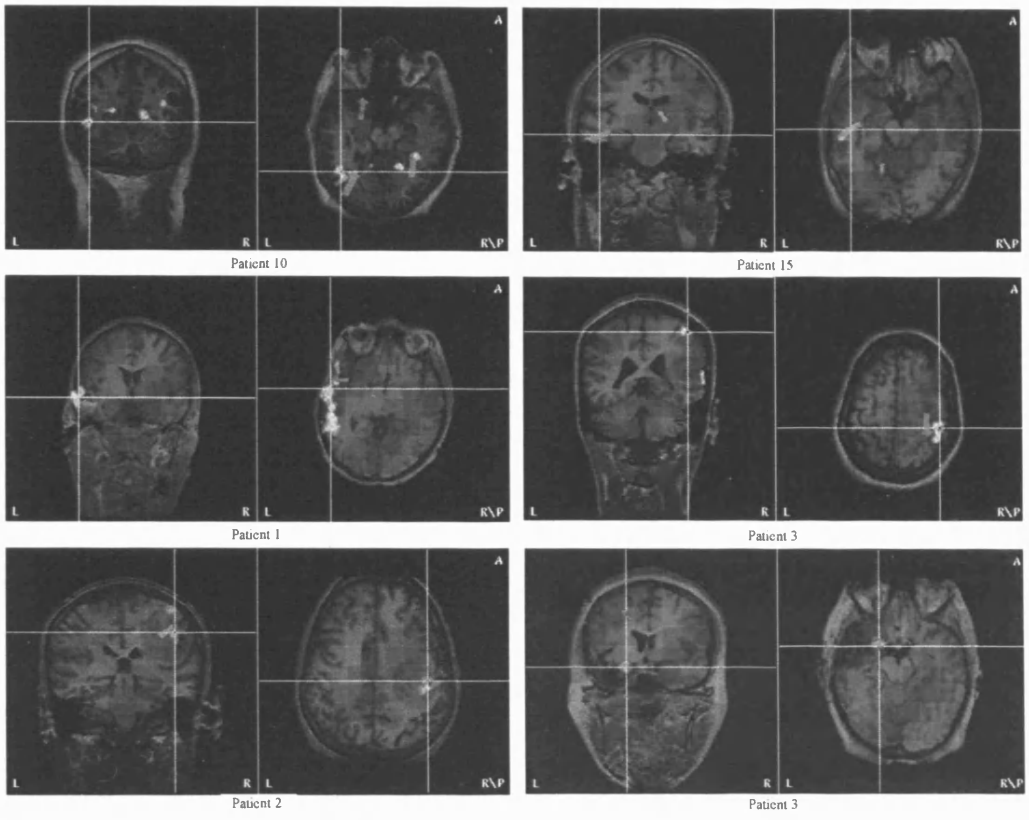

Figure 18: *Illustration of the results of multiple unconstrained moving dipoles model (MDM) at* t_2 *and registered BOLD localisations superimposed on T1-weighted anatomical scans for all patients. The dipoles are shown in light blue and the BOLD activations using the hot metal colour scheme. The cross-hair indicates the peak of the BOLD activation or one of the BOLD activations. Patients 1, 2, 3, and 15 each have a single activation. In patient 1, the cross-hair indicates the point chosen for the measurement, at a local BOLD maximum. Patient 10 has three activations, in the right*

and left occipital regions. Patient 5 has one activation in the right temporal and one in the right parietal region.

The number of moving dipoles used varies between 1 and 3. In all cases, the MDM explains at least the same amount of variance as the STSM. For t_1 EV is greater than 90% in 5/6 cases for MDM and in 3/6 cases for STSM; for t_2, EV is greater than 90% in all cases for MDM and 5/6 cases for STSM.

The results of the comparison between the MDM and BOLD findings are summarised in *table 3* and illustrated in *figure 18.* In all cases, at least one of the moving dipoles is located in the same lobe as the BOLD activation. In the case of patient 10, where two activations are located in different lobes, there is a dipole located in the same lobe as each activation. In the case of patient 1, it is important to note that the BOLD activation is the largest found in the study and that the EEG field is relatively complex, see *figures 18 and 19*. Furthermore, in the case of patient 3, the BOLD activation is located in the left mesial-temporal region. In terms of distance between dipole and structural abnormality, these do not differ from the dipole-to-BOLD values. The results for STSM are consistently inferior to the MDM results, with a mean distance of 4.2 cm.

Discussion

This section is based on the first report of the direct comparison of independently obtained EEG source modelling and spike-triggered fMRI findings (Lemieux et al., 2001b). Although more sophisticated source models are currently available, e.g. based on current density distributions, in this report dipole-based models were evaluated because they are the simplest available models and because it has been previously shown that they can be useful in analysing EEG activity associated with a wide range of generators. For example, single moving dipoles were used to model the generators of

IED associated with focal brain lesions successfully (Krings et al., 1998), while spatio-temporal source models have proven useful in the analysis of temporal lobe spikes (Merlet et al., 1998; Merlet and Gotman, 1999).

Table 3. *Summary of source analysis and BOLD comparison findings*

Patient no	**N**	**t_1**		**t_2**	
		EV (%)	***d* (cm)**	**EV (%)**	***d* (cm)**
1	2	75	-	92	1.7
2	1	95	2.1	95	1.3
3	1	94	5.4	94	5.1
10	3	96	3.3 [3.3]	98	3.2 [4.1, 4.3]
15	3	92	3.7	92	1.0
17	2	95	3.1 [3.3]	98	1.0 [3.3]

Table 3: N *is the number of dipoles used.* d *is the distance between BOLD activation and the nearest dipole; in cases with multiple BOLD activations, the mean distance between each activation and the nearest dipole is given in parentheses.* t1 *are the negative and* t2 *the positive peaks of the averaged spikes.*

It was found that the moving dipoles model tends to fit the EEG data better than the spatio-temporal model. This is not surprising in light of the model's relative lack of constraints. On the other hand, this model is usually considered the least realistic, since it is difficult to reconcile it with current physiological knowledge on the generation of EEG events. It was found that the number of dipoles necessary to fit the data satisfactorily to range between 1 and 3.

The distance for t_2 was generally smaller than for t_1, apart from a single case. The dipole

or one of the dipoles was located in the same anatomical region as (or overlap) at least one of the BOLD activations, with a mean separation of 3.5 cm for t_1 and 2.2 cm for t_2. The significance of this difference cannot be ascertained in such a small sample, but may nonetheless reflect a combination of the differences in the physiological processes that are imaged by the two techniques and propagation effects (see below).

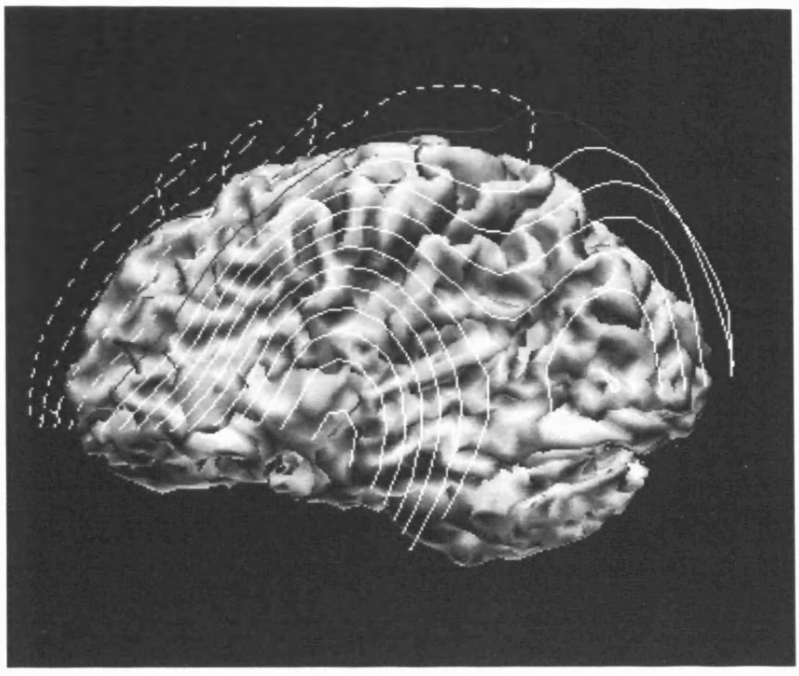

Figure 19: *Potential distribution for averaged spikes from patient 1 at* t_2. *It shows a complex pattern over the left temporal/parietal region. Soils lines represent positive values and dashed lines represent negative values; 20 μV/increment; Reference, common average.*

The mean BOLD to dipole model distance for patients 1, 2, 10, 15, and 17 is 1.6 cm. In these cases, the generator or generators appear to be relatively superficial. The anatomical separation of the dipole model and the BOLD signal change in patient 3 most likely reflects the effects of propagation. There is an increasing body of evidence to suggest that scalp detected spikes are rarely associated with deep brain activity alone

but reflect time-locked propagation with secondary activation of the superficial cortex (Alarcon et al., 1994; Merlet and Gotman, 1999). It is well established that a major pathway for spike propagation from the hippocampus is through the uncinate fasciculus to the frontal cortex (Kendrick and Gibbs, 1958) which could well account for the deep hippocampal BOLD activation time locked to the scalp detected ipsilateral frontal spiking and associated dipole model.

In contrast to EEG-derived localisation methods, which rely on mathematical modelling techniques, EEG-triggered fMRI uses a direct biological measurement. At present no explicit biological model exists for the spatio-temporal relationship between the generators of IED and the BOLD response. It was already remarked that source models derived from scalp EEG and BOLD changes would not always to be expected to agree based on biological considerations. It was also noted that the mean BOLD-dipole separation is larger than the 1.1 cm mean separation between scalp EEG-derived point dipoles and the maximal potential measured using depth electrodes (data also acquired on two separate occasions) measured by Merlet and Gotman (1999), though the significance of this difference is difficult to assess at this stage. No similar intra-cerebral data was available in our patient group for comparison.

In summary, the potential sources of discrepancy between dipole and BOLD localisation are as follows from the fundamental to the purely methodological: (1) The different neurophysiological bases of the two measurement methods, and in particular the crucial issue of neurovascular coupling. Essentially, EEG reflects synchronised neuronal activity while fMRI reflects changes in local cerebral blood flow, oxygen consumption and blood volume associated with changes in neural activity. The exact nature of this association in the realm of normal brain function remains the topic of much investigation, and has been scarcely touched in pathological brain function. (2) Issues related to the BOLD data acquisition, namely: local vascular architecture on

BOLD fMRI (Disbrow et al., 2000); effect of scanner field strength on the BOLD measurement, which restricts sensitivity mainly to large vessels at 1.5T. (3) Noise: Physiological, whereby EEG and fMRI will pick up brain activity not related to the pathology; Instrumental, related to both EEG and fMRI acquisitions. (4) Differences in brain or disease state between the two experiments due to sleep-wake state, drug levels, seizure history, that may not have a significant effect on individual spike morphology but nonetheless introduce a degree of variability in the spatial distribution of epileptogenicity. (5) Source modelling limitations: Although a conduction model of the head based on each individual subject's MRI scan was used, the accurate estimation of the skull thickness is difficult based on the imaging data used. Multiple, spatially distributed sources can be falsely demonstrated as a single dipole by a source analysis algorithm. (6) EEG-triggered fMRI limitations: the restricted temporal resolution can lead to false localisation by identifying brain areas activated by propagation effects. (7) Uncertainty in electrode position and registration error due to image distortion: previous experience indicates that model-based electrode localisation uncertainty is of the order of 5 mm; for our EPI sequence, a geometric distortion of the order of one pixel (3.75 mm) can be expected in the phase-encode (A/P) direction (Jezzard and Balaban, 1995). In the case of patient 1 (see *figure 18*), while some of the signal may arise from large, superficial vessels there may be an effect of mis-registration. Although effective distortion correction and co-registration methods have been proposed for EPI functional images they rely on the acquisition of special data and require special software, and thus have not yet been applied widely (Jezzard and Balaban, 1995; Studholme et al., 2000). Nonetheless this is an important issue, which may also contribute to a systematic bias across subjects, and has to be addressed in future work. The relative contributions of the above factors to the non-concordance seen between fMRI activations and EEG foci observed are only speculative. Furthermore, factors (1) and (2) are more likely than

others to contribute to a systematic bias (i.e. separation between BOLD and dipole localisation greater than the measurement uncertainty) than an increase in variance. In particular, evidence from combined BOLD and invasive EEG measurements indicates that the combination of some of the more fundamental factors listed above contribute to only a partial spatial overlap of the electrophysiological and BOLD maps associated with normal brain function (Disbrow et al., 2000). Within the limitations of source modelling based on scalp measurements, the results are consistent with the findings that electrical generators are in close proximity or overlap the BOLD activation. This may reflect a commonality of the neurovascular coupling between normal and pathological brain activity.

The issue of BOLD activation volume is important as it is widely acknowledged that the true generators of epileptiform activity are not point sources. In the context of pre-surgical assessment, the extent of the epileptogenic zone is an important factor. In terms of this study, the effect of activation extent for the purpose of assessing the agreement between dipoles and BOLD would be small given that in most cases studied here, the extent of the activation along the line joining the dipoles and the activation centre is small compared to the dipole-to-BOLD centre distance, *d* (see *figure 18*). In the case of patient 17, the distance from the dipole to the nearest edge of the BOLD activation was 0.5 cm, compared to 1 cm for *d*. It is important to note that volume of activation obtained in a given experiment will be dependent on at least the following factors: signal-to-noise ratio (which incorporates measurement and intrinsic factors), amount of spatial smoothing applied and significance threshold level chosen.

It was already shown that individual spikes (in patient 1, *table 2*) can give rise to significant BOLD activation (Krakow et al., 2001b). Furthermore, the new technique of continuous event-related EEG-fMRI (Lemieux et al. 2001a), made possible by suppression of the imaging artifact in the EEG (Allen et al., 2000), with its potential

increase in sensitivity and much improved temporal resolution should allow us to better study the spatio-temporal characteristics of spike-related BOLD signal changes. This, combined with the recording dense-array EEG during fMRI (Bonmassar et al., 1999), will provide the opportunity of studying electrophysiological and vascular changes measured simultaneously for individual events, and removing the effects of grouping and averaging of events.

Given the varying nature of the underlying substrates in the group of patients and the small number of subjects studied the results are suggestive of the validity and complementarity of both methods to localise generators of IED. It can be concluded that in all cases with equivocal information on localisation, a combination of EEG-correlated fMRI and EEG source analysis may enhance the analysis.

6.2. Multimodal MR imaging: Combination of EEG-correlated fMRI with other MR modalities

A correlation of structural with functional information is essential to understand the processes underlying focal epilepsies (Duncan, 1997). This is in particular evident in patients with malformations of cortical development, a common cause for intractable focal seizures. Brains with malformations of cortical development may differ from normal brains in both functional and structural organisation (Raymond et al., 1995, Sisodiya et al., 1997).

In this section the integration of complementary functional and structural data acquired with MRI in a patient with localisation-related epilepsy due to cortical dysgenesis is demonstrated (Krakow et al., 1999a). Different MRI techniques can be useful in the field of epilepsy to investigate the microstructural organisation of brain tissue, the concentrations of cerebral metabolites and neurotransmitters, and local changes of blood oxygenation associated with epileptic activity and physiological brain activity. Here

results of four MR techniques are presented and discussed: (1) Functional MRI triggered by IED; (2) Functional MRI of the motor system; (3) Diffusion Tensor Imaging (DTI) to measure mean diffusivity, fractional anisotropy and fibre orientation; (4) Chemical Shift Imaging (CSI) to obtain a quantitative metabolic map of N-acetyl-aspartate (NAA).

Methods

Patient

A 22-year-old right-handed man with refractory epilepsy since age one year had simple partial seizures with jerking and numbness of the left sided limbs, complex partial and secondarily generalised tonic-clonic seizures (patient 2 of *table 2*). Neurological examination revealed a mild left hemiparesis. Interictal EEG demonstrated frequent focal spikes and sharp waves over the temporal and parasagittal region of the right hemisphere. Standard structural MRI showed subcortical nodular heterotopia of the right hemisphere with a large mass in the central region and a smaller nodule in the medial parietal lobe.

All additional MR data was acquired with a 1.5 tesla Horizon EchoSpeed MRI scanner (General Electric, Milwaukee, USA) using the following MR techniques:

(1) EEG-triggered fMRI and fMRI of the motor system

The EEG/fMRI experiment was performed as described in section 5.1. Acquisitions representing 47 activation and control states each were sampled non-periodically. The SPM96 package was used to perform spatial realignment and statistical analysis, as described earlier. The significance threshold was set to $p<0.001$ and the extent threshold to $p<0.05$. In addition, a BOLD fMRI block design experiment of self paced finger tapping of the left hand was carried out.

(2) Chemical Shift Imaging

The concentration of N-acetyl-aspartate (NAA) can be seen as a measure of neuronal functioning and integrity. CSI was performed with a 24x24 matrix over a 24 cm FOV (TE = 30 ms, TR = 3 s), giving 1 cm in-plane resolution. The slice was 2.25 cm thick, for a nominal voxel volume of 2.25 cc. A region of interest (11 cm x 7.5 cm) was prescribed using PRESS localisation. Spectra from each voxel were extracted and fitted in the frequency domain using LCModel (Provencher, 1993). Quantitative metabolite maps were produced as previously described (McLean et al., 1998), and overlayed upon a reference anatomic image.

(3) Diffusion Tensor Imaging

Diffusion-weighted MR imaging can be used to study cerebral microstructure, in particular the orientation of fibres in the white matter. In the white matter of the brain diffusion is directional (anisotropic) because water molecules diffuse predominantly parallel to tracts (Basser and Pierpaoli, 1996). Diffusion tensor imaging (DTI) provides quantitative measures of the magnitude and directionality of water diffusion in a three dimensional space and can be used for accurate studies of fibre orientations in vivo (Hsu et al., 1998). The principal eigenvector represents the principal direction of diffusion and can be used to display the direction of the fibre tract axis. Maps of the anisotropy of water diffusion give information about the degree of directionality. Highly directionally organised tissues have high anisotropy

A single shot inversion recovery prepared spin echo EPI based diffusion-weighted sequence (TR = 5000 ms, TE = 78 ms, TI = 1835 ms, FOV 24 cm, acquisition matrix 96x96, 5 mm slice thickness, 5 mm inter-slice gap) was used. Two b-values were applied in 7 non-coliniar directions at 14 slice positions (b_{max} = 703 s/mm^2). Two interleaved series with five averages were acquired. The fractional anisotropy and mean diffusivity were calculated on a pixel-by-pixel basis (Basser et al., 1996). The mean diffusivity is a measure of the magnitude of diffusion in mm^2/s. The fractional

anisotropy index is a scalar index of anisotropy which scales from 0 (isotropic medium) to 1 (maximum anisotropy).

In addition, a norm fractional anisotropy brain was created by averaging the spatially normalised anisotropy maps of 20 control subjects and generated maximum intensity projections (MIPs) using ANALYZE 7.5 software (Biomedical Imaging Resource; Rochester, Minnesota: Mayo Foundation, 1996). The MIP of the normal anisotropy brain was overlaid with pixels with significantly (>mean -2 SD) reduced anisotropy of the patient.

Results

The fMRI activation map is presented in *figure 13*. It reveals a single significant BOLD activation associated with interictal discharges (maximum Z-score = 3.9), located in the lateral part of the large MCD adjacent to its cleft. The activated area showed co-localisation with the EEG spike focus and was reproducible in three studies.

Figure 20a shows an overlay of a quantitative NAA map upon a reference anatomic image. The normal-appearing tissue and parts of the malformation appeared mainly yellow, indicating a relatively uniform high concentration of NAA. The NAA was abnormally low along the medial border of the MCD. In the same area, the DTI revealed a clearly higher mean diffusivity (values around 1.0 x 10^{-3} mm^2/s; *figure 20b*) and a lower fractional anisotropy (values around 0.4; *figure 20c*) than in the surrounding tissue. On T1-weighted images, this area did not differ from the remaining MCD, and no signs of oedema were visible on T2-weighted images. In addition, there was reduced anisotropy throughout the brain, including normal appearing white matter (mean diffusivity in white matter of normal control subjects: mean 0.75 x 10-3mm2/s (SD 0.05) x 10-3mm2/s, fractional anisotropy in control subjects: mean 0.76 (SD 0.05) *(figure 21d)*. Maps of the principal eigenvector showed that fibres were deviating from

their usual rostral-caudal orientation (in control subjects the angle between the AC-PC line and the pyramidal tract ranged from 50° to 80°) passing around the malformation *(figure 21c)*, which explained the findings of the fMRI finger tapping experiment: In this experiment there was no fMRI activation in pixels inside the heterotopic grey matter but it occurred in pixels adjacent to the heterotopic grey matter *(figure 21b)*.

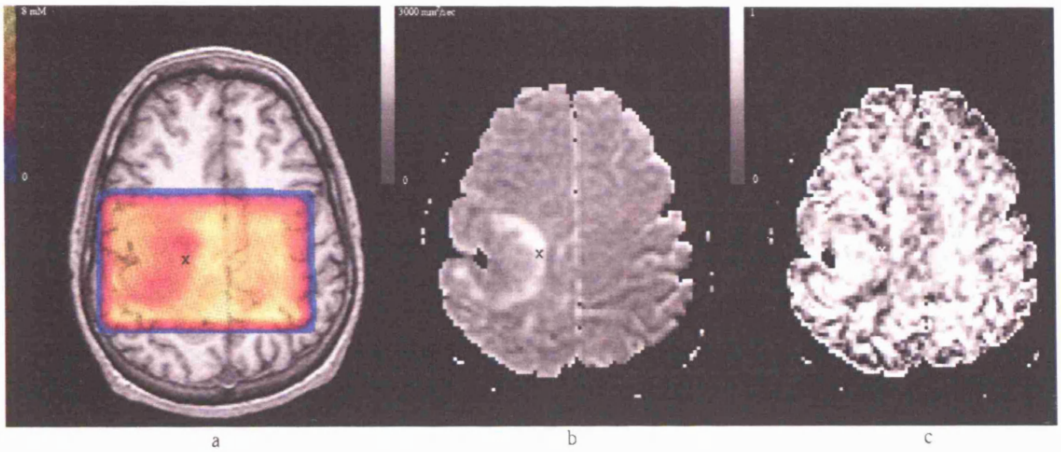

Figure 20: *Quantitative metabolite map of N-acetyl-aspartate (NAA) (a). Yellow indicates high, red and blue lower concentrations of NAA. Mean diffusivity (b) and fractional anisotropy (c) map. The area with a high mean diffusivity showed co-localisation with the region of reduced NAA concentration and fractional anisotropy, indicated by a cross (x).*

Discussion

The MR techniques of this study, which can be applied during a single session of less than three hours, provide information about the generation of interictal epileptiform

discharges and neuronal and micro-structural organisation of the epileptogenic lesion and the surrounding tissue which is not available with other non-invasive techniques.

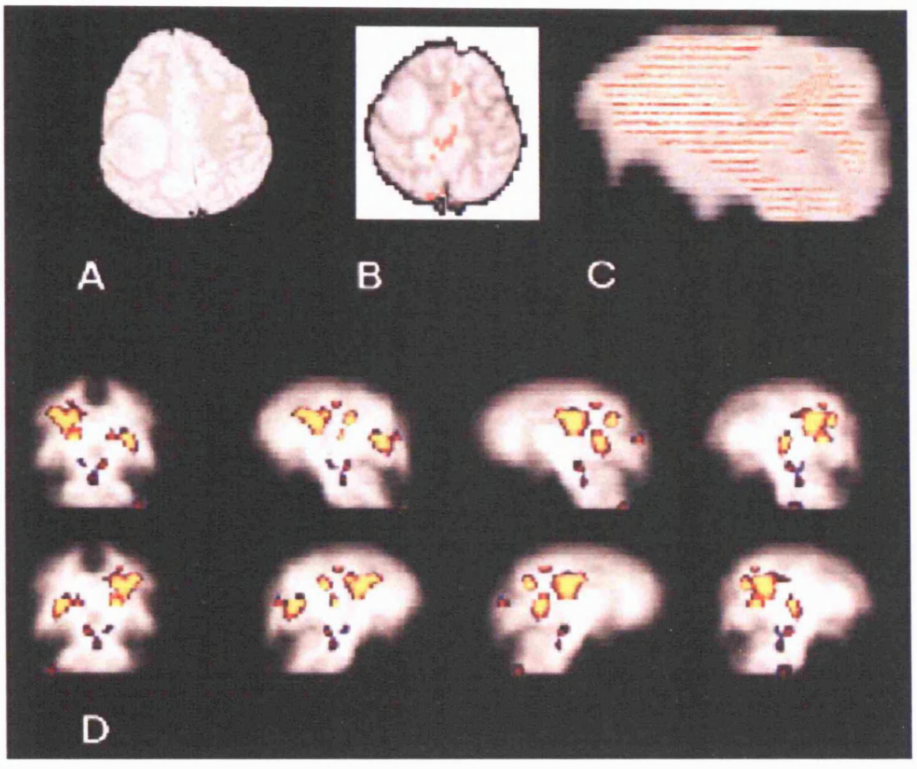

Figure 21: *(A) T2 weighted anatomical image showing a large nodular heterotopia area in the right central region and a smaller one in the medial parietal lobe (left on images is patient's right). (B) fMRI experiment (finger tapping of the left hand) showing widespread activation in the right hemisphere sparing the dysgenetic area in the central region. There is some activation in the parietal dysgenetic region. (C) Map of the principal eigenvector (sagittal view) showing that fibres with rostral-caudal orientation (presumably the pyramidal tract) are passing around the central dysgenetic area. (D) Maximum intensity projections (MIP) of a normal brain of anisotropy of water diffusion overlayed with pixels with significantly (< mean -2 SD) reduced anisotropy of the patient showing widespread bilateral loss of directional organisation of white matter (coronal MIP views rotated in 45° steps starting with an anterior view).*

Using EEG-triggered fMRI a brain area within the MCD involved in generating IED was identified *(figure 13)*. Due to the high temporal resolution of fMRI, changes of blood flow and oxygenation linked to single epileptiform discharges can be identified (Warach et al., 1996). The size of the fMRI activation is relatively small compared to the anatomical extent of spiking cortex usually identified by electrocorticography. This might be due to the fact that the sensitivity of our fMRI technique was not high enough to identify the whole extent of activated cortex. As the fMRI was triggered after IED, the activated cortical area contributes to the „irritative zone". As discussed previously, this is not identical with the „epileptogenic zone", but typically has a close spatial relation (Lüders et al., 1993). The pattern of cortical activation during finger tapping differed from the pattern found in subjects without neurological disease. The activation was widespread, but spared the malformation of cortical development. The possibility that some cortical activation below the threshold of fMRI occurred within the heterotopic grey matter could not be excluded. However, the fMRI study indicated an abnormal functional organisation of the cortex involving large regions in the right hemisphere consistent with previous PET studies (Richardson et al., 1998).

DTI revealed a heterogeneous structure of the MCD that was not evident on standard MRI: The centre of the malformation appeared similar to normally organised grey matter, while the periphery showed abnormalities of micro-structural organisation: In this area the tissue showed a lower density than normal grey matter (indicated by a high mean diffusivity, *figure 20b*) and was less structurally organised than white matter (low fractional anisotropy, *figure 20c*). This area was identical with the region showing the lowest NAA-concentrations *(figure 20a)*, also indicating an area of impaired neuronal function (Hugg et al., 1996, Cendes et al., 1997). Interestingly, the area with the most abnormal micro-structural organisation and NAA-reduction was distinct from the area identified with fMRI. It can therefore be assumed that the histological abnormalities

indicated by DTI and CSI are not necessarily identical with the area generating the epileptic activity. Whether this mismatch between micro-structural and functional abnormalities within the lesion is specific for this particular patient, or is a common finding in lesional epilepsies is important to determine in larger studies of a population of patients, preferably including surgical outcome data and histological correlation. Additionally, DTI provided information about neuronal pathways of the brain ("MR tractography"). Maps of the principal eigenvector of the diffusion tensor showed that fibres with rostral-caudal orientation (presumably reflecting the pyramidal tract) deviated "avoiding" the malformation *(figure 21c)*. Displaced but largely intact motor pathways might be the imaging correlate of the mild hemiparesis in this patient. Comparison of the patient's diffusion anisotropy with that in a group of normal controls revealed evidence for widespread regions of reduced anisotropy in the white matter not only affecting the malformation but also the normal appearing white matter in the contralateral hemisphere *(figure 21d)*. This is consistent with a loss of directional organisation of white matter (Wieshmann et al., 1999).

In conclusion, the ability to localise brain regions which show abnormal micro-organisation and are involved in generating epileptiform activity may improve understanding of the pathophysiology of epilepsy and associated neurological deficits and advance specific surgical strategies related to different pathologies. Further characteristics of epileptogenesis may become approachable in vivo if not only fMRI, but also diffusion and chemical shift imaging are correlated with epileptic activity identified with concurrent EEG recording.

6.3. Fixation-off sensitivity as a model of continuous epileptiform discharges: EEG, neuropsychological and functional MRI findings

Fixation-off sensitivity (FOS) refers to an electroencephalographic (EEG) abnormality

elicited by elimination of central vision and fixation. The EEG findings are characterised by sustained occipital or generalised epileptiform discharges during eye closure, complete darkness or unpatterned vision, which disappear on binocular or monocular fixation. FOS is most frequently found in children with benign childhood epilepsy with occipital paroxysmal activity (BCEOP). Only a few cases of FOS in adult patients with epilepsy are described in the literature (Panayiotopoulos, 1998).
In this section the electro-clinical findings of an adult with FOS are demonstrated as a human model for the study of epileptiform discharges. FOS occurs predictably and is not associated with clinical features such as movement impeding EEG and MRI. The main aims of this study were to assess whether the epileptiform activity is associated with (1) transitory cognitive impairment and (2) changes of cerebral perfusion detectable with BOLD fMRI.

Patient and Methods

The patient was a 27 year old male with an unremarkable medical history until age 20 when he gradually developed difficulties walking down stairs and slopes because of worries that he may fall. These problems generalised over several years leading to a psychiatric diagnosis of agoraphobia, panic disorder, and obsessive compulsive disorder. The neurological examination was unremarkable besides a slightly unsteady gait. An EEG, which was performed because of occasional falls, revealed FOS. He never experienced, however, any symptoms indicative of epileptic seizures, but had a positive family history of epilepsy. His deceased maternal grandmother had grand mal epilepsy and one of his five siblings was diagnosed with myoclonic epilepsy.

Video-EEG monitoring

30 channels of scalp EEG were recorded for 22 hours. The EEG recording covered

periods with spontaneous eye opening and closure, sleep, tests for eliminating central fixation and central vision (including complete darkness, monocular and binocular Frenzel lenses, and homogeneous visual fields), and photic stimulation.

64-channel-EEG source analysis

64-channel EEG was recorded using a QuickCap (Neuroscan, Sterling, Virginia, USA). Five two-second epochs beginning one second before the fixation-off discharges were extracted from the recording for EEG source analysis. Localization analysis was performed based on the first spike and wave complex of each epoch using the Curry 3.0 software (Neuroscan) with a realistically-shaped boundary-element conduction model. Spatially-constrained MUSIC dipole scan and current density map generator models were applied.

Neuropsychological assessment

Parallel forms of three cognitive tasks were performed by the patient during EEG recording under the two conditions "eyes open" and "eyes closed".

1. The digit span task from the WAIS-R was used.
2. In the story recall task the patient heard a short passage containing 30 ideas and was then asked to immediately recall as much as he could.
3. In the list learning task the patient was read a list of 15 words and asked to repeat as many words as possible following each presentation. Five learning trials were presented. To control for timing effects the two conditions were alternated between the tests.

fMRI

Data were acquired using a 2 tesla Magnetom VISION (Siemens, Erlangen, Germany)

MRI system. Contiguous multislice T2*-weighted fMRI images were obtained (echo time = 40 ms) with echo-planar imaging (32 axial 3 mm slices, 3.2 seconds per volume). Five epochs of the eyes open and three of eyes closed condition were acquired, each consisting of 10 volumes (the planned image acquisition was not completed due to claustrophobia of the patient). Eye closure was monitored using the Eyetracking system, Model 504 (Applied Science Laboratories, Bedford, MA, USA). Scanning data were processed and analysed using Statistical Parametric Mapping (SPM99b) (Friston et al., 1995). All volumes were realigned and the images were spatially normalised and smoothed (8 mm). The two conditions were compared with a t-statistic on a voxel-by-voxel basis.

Results

EEG

The resting record showed beta-rhythm with occasional 8 Hz alpha-rhythm of medium amplitude on eye opening. With eyes closed, there were continuous spike and wave complexes associated with 3-4 Hz slow wave activity at 40-100 μV in the posterior regions bilaterally. This activity commenced immediately on eye closure and attenuated with eye opening *(figure 22)*. When central fixation and vision were eliminated, the posterior discharges re-appeared and were then unaffected by eye opening or eye closure. The discharges persisted during light sleep and disappeared during slow wave sleep. There was no evidence for photosensitivity.

Neuropsychological assessment

Scores of both the story recall and the list learning tasks were significantly lower in the eyes closed-condition. In the eyes open condition the scores fell in the 75^{th} - 90^{th} percentile range for the story recall and the 50^{th} percentile range for the list learning

task. In the eyes closed condition the scores on these tasks fell at the 25th and below the 2nd percentile, respectively. There was no significant difference in the performance on the digit span tasks between the two conditions.

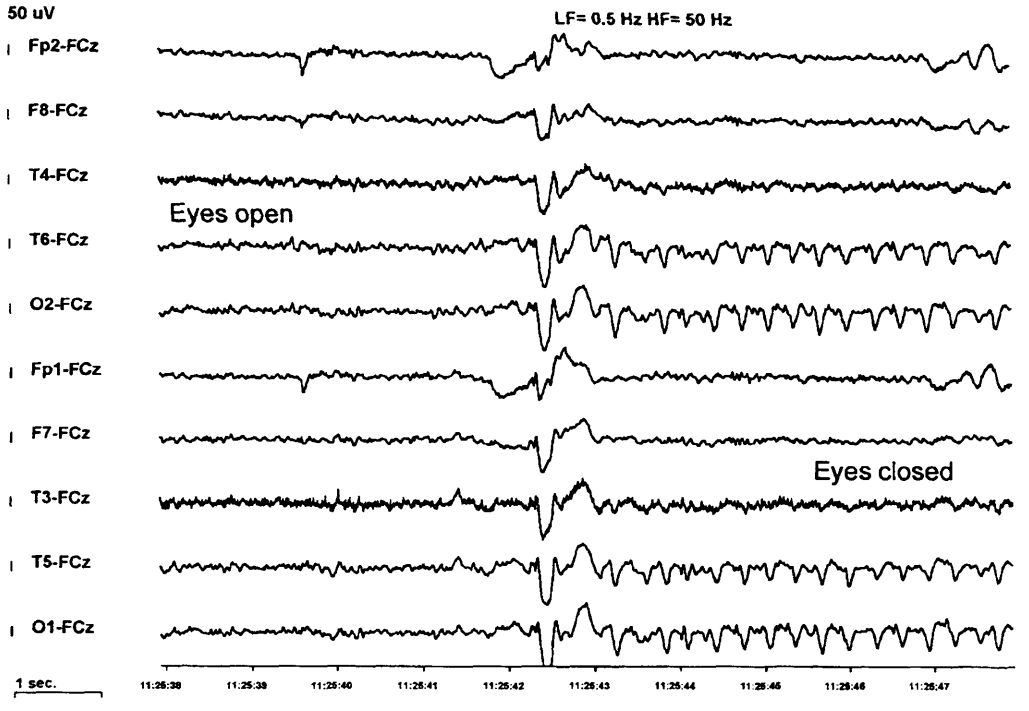

Figure 22: *Video-EEG recording. Ten EEG channels of a bipolar montage are displayed. Bilateral occipital spike and sharp and slow wave discharges are immediately induced by binocular fixation-off (eye closure).*

fMRI and EEG source analysis:

The fMRI results are presented in *figure 23*. The comparison "eyes open" to "eyes closed" showed, as expected, an activation of the primary visual cortex and neighbouring extrastriate regions *(figures 23a and 23c)*. The "eyes closed" state revealed a bilateral parieto-occipital activation laterally adjacent to the region activated during "eyes open" *(figures 23b and 23d)*. Additional smaller activated regions were

localised in the right anterior cingulum and bilateral in the superior frontal gyrus and fronto-basal regions (*figure 23b*).

Source localisation based on both EEG generator models and over all selected epochs had a clear occipital maximum *(figure 24)*.

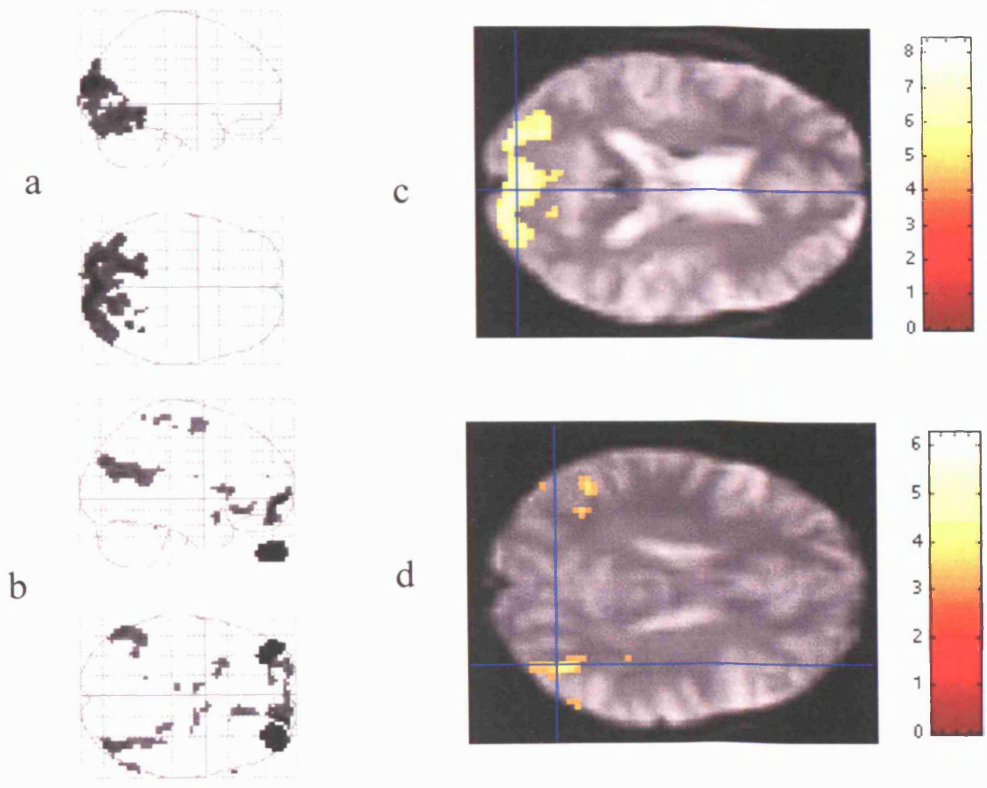

Figure 23: *SPM activation map of the fMRI data. Areas of significant BOLD signal changes are displayed in a sagittal and axial glass view (a,b) and overlaid on an axial anatomical image (c,d). The eyes open state is associated with an occipital visual activation (a,c), the fixation-off discharges during eye closure with a bilateral parieto-occipital activation laterally adjacent to the visual activation and smaller activations of the frontal lobe (b,d).*

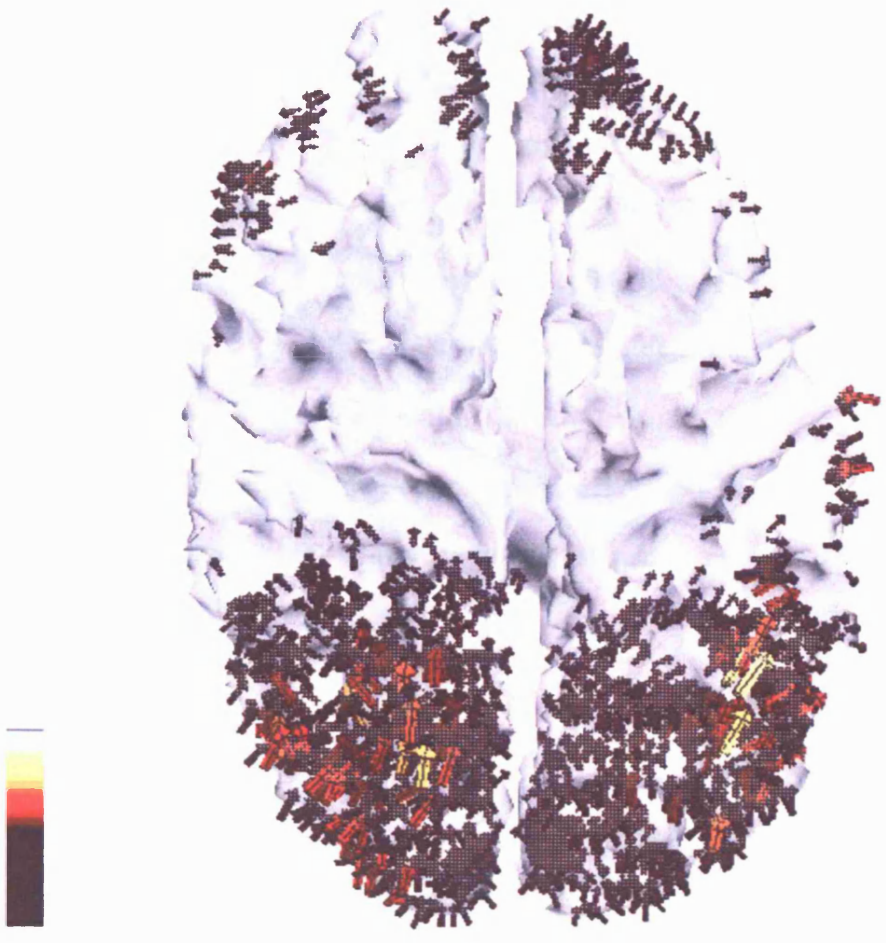

Figure 24: *Current density map based on a 64-channel EEG recording showing a bilateral occipital source localisation.*

Discussion

This is the first report of an adult patient with marked FOS and no history of epilepsy (Krakow et al., 2000b). The EEG showed the typical features of FOS with continuous epileptiform discharges during elimination of central vision and fixation, including light sleep. Although the patient never experienced any clinical symptoms which could be attributed to his FOS, neuropsychological testing revealed cognitive impairment that occurred simultaneously with the epileptiform discharges. This is in keeping with reports on transitory cognitive impairment with focal (Binnie, 1987) and generalised (Rugland, 1990) epileptiform discharges in patients with epilepsy. In contrast to studies

in epilepsy patients, measurements of cognitive performance in FOS are not confounded by effects of antiepileptic drug therapy and seizures, and the predictable occurrence of discharges facilitates the experimental set-up and interpretation of results.

The involvement of fronto-central regions has been considered to be important for the manifestation of cognitive impairment during epileptiform EEG discharges (Aldenkamp, 1997). A possible explanation of the cognitive dysfunction in FOS with an occipital EEG focus is provided by fMRI which showed not only activation of parieto-occipital, but also of frontal lobe structures associated with the fixation-off discharges. This might indicate a more widespread functional disturbance than suggested by the localised scalp EEG changes.

The fMRI activations indicate an increased blood flow related to the epileptiform activity, which is in keeping with previous fMRI studies showing BOLD signal changes related to focal seizures (Jackson et al., 1994), and focal (Krakow et al., 1999b) and generalised (Warach et al., 1996) interictal epileptiform discharges. In contrast, a recent fMRI study failed to detect BOLD signal changes in relation to brief photoparoxysmal spike-wave activity evoked in patients with photosensitive epilepsy (Hill et al., 1999). Photosensitivity is considered to have opposite mechanisms of excitation and inhibition to that of FOS (Panayiotopoulos, 1998).

In the interpretation of the fMRI results the lack of a baseline condition in FOS has to be taken into consideration. Both conditions ("eyes open" and "eyes closed") are associated with a partly overlapping occipital activation. Therefore the area of visual activation *(figures 23a and 23c)* appeared to be spared in the activation of the fixation-off discharges *(figures 23b and 23d)*, although the pattern of the surrounding fMRI activation and the EEG source reconstruction strongly suggest an involvement of the visual cortex in generating the discharges.

In conclusion, the applied methods could enhance the understanding of an EEG

phenomenon such as FOS by demonstrating transitory cognitive impairment in an otherwise subclinical condition and localising the underlying generators of the discharges with high spatial resolution.

Chapter 7

Further applications and future developments

7.1. Further applications: EEG-correlated fMRI beyond epilepsy

The development and application of EEG-correlated fMRI was so far mainly carried out in the field of epilepsy research. The efforts were driven by the need of further non-invasive tools to identify and localise epileptic activity. However, because EEG and fMRI jointly can provide information about the timing and location of brain activity in general, it is reasonable to expect that EEG-correlated fMRI will allow investigators to probe for the generators of physiologic states or cognitive evoked potentials.

Applications that may be appropriate to consider, in addition to epilepsy, include the evaluation of the fMRI generators related to physiological EEG events and oscillatory rhythms such as alpha rhythm, sleep spindles, and cognitive or more standard clinical evoked potentials (EP) (Schomer et al., 2000).

The recording of EP inside the fMRI (Bonmassar et al., 1999) has proven exceptionally difficult because of the small amplitude of the signal which ranges from 1 to 10 μV and the relative amount of random noise present which may be between 20 und 200 μV (Bonmassar et al., 1999). In the first study performed by Bonmassar et al. visual pattern reversal EP were measured (full-field black and white checkerboard visual stimulus with 2 Hz or 4 Hz reversal frequency). In a 1.5 tesla magnet the visual evoked potentials waveforms were clearly extractable by epoch selection and averaging. The concurrent fMRI showed activation of early visual areas (V1 and V2).

A study performed by Goldmann et al. (2001) used EEG-correlated fMRI to identify the generators of alpha rhythm. Six subjects were studied during eyes closed rest. Sixteen channels of scalp EEG were recorded, MR scanning was preformed on a General Electric 3 Tesla imager using EPI. A software described in Goldman et al. (2000) was

used to remove scanner and pulse artifact. Then, the average power in the alpha band (8-12 Hz) was calculated at each TR using a Fast Fourier Transform. These curves were then convolved with a hemodynamic response function and a voxel-wise correlation was performed.

Two prominent correlations between the BOLD response and the alpha power were found: A negative one in the occipital cortex and a positive one in the thalamus. These anatomic correlations were not present for the other EEG frequency bands. The results support the hypothesis that the alpha rhythm represents a state of decreased afferent input associated with neocortical synchronisation that is driven by the thalamus.

The next section gives an example how EEG-correlated fMRI can be used to monitor the state of vigilance and sleep during fMRI experiments.

Monitoring of sleep-wake cycle during fMRI experiments

If EEG is recorded during MRI scanning (e.g. for spike-triggered fMRI in patients with epilepsy) it can be observed that patients or probands often fall asleep inside the scanner despite the noisy and narrow environment. Hence, EEG-correlated fMRI can also be used to study the sleeping brain. The EEG recording (with additional EMG and EOG recording) enables on-line monitoring of the sleep stages while the fMRI can reveal a profile of brain activation and deactivation during sleep with high spatial resolution. Sleep studies can focus on a sleeping brain unchallenged with specific manipulations in terms of external cognitive stimuli to study activation-deactivation patterns compared to the waking state. Alternatively, cognitive information can be offered to the sleeping brain in form of sensory stimuli. Many previous electrophysiological studies have examined the surface cortical-evoked responses to a variety of stimulus-related paradigms, demonstrating strong evidence that in several stages of sleep information can be processed, retained, and even modified. However, as with the wake state, these

EEG techniques suffer from poor spatial resolution, leaving explanatory models of information processing across the sleep states largely speculative (Walker and Hobson, Neuron 2000). In the following section a study of specific auditory processing in waking versus non-REM sleep using EEG-correlated FMRI is presented, which is one of the first taking advantage of the superior spatial resolution of fMRI. This study was performed at the Wellcome Institute of Cognitive Neurology, Institute of Neurology, University College London in cooperation with Dr. Chiara Maria Portas.

Introduction

The degree of cognitive activity taking place in a sleeping brain is a current matter of interest (Cote and Campbell 1999; Perrin et al., 1999). Although the electrophysiological studies described above show that some aspects of sensory processing are preserved during NREM sleep, they lack the spatial resolution to identify the neuroanatomical substrates underlying this process. In this study, fMRI was combined with EEG to investigate 'if' and 'how' the brain responds to sensory processing across different levels of consciousness. First, it was tried to establish to what extent auditory stimuli presented during sleep are associated with brain activity and hemodynamic changes associated with auditory processing were compared between in sleep and wakefulness. Second, it was considered whether, during NREM sleep, the brain may differentially process stimuli having special affective significance. To test this hypothesis, two types of auditory stimuli were presented, matched for their intensity and duration but with different affective significance: pure tones (beep) and the subject's own first name.

Subjects

A total of 12 healthy volunteers (10 males and 2 female, age 23-34) participated in the

study. They had negative history for neurological, psychiatric disorders or sleep abnormalities. Three subjects were used in a pilot study to test the experimental procedure. Two more subjects had to be excluded from the group analysis due to severe movement artifacts present in the data acquired. Thus, results from 7 subjects (5 males and 2 females) were used in the data analysis.

Experimental protocol

To ensure that subjects would sleep in the uncomfortable and noisy MRI environment the sleep propensity was increased by sleep depriving the subjects for 24 hours prior to the experiment, under continuous supervision. On the day of the experiment subjects were prepared for polygraphic recording and then placed inside the scanner (8.00 a.m.). To minimise movement artifacts due to sleep, the subject's head was immobilised with special pads. During a 2 hour scanning period (including wakefulness and sleep) subjects were presented binaurally, using a headphone, with trains of auditory stimuli of two types alternated with periods of silence (baseline condition). In the baseline condition there was no auditory stimulation other than the scanner noise *(figure 25)*. A pure tone (beep, 1400 Hz sine waves, 500 ms duration, 80 db intensity) was used as neutral stimulus and presentation of the subject's own name (500 ms duration, 80 db intensity) was used as stimulus having special affective significance. Previous studies have shown that a person's own name is an intrinsically meaningful stimulus (Brain, 1958; Oswald et al., 1960; McDonald et al., 1975; Fischler et al., 1987, Voss and Harsh, 1998) and its saliency stands out against presentation of other first names (Berlad and Pratt, 1995; Perrin et al., 1999). In addition, the subject's own name offers the same level of affective saliency across subjects. A total number of 160-180 'events' (pre-recorded trains of stimuli or baseline) were presented in random order during matching bursts of functional measurements (see section below). In the gaps between bursts of

fMRI measurements the recorded scanner noise was replayed in order to produce a constant background noise through the duration of the experiment (see *figure 25).*

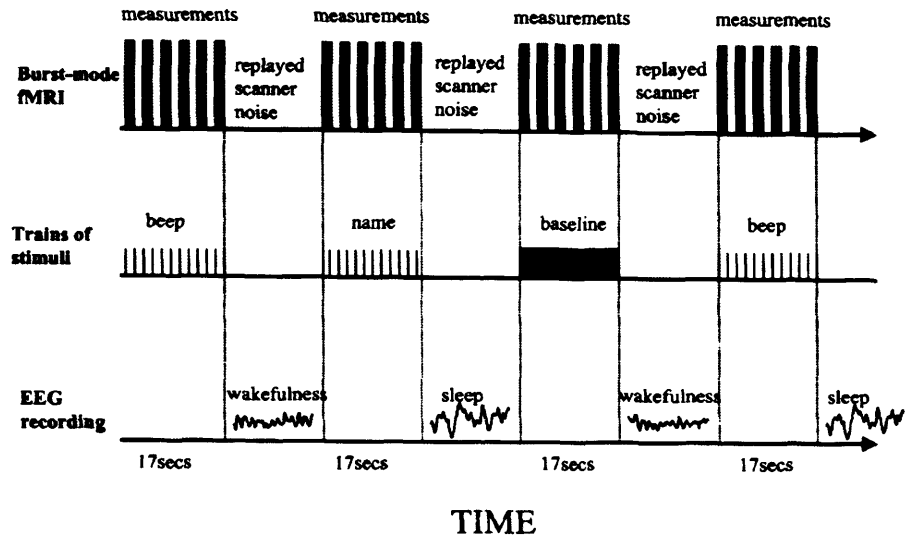

Figure 25: *A schematic of the experimental design of the EEG/fMRI study on auditory processing across the sleep-wake cycle. The figure shows the time relation between functional measurements, EEG recording, presentation of auditory stimuli, and replay of MR scanner noise.*

Functional data acquisition and analysis

To detect brain activation associated with processing of auditory stimuli across the sleep-wake cycle, a burst-mode fMRI was used (Josephs et al., 1999). This technique involves the acquisition of short 'bursts' of measurements (6 measurements per burst in this study). In the gaps between bursts it is possible to monitor behaviour and/or electrophysiological parameters (e.g. EEG recording). During a two hour experimental session 160 - 180 bursts (matching the number of events) were acquired for each subject (corresponding to approximately 1000 volumes). Each volume consisted of 34 slices (2 mm thickness). With this procedure each volume covered the whole brain (with the

exception of the lowest part of the cerebellum); the voxel size was 3x3x3 mm, and the acquisition time (TA) was 2.88 seconds. Each burst had approximately 17 seconds duration (same as the gaps) (see *figure 25*). Before proceeding to fMRI data analysis all volumes were realigned, motion corrected, normalised (Friston et al., 1995) to a standard template (Montreal Neurological Institute; Evans et al., 1994) and smoothed using a 6 mm FWHM Gaussian kernel. Statistical inference was obtained using SPM99. Data were analysed by modelling the evoked hemodynamic responses for the different stimuli as boxcars convolved with a synthetic hemodynamic function (hrf), in the context of the general lineal model (Josephs et al., 1997). Six event types were defined: name, beep and rest in sleep and wake. Differential effects were tested by applying appropriate linear contrasts to the parameter estimates for the hrf regressors of each event, resulting in a t-statistic for each voxel. These t-statistics (transformed to Z-statistics) constitute a Statistical Parametric Map. The corresponding p values were corrected for multiple comparisons across the entire brain, in the context of Gaussian random field theory, except where otherwise indicated.

Data were first analysed individually for each subject and then as a group. A fixed effects model was used to estimate the *main effect* of state (sleep or wakefulness) over each type of event (*beep*, *name*, baseline). State by event interactions (e.g. auditory-related brain activity during sleep was compared to auditory- related brain activity during wakefulness), and state by event-type interactions (i.e., *name*- versus *beep*-related brain activity during sleep compared to *name*- versus *beep*-related brain activity during wakefulness were also studied; for a detailed review of interaction analysis see Price et al., 1997). Significance was accepted for $p<0.001$ uncorrected or $p<0.05$ corrected for multiple comparisons (Friston et al., 1994).

EEG data acquisition and analysis

Sleep and wakefulness electrophysiological correlates were assessed by polygraphic recording obtained during bursts of measurements *(figure 25)*. Gold electrodes were applied on the scalp (A1, A2, C3, C4) according to the International 10/20 system (Jasper, 1958) for EEG, on the outer canthus-external meatus for electrooculogram (EOG), under the chin (submental muscles) for electro-myogram (EMG). The EEG recording during the fMRI experiment was performed as described in section 5.1. Data were visually analysed on-line and off-line by two different raters to distinguish sleep from wakefulness according to Rechtschaffen and Kales (1968) *(figure 26)*.

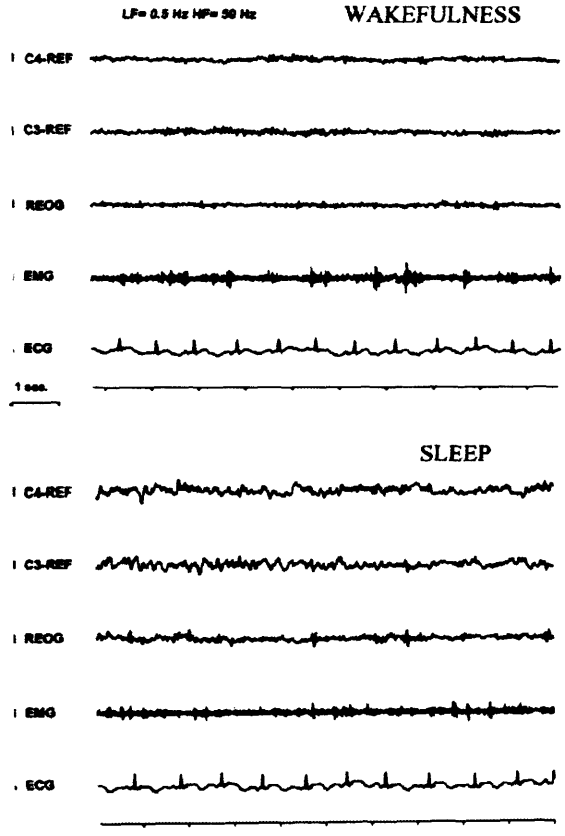

Figure 26: *Example of a polygraphic recording inside the MR scanner. During quiet wakefulness the EEG is characterised by alpha-activity (upper panel), while sleep is characterised by high amplitude theta and delta activity (lower panel). The amplitude of the EMG-activity and the heart rate is also decreased during sleep compared to wakefulness. The calibration bar used for EEG, EOG, and EMG channels corresponds for 50 μV, for the ECG channel corresponds for 500 μV.*

To increase the number of 'events' in relation to the 'state' all NREM sleep stages were collapsed into one. REM sleep epochs were too rare and short (due to the short scanning time and to the 'total sleep deprivation' protocol) and were excluded from the data analysis. Epochs which included state transitions or combination of waking and sleep were also excluded from data analysis. Thus, only two states were considered: sleep and wakefulness.

For EEG/fMRI data matching, each EEG recording epoch was paired with the preceding burst of measurements and auditory event *(figure 25)*. It was considered that because each train of auditory stimuli ended just before the outset of an EEG-epoch, such EEG-epochs would closely reflect the occurrence (or lack) of wakefulness during the preceding burst of measurements.

Results

Hypnograms showed in all subjects an alternation between wakefulness and sleep periods. NREM sleep will be referred to as 'sleep'. Most subjects fell asleep immediately after the start of the experiment and spent most of the sleeping time in stages II and III. An example of a subject's polygraphic recordings is shown in *figure 26*.

The mean number of awakenings was 10 per subject and the majority was due to the presentation of the subject's own name *(figure 27)*. The most important finding of this study was that the pattern of brain activation associated with auditory stimulation was remarkably similar during wakefulness and sleep. In particular, processing of the auditory stimuli (*name* or *beep*) produced bilateral activation in auditory cortex (superior temporal gyrus, BA 41/42), thalamus and caudate in wakefulness and sleep *(figure 28)*.

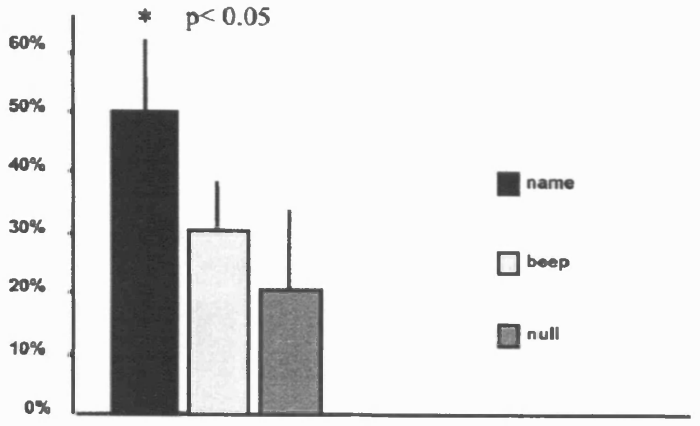

Figure 27: *The affective saliency of the stimuli was estimated as percentage of awakenings in relation to the time of stimulation. The graph shows the percentage of awakenings in relation to the type of auditory stimulation. Name is significantly more arousing than beep (ANOVA followed by post-hoc comparison p <0.05).*

However, when the stimuli-related brain activity during sleep was compared to stimuli-related brain activity during wakefulness, a decreased activation was found in the left parietal cortex (BA 7) and bilaterally in the prefrontal cortex (BA 47), thalamus, cingulate gyrus (BA23/24) and peri-amygdala regions.

Direct comparison between the two event types (*name* versus *beep)* revealed higher activation of the middle temporal gyrus and orbito-frontal cortex bilaterally in response to the *name* in both wakefulness and sleep *(figure 28).*

Finally, activations associated with the interaction between stimulus type and state were assessed. That is, *name*- versus *beep*-related brain activity during sleep with *name*- versus *beep*-related brain activity during wakefulness were contrasted. Because there was interest in those brain regions which responded more to the presentation of the

subject's own name, compared to beep, in sleep than in wakefulness, the interaction was masked with a contrast coding for the simple main effect of name versus beep in sleep. This comparison showed increased activation in the left amygdala and left prefrontal cortex (BA 46).

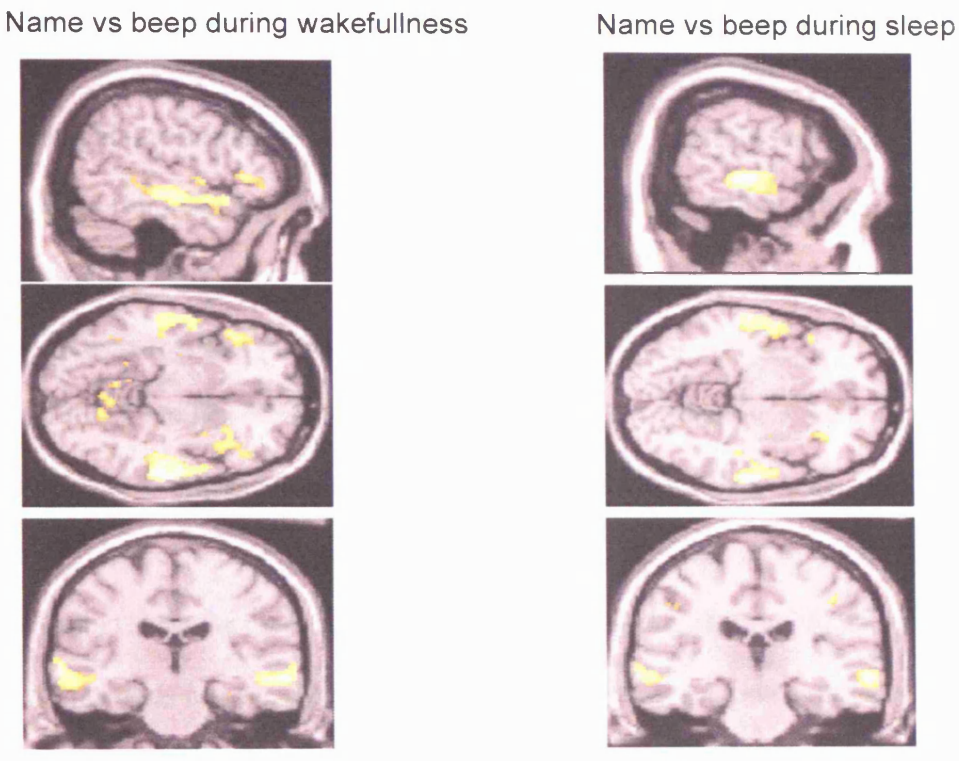

Figure 28: *SPM activation map of auditory stimulation in wakefulness and in sleep. There is a bilateral activation in the superior temporal gyrus and thalamus in both wakefulness and sleep. These brain areas are more activated in relation to name compared to beep presentation in both wakefulness and sleep.*

Discussion

This section presents the first fMRI study to investigate auditory processing as a function of the level of consciousness (Portas et al., 2000). The first significant result of

this study is that the pattern of brain activation associated with auditory stimulation was strikingly similar in wakefulness and sleep, suggesting that sensory processing occurred in both conditions. However, qualitative differences were found in brain activation associated with auditory processing during sleep compared to wakefulness. The reduced regional activity during sleep, compared to wakefulness, in the left parietal and, bilaterally, in the prefrontal cortex, thalamus and cingulate gyrus (part of the limbic system) suggests that these areas may be involved in the further processing and perceptual integration of sensory inputs likely to occur during wakefulness only. Indeed, a role for frontal and parietal regions (Kleinschmidt et al., 1999, Lumer et al., 1999, Portas et al., 2000) and the thalamus (Hugdahl et al., 1991, Portas et al., 2001) in conscious perception has previously been proposed.

Recent PET studies of vegetative patients showed that their primary auditory cortex responds to auditory stimulation (Laureys et al., 2000). However, a significant alteration in functional connectivity between the auditory cortex and multimodal (parietal cortex) and limbic areas was reported. The authors suggested that these 'functional' disconnections restrict cortical processing and prevent perceptual integration in vegetative patients. In this respect, Laureys's results are entirely consistent with this study. Residual input processing in vegetative patients in relation to other sensory modalities has also been shown (Owen et al., 1999). Furthermore, a selective decrease of activity in association cortices (parietal and prefrontal regions) during REM sleep in healthy volunteers has been reported (Maquet et al., 1996). REM sleep is a state in which the brain is highly aroused and the activity in the thalamo-cortical system is similar to wakefulness (Llinás and Ribary, 1993). However, sensory awareness is rarely achieved (Burton et al., 1988) and the threshold for awakening is as high during REM sleep as in delta sleep (Rechtschaffen et al., 1966). It is conceivable that the dampened activity in association regions during REM sleep is sufficient to prevent awareness and

contextualisation of sensory stimuli despite the high degree of brain arousal. Despite the intrinsic difference between REM and NREM sleep (Llinás and Pare, 1991), it seems that a similar decrease in association cortices activity may occur in the two states. This might explain the common perceptual impairment. The present findings argue in favour of this hypothesis.

The second aim of this study was to investigate if, during sleep, the brain responds in a different fashion to different stimuli as a function of their significance. Behavioural and electrophysiological evidence support this possibility. For example, some auditory stimuli produce more awakenings than others regardless of their intensity, e.g. young mothers are woken up by their infants lightest movements (Nishihara and Horiuchi, 1998). In addition, a waveform called "mismatch negativity" elicited by deviant tones in wakefulness, is also present during sleep (Nordby et al., 1996, Pratt et al., 1999). Similarly, other electrophysiological studies suggested that certain processes of attention and memory-related operations involved in auditory processing remain operative during sleep (Bastuji et al., 1995, Nordby et al., 1996, Brualla et al., 1998). Of particular interest is the recent study by Perrin et al. (1999), reporting that, during REM and NREM sleep, presentation of the subject's own name elicited a cognitive response comparable to that occurring during wakefulness as shown by enhancement of the P300 component. Such responses were not shown for presentation of other first names. Taking advantage of the higher spatial resolution of fMRI compared to event related potentials, we were able to identify selective areas of brain activation associated with processing of significant (subject's own name) and neutral (beep) auditory stimuli across the sleep-wake. Presentation of *beep* or subject's own *name* induced a similar pattern of activation in the auditory cortex, thalamus and caudate bilaterally. However, when *name-* was compared to *beep-* related brain activity, higher activation was present in the middle temporal gyrus and orbito-frontal cortex bilaterally both in wakefulness

and sleep. This difference is likely to reflect complex semantic processing (Binder et al., 1997) essential for name processing only.

More importantly, when specifically the effect of *name* versus *beep* in sleep compared to wakefulness was tested, higher activation in the left amygdala and left prefrontal cortex was found. These responses to the presentation of subjects' own name were unrelated to the physical difference between the stimuli and only present during sleep. Thus, the results suggest that when subjects were listening to their own name during sleep some brain regions were selectively more responsive than in any other condition. The evidence that the amygdala may play a role in mediating the response to auditory stimuli with affective significance is not surprising. The role of the amygdala in detection of stimuli with affective content is well established (e.g., LeDoux, 1996) and amygdala responses to behaviourally-relevant stimuli can occur without awareness (Morris et al., 1998; Whalen et al., 1998). The present study extends these findings to the unconscious state represented by sleep. The lateral nucleus of the amygdala receives profuse projections from the auditory thalamus and auditory cortex (Romanski et al., 1993). Information from the lateral nucleus flows to the central nucleus and from here to several cortical and subcortical areas. It can be suggested that following the detection of relevant emotional stimuli during sleep, the amygdala may activate the dorsolateral prefrontal cortex, inducing arousal and sustaining a basic level of sensory awareness (Armony and LeDoux, 2000). Although the amygdala is not directly connected to the dorsolateral prefrontal cortex, it projects to the medio-dorsal thalamic nucleus, one of the major areas feeding into the prefrontal cortex. The amygdala also projects to non-specific systems involved in the regulation of cortical arousal (Amaral et al., 1992). The prefrontal cortex would then determine the consequences of the "alarm effect". Such effect may progress to full awakening and acknowledgement of the input or to sensory neglect. The role of the prefrontal cortex in "selection" is well established (Frith

et al., 1991, Hyder et al., 1997).

In summary, this study demonstrated that the sleeping brain is able to process auditory stimuli. In addition, the existence of a functional network capable of detecting and facilitating processing of emotionally- relevant inputs during sleep can be postulated.

7.2. Future developments: Continuous EEG-correlated fMRI

The potential advantages of continuous EEG/fMRI have already been discussed in previous chapters. However, the large EEG artifacts induced by image acquisition during fMRI have precluded simultaneous EEG and fMRI recording before sufficient methods for removing imaging artifacts became available. Since 1999, several techniques for reducing imaging artifact have been reported (Felblinger et al., 1999, Sijbers et al., 1999, Hoffmann et al., Cohen et al., 2001).

This section reports on the initial imaging findings with a new technique for the simultaneous and continuous acquisition of functional MRI data and EEG recording. This technique is based on an EEG recording system and an artifact reduction method presented by Allen et al. (2000). In summary, this recording system has a large dynamic range to capture both low-amplitude EEG and large imaging artifact without distortion (resolution 2 μV, range 33.3 mV), 5-kHz sampling, and low-pass filtering prior to the main gain stage. Imaging artifact is reduced by subtracting an averaged artifact waveform, followed by adaptive noise cancellation to reduce any residual artefact *(figure 29).*

Introduction

In fMRI, knowledge of the brain's state throughout data acquisition is essential as the method relies on contrasts between images acquired in different brain states. In the standard so-called block design fMRI experiments this is accomplished by imposing a

succession of stimulation and rest periods of fixed duration. More recently, the advent of event-related fMRI has allowed the analysis of events with variable or random presentation sequences (Josephs et al., 1997).

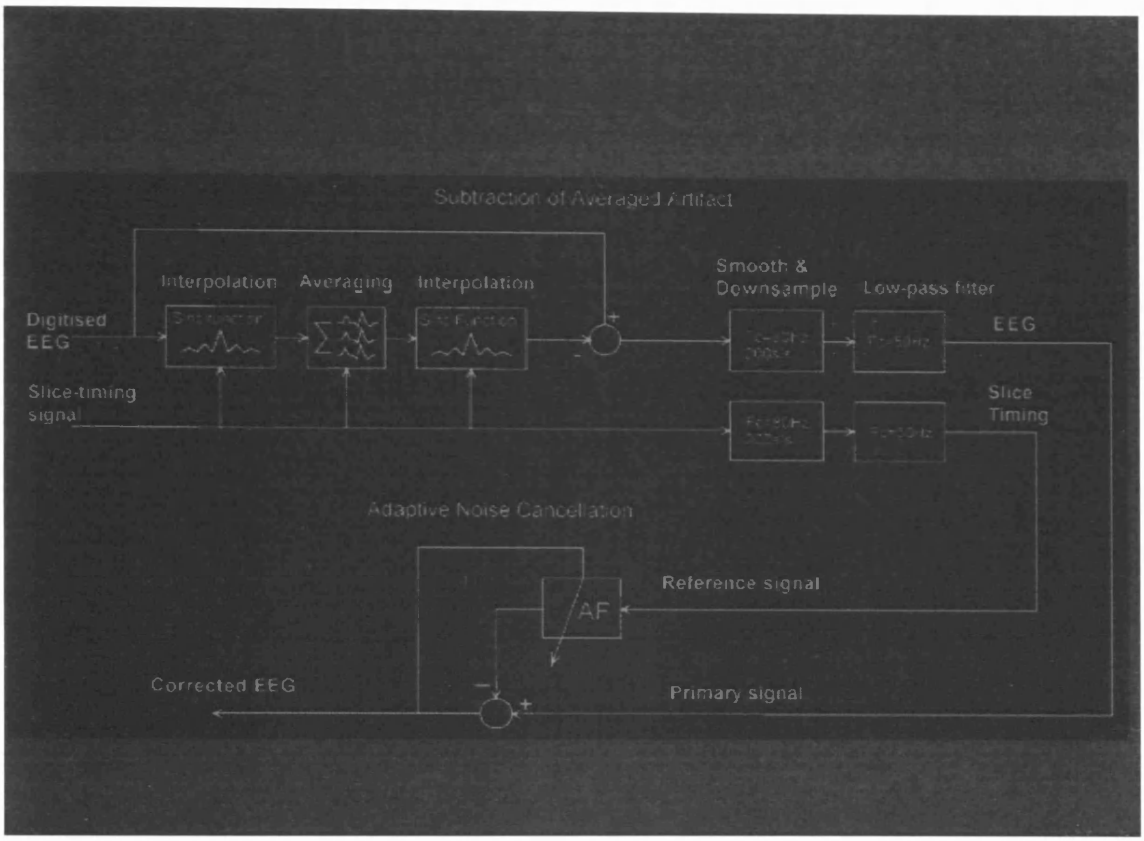

Figure 29: *Schematic of the image artifact reduction algorithm proposed by Allen et al. (2000), which was used for the continuous and simultaneous EEG/fMRI experiment.*

In epilepsy, the localisation of the generators of IED is important for clinical and basic science purposes. Although increasingly sophisticated electrophysiological measurement methods have been developed, e.g. EEG with up to 256 channels, the lack of an independent means of measuring the abnormal brain activity has limited the validation of source localisation methods. The advent of safe and high-quality EEG recording inside the MRI scanner has given us the tools necessary to compare BOLD image contrast and EEG-derived localisation information (Ives et al., 1993; Lemieux et

al., 1997; Allen et al., 1998). EEG-triggered fMRI, where the fMRI data is acquired at a fixed interval following events of interest (e.g. epileptiform spikes) and 'rest' periods, has already demonstrated the usefulness of EEG/fMRI in the investigation of epilepsy (Warach et al., 1996; Krakow et al., 1999b). However, it suffers from two main limitations, both linked to the obliteration of the EEG during the image acquisition. First, there are constraints on the scanning rate and the duration of each scan: the minimum time gap between successive image acquisitions must be of the order of 15 seconds (for 1.5 tesla scanners) in order to avoid signal variations due to T1 signal decay and the maximum duration of each image acquisition must be less than the expected duration of the BOLD response in order to ensure proper separation of the responses from events which may occur during image acquisition, and therefore be undetected. These limits on the scan acquisition parameters can also be expressed in terms of the spontaneous event ('spiking') rate, which highlights the implications for patient selection. The event rate must be low enough such that the mean separation between events is at least as large as the minimum scanning interval (~15 seconds) to avoid the effects of undetected events (due to EEG obliteration) but also high enough to allow acquisition of sufficient image data in a 45-minute period[1]. Second, the spike-triggered approach relies on assumptions about the BOLD response peak time and duration; in our experimental design we assumed that the BOLD response to spikes peaks around 5 seconds and has returned to baseline 15 seconds post-event for all spikes and in all subjects. Given the difficulty of measuring the temporal characteristics of the HRF associated with spikes using the triggered approach, there is uncertainty about the optimality of this model. Given these limitations, larger studies have found BOLD activations associated with interictal spikes in approximately 50% of the patients studied (Krakow et al., 1999b).

Recently, a new system capable of recording good quality EEG throughout the fMRI

[1] Patient discomfort and movement can become significant factors after 45-60 minutes.

acquisition through removal of a well-characterised image acquisition artifact was described (Allen et al., 2000). This method should enable the identification of all EEG events and the use of a more sophisticated event-related fMRI approach by allowing the acquisition of images at random time-lags in relation to the EEG events of interest (Josephs et al., 1997). As discussed by Aguirre et al. (1998), precise knowledge of the HRF in individual subjects and experimental conditions is an important factor in the optimal acquisition and analysis of event-related fMRI. Therefore, the initial aim of this study was to illustrate how the shape of the HRF associated with epileptiform discharges can be characterised.

In this section, the initial imaging findings from the first experiment with continuous EEG/fMRI and event-related analysis of epileptic events are summarised.

Methods

Patient and Data

The study was performed on a 50-year-old patient with intractable partial and secondary generalised seizures (patient 1, *table 2*). This patient was studied because previous spike-triggered fMRI studies had revealed consistent BOLD activations, in agreement with previous electroclinical findings (Krakow et al., 1999b, Krakow et al., 2001c).

Continuous EEG/fMRI

The EEG recording was performed as described in section 4.1. On-line pulse and imaging artifact removal was used to monitor the EEG during the experiment (Allen et al., 2000, *figures 5 and 29*). In summary, the EEG acquisition system uses careful design of filtering and gain sections of the EEG amplifier to avoid saturation during image acquisition, digitisation at 5000 Hz of EEG data and a scanner generated slice-timing pulse. For each channel, online subtraction of a running time-averaged waveform

(synchronised with the slice-timing pulse) is followed by adaptive noise cancellation and a running time-averaged EEG signal synchronised to the ECG is subtracted to remove the pulse induced artifact (Allen et al., 1998). Validation was based on comparative spectral analysis and accuracy of the identification of separately recorded spike-wave complexes (median amplitude: 74 μV) added to EEG recorded in five subjects (Allen et al., 2000).

The experiment was conducted on a 2 tesla MRI scanner (Siemens Magnetom Vision; Siemens, Erlangen, Germany). 1200 volumes each consisting of 20 axial slices (1.8 mm thick, 1.2 mm gap; TE: 40 ms; TR/slice: 76 ms; FOV: 192 mm; 64x64 image matrix) were acquired continuously over a period of 30 min 24 sec. The BOLD echo-planar images were registered to the T1 volume using SPM99 for visualisation purposes (Ashburner et al., 1997).

EEG and fMRI Analysis

The EEG recording was examined retrospectively to identify spike and sharp wave complexes and record the corresponding fMRI slice number (from the slice pulse channel; range: 1 to 24000).

The fMRI data were realigned, spatially normalised and smoothed (Gaussian kernel; FWHM: 6 mm) using SPM99 (Friston, 1995; Ashburner and Friston, 1999). The fMRI event slice number was then used as input for an event-related analysis of the time course of BOLD activation using a windowed Fourier expansion (8 sines, 8 cosines, plus constant term; window width = 64 sec) and the resulting SPM{F} was thresholded at $p<0.001$ (uncorrected) (Josephs et al., 1997).

Results

In the EEG, background activity was observed that was lesser on the left with irregular

theta-delta activity (3-6 Hz) and predominant alpha activity (8 Hz) over the right. There were frequent IED maximal over the left temporal region. Of these, high amplitude stereotyped sharp waves (>200μV) with phase reversal over electrode position T3 (left mid-temporal) were the most prominent feature. Thirty-seven of these were identified by an expert observer in the entire recording (mean inter-spike interval was 51 seconds), labelled and used for the fMRI analysis. *Figure 30* illustrates an EEG segment recorded inside the scanner during fMRI and shows a typical spike and slow wave complex. The thresholded SPM{F} revealed an activation located in the left temporal region similar to the activation previously obtained using the spike-triggered method, as shown in *figure 31*. *Figure 10* shows the result of the experiment using spike-triggered fMRI in the same patient (see section 4.1). The *Z* score for the maximum activation was 7.1. For the continuous EEG/fMRI experiment the F ratio of the highlighted (maximum) voxel is 5.23 ($P_{corrected} = 0.001$).

The time course of the activation at the maximum activation voxel (highlighted in *figure 31*) peaks at approximately 9 seconds post-spike (*figure 32*).

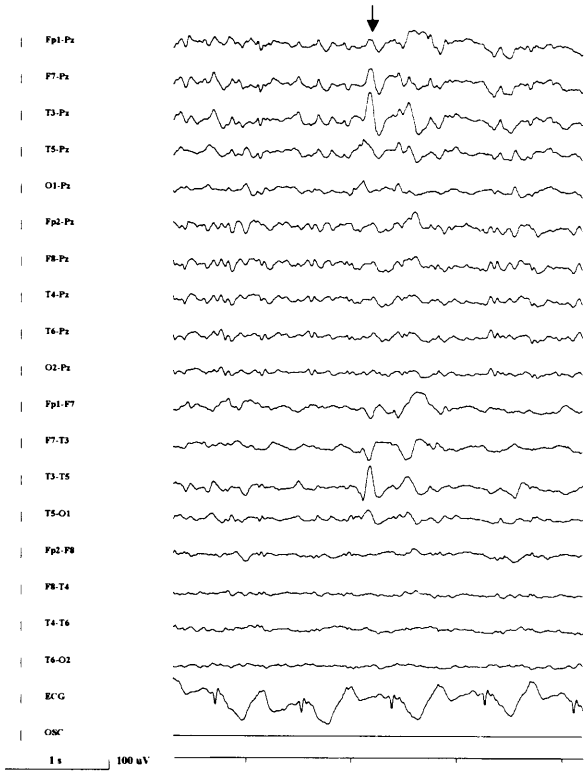

Figure 30: *An EEG section recorded inside the MR scanner, showing a typical spike of patient 1 (table2). The upper 10 traces show a referential montage, the lower traces a bipolar montage of bitemporal chains, the ECG (used for pulse artifact subtraction), which is distorted due to the static magnetic field, and the slice acquisition pulses (used for image acquisition artifact subtraction and EEG/fMRI synchronisation). The section above was recorded before the start of the fMRI acquisition, with pulse artifact subtraction. The section on the next page was recorded during the fMRI acquisition, with pulse and image acquisition artifact subtraction. Both sections show a typical epileptiform discharge with phase reversal over T3 (indicated by the arrow; peak-to-peak amplitude ~200 μV). There is an asymmetry of the background activity, with irregular slow activity on the left.*

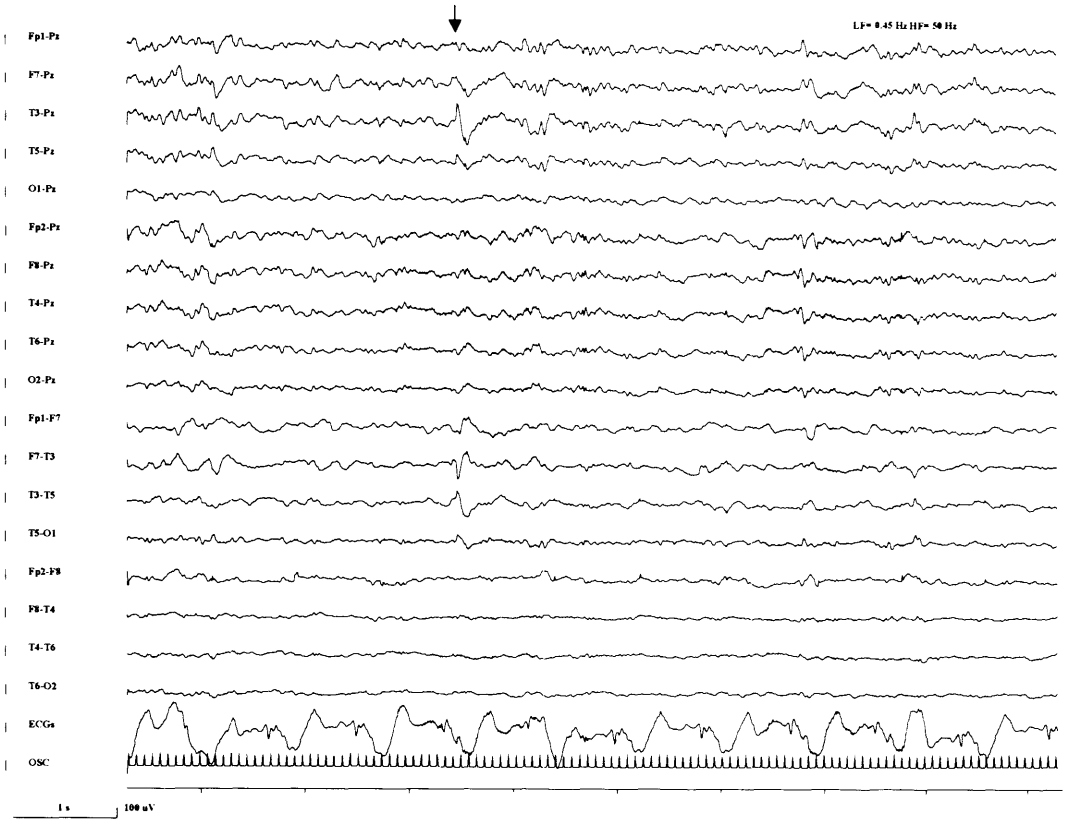

Discussion and Conclusions

In this study an event-related fMRI analysis of EEG events from continuous and simultaneous EEG/fMRI acquisition was performed for the first time to obtain spatio-temporal patterns of activation (Lemieux et al., 2001a).

The BOLD activation derived from these data was concordant with previous scalp and intracranial EEG findings, as well as results from previous fMRI studies obtained using spike-triggered EEG/fMRI. This result tends to reinforce the confidence in the method's capacity to provide good quality EEG. Regarding the difference in the appearance of the activations derived from the two techniques, these can result from a combination of the following methodological and biological factors: First, variability of the EEG events between the experiments, which is always a possible limitation of repeated studies. However, there were no significant changes in the patient's EEG pattern noted throughout the period spanning the spike-triggered fMRI and continuous EEG/fMRI

experiments, as illustrated in *figures 10* and *31*. Second, and perhaps most importantly, the nature of the questions answered by the analysis is different between the two methods. In the spike-triggered approach, the question is: "which voxels show a significant signal increase between 'rest' and 'activation' images?" and is expressed as a *t* test. This is in contrast to the event-related approach demonstrated here to measure the shape of the HRF, for which our questions are: "which voxels show a pattern of signal change that is consistent across events and that explains a sufficient proportion of the signal variance?", expressed as a F-ratio, and "what is this pattern?". Therefore, the extent and significance of the derived activations for the two types of data are not directly comparable. Although an event-related approach can also be used to address the first type of question, this would require the assumption of a specific form for the HRF (Aguirre et al., 1998). As noted previously this study is part of the current efforts of characterizing the shape of the HRF for IED in order to derive an optimal experimental strategy.

The time-course of the BOLD activation was consistent with the characteristic shape of the expected physiological HRF (Aguirre et al., 1998). In particular, the observed response is consistent with a peak at 5-9 seconds latency followed by an under-shoot. This knowledge, combined with the fact that the maximum amount of data is acquired in a given total experiment time, should lead to improved sensitivity and efficiency of EEG/fMRI experiments (Dale et al., 1999).

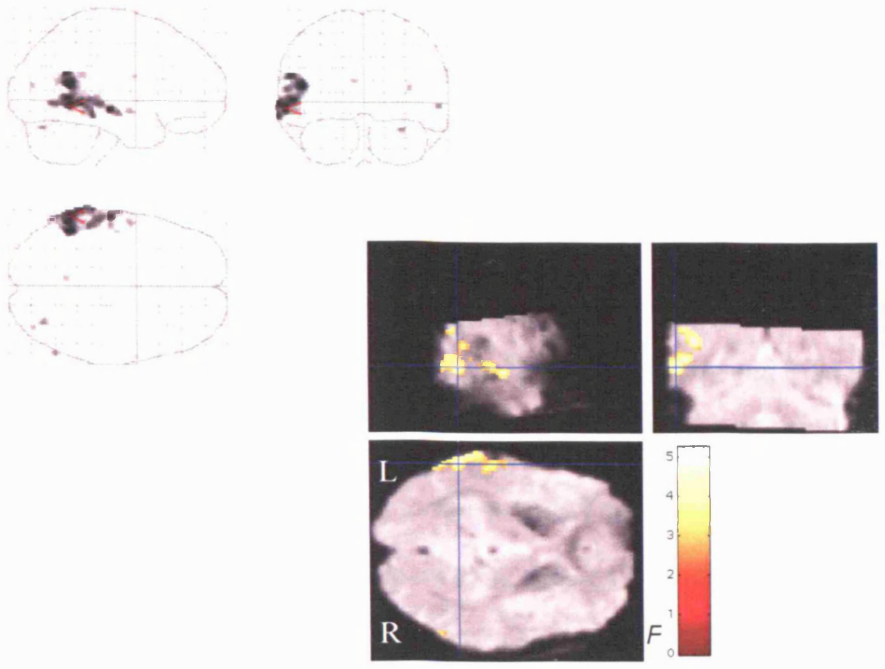

Figure 31: *SPM{F} of the spike-related events in the continuous EEG/fMRI experiment. Highlighted cluster projected onto orthogonal slices of the mean EPI, showing activation localisation in the left temporal lobe.*

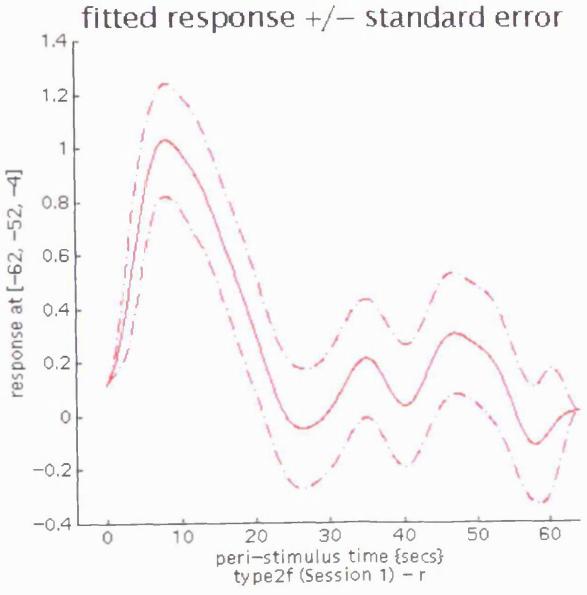

Figure 32: *Time course of the BOLS response at the highlighted voxel (cross hairs at figure 31). The response is expressed as a percentage of the mean whole brain signal.*

Chapter 8

Summary of the main findings

This thesis describes the technique of EEG-correlated fMRI and the application of this method to patients with epilepsy. Since the first report on EEG recordings inside a MR scanner more than a decade ago (Ives et al., 1993), important technical improvements have been achieved with respect to patient safety, EEG quality and MRI artifacts (Krakow et al., 2001a). Several of the landmark publications in these fields are included in this thesis. In particular, methods to remove EEG artifacts which occur inevitably on EEG recordings in the MR environment have enabled a wider application of the method to study pathological and physiological brain function. A first milestone was a method to remove pulse artifact on-line from intra-MR EEG recordings (Allen et al., 1998). This made the reliable on-line detection of EEG-events (e.g. epileptic spikes) possible and thus enabled *spike-triggered fMRI* experiments. In this approach, the EEG is observed on-line during the experiment and fMRI acquisitions are triggered manually with a defined temporal delay after an EEG event of interest occurs. More recently, methods for removing the image acquisition artifact were introduced (Allen et al., 2000), which permit simultaneous und continuous EEG/fMRI. This technique is likely to replace EEG-triggered fMRI for most applications if it becomes broadly available (Lemieux et al., 2001a). By recording all events during an experiment, simultaneous und continuous EEG/fMRI makes it possible for the first time to exploit the full power of both modalities. Therefore, the applicability of EEG/fMRI will be enhanced by expanding the spectrum and frequency of events that can be acquired and analysed. The availability of continuous EEG and fMRI data will allow the study of the relationship between the BOLD response on the one hand and the morphology (amplitude, duration, etc.) and relative timing of EEG events on the other (event interaction effects (Friston et al., 1998)). Furthermore, it may be possible to study propagation effects by exploiting

the ability of event-related fMRI to provide a superior temporal resolution to scanning repetition time (Josephs et al., 1997).

So far, the development of EEG-correlated fMRI was mainly expedited by epilepsy research groups. Their motivation was the necessity for further non-invasive diagnostic tools to localise epileptic activity in patients with focal epilepsy, in particular in patients undergoing presurgical evaluation. The available diagnostic methods are either invasive (intracranial EEG recordings) or expensive (video-EEG-telemetry), or both, and in many patients the results are ambiguous. Therefore, a method to identify brain activity non-invasively with high spatial and sufficient temporal resolution has the potential to add valuable information to the diagnostic work-up of patients with epilepsy.

From the functional imaging methods routinely applied to epileptic patients, PET and SPECT, it is well known that ictal epileptic activity leads to an increased blood flow and metabolism. The same can be presumed for interictal epileptic activity, although this phenomenon cannot be studied by these methods due to their low temporal resolution. In 1988, it was shown for the first time that also MRI is sensitive to abnormal perfusion associated with ictal activity (Fish et al., 1988). In the following years, BOLD fMRI was used to study epileptic seizures in a few case report studies (Jackson et al., 1994, Detre et al., 1995, Warach et al., 1996, Salek-Haddadi et al., 2002). However, for technical and methodological reasons, ictal fMRI will be restricted to exceptional cases (Salek-Haddadi et al., 2002).

The first case study on imaging interictal epileptiform activity using EEG-triggered BOLD-fMRI was reported by Warach et al. in 1996. In the following years, the ability of EEG-triggered fMRI to identify generators of interictal epileptiform activity was confirmed by various research groups. In chapter 5, the so far largest study on EEG-triggered fMRI in patients with focal epilepsy is presented. In 24 consecutive patients, fMRI acquisitions were manually triggered after IED and periods of EEG without

epileptiform activity. Using SPM, cortical activations corresponding to the presumed generators of the IED could be identified in twelve out of the 24 patients. In the remaining patients no significant activation (n = 10) was present, or the activation did not correspond to the presumed epileptic focus (n = 2). The relative high percentage of negative results hinders so far the wider clinical application of EEG-correlated fMRI. However, in selected patients this technique has the potential to be useful in the presurgical workup of patients with medically refractory focal seizures. The basis for successful epilepsy surgery is accurate localisation of the epileptogenic zone is (Lüders et al., 1993). This information is derived from the convergence of diverse investigations. In some patients, particularly with neocortical cryptogenic epilepsy, additional intracranial EEG recordings often have to be applied to reliably identify the epileptic focus. EEG-correlated fMRI might have the potential to replace invasive techniques in selected patients or, at least, provide additional information to guide the placement of invasive intracranial electrodes where necessary. However, in a clinical interpretation it has to be considered that the source of interictal discharges (irritative zone) is not identical with the seizure onset zone or the epileptogenic zone (Alarcon et al., 1994). Before EEG-triggered fMRI can be used as a decisive method in the presurgical assessment, further studies are needed to determine the types of epilepsy in which this technique can effectively identify the seizure onset zone. This needs comparison of fMRI results with extra-/intracranial ictal video-EEG telemetry and surgical outcome in relation to resection of the activated area. Technical improvements in EEG/fMRI may allow more detailed analysis of the characteristics of the BOLD signal change. It will be of particular interest to investigate spike-related BOLD signal changes identified from areas within the epileptogenic zone compared to propagated spikes.

In another study (chapter 5.2) it was demonstrated that in selected patients individual (as opposed to averaged) focal IED can be associated with hemodynamic changes detectable with fMRI. In the patient studied, 15 out of 43 spikes (34.9%) were associated with a significant fMRI activation showing co-localisation with the result of the averaged data and the area of spiking cortex previously identified with electrocorticography. Only examination of single hemodynamic responses provides information about the unique aspects of an individual event. In spike-triggered fMRI this is of particular interest for several reasons:

1. It allows study of the relation between the morphology of individual EEG events and the hemodynamic response provided by fMRI. Thus, the question whether characteristics like amplitude or waveform of individual spikes influence the fMRI activation can be addressed.

2. It can help to reveal variable localisation of spike generators, which is of particular importance in patients with multifocal spikes.

3. Recording multichannel EEG inside the MR scanner would allow EEG source modelling of individual spikes and comparison of the solutions with the fMRI activation. Waveform-variability is a common problem in the averaging of apparently similar spikes and can introduce localisation errors (Michel et al., 1999). Cortical activations identified with single spike-triggered fMRI would allow constraints to be placed on source modelling of individual spikes and thus improving EEG modelling.

4. It provides confidence that signal-to-noise characteristics of spike-triggered fMRI is sufficient to apply this method also to epilepsy patients who have infrequent interictal spikes, which has implications for experimental design and patient selection criteria.

Chapter 6 of this thesis gives examples of combination of EEG-correlated fMRI with other modalities to obtain complementary information on interictal epileptiform activity or epileptic foci. A study compared spike-triggered fMRI activation maps with solutions

of EEG source analysis based on 64-channel scalp EEG recorded in a separate session outside the MR scanner. The BOLD and structural images were coregistered, allowing the measurement of distances between the generator models and BOLD activation(s). Six patients were studied. In all cases dipole models could be found that explained a sufficient amount of the data and that were anatomically concordant with the BOLD activation. The overall mean distance between the main moving dipole and the centre of the nearest BOLD activation was 3.5 and 2.2 cm for the negative and positive peaks, respectively. It is discussed why solutions of source analysis derived from scalp EEG and BOLD changes are not expected to agree completely, and potential causes of the discrepancy are given. However, the degree of agreement between the BOLD and the EEG source localisation indicates that the combination of these techniques offers the possibility of advancing the study of the generators of epileptiform electrical activity. In a further case report study, the combination of spike-triggered fMRI with other MRI-modalities like diffusion tensor imaging and chemical shift imaging is demonstrated. This multi-modal MR imaging allows the identification of brain regions, which show an abnormal micro-organisation and are involved in generating epileptiform activity, thus providing complementary information to structural MR images of localisation-related epilepsy.

In chapter 7, further applications and future developments of EEG-correlated fMRI are discussed. The investigation of physiological EEG events or rhythms and the simultaneous recording of evoked potentials and fMRI data are presented as potential fields of interest for EEG/fMRI experiments. Furthermore, EEG-correlated fMRI might be a useful technique to investigate the effect of changes of vigilance or sleep on cognitive tasks. In this context, an fMRI study on auditory processing is presented, in which a concurrent EEG recording was used to monitor vigilance and sleep stages. In this study it could be demonstrated that the sleeping brain is able to process auditory

stimuli. In addition, the existence of a functional network capable of detecting and facilitating processing of emotionally- relevant inputs during sleep was postulated. Understanding how sensory stimuli are processed in a state of reduced consciousness might be of general interest as it might help to comprehend how residual cognitive activity operates during states of 'unconsciousness' other than sleep (e.g. anaesthesia or comatose states).

Finally, the initial imaging findings with the technique for the simultaneous and continuous acquisition of fMRI and EEG data are presented as an outlook to the future potential of EEG-correlated fMRI.

In conclusion, the fundamental technical problems of EEG-correlated fMRI have been largely solved. It is now possible to record safely a high quality EEG inside the MR scanner without compromising the MR signal. EEG-correlated fMRI has proved useful to provide insights into the generation of epileptiform activity in patients with focal epilepsy. In selected patients with frequent IED, EEG-correlated fMRI has the potential to reproducibly indentify cortical areas involved in generating IED, i.e. the irritative zone. So far, the sensitivity of the method is in the range of 50%. To determine the specificity of the method, further studies are necessary to compare the EEG/fMRI results with the diagnostic gold standards, which are intracranial EEG recordings and postoperative outcome after epilepsy surgery. Until these results are available, the utility of EEG-correlated fMRI in clinical epileptology cannot be definitely determined. However, the recently introduced methodology of simultaneous and continuous EEG-correlated fMRI is likely to enable further applications in different areas of functional neuroimaging, e.g. studying the effects of vigilance and sleep on brain metabolism and cognitive processes.

References

Aguirre GK, Zarahn E, D'Esposito M. The variability of human, BOLD hemodynamic responses. Neuroimage 1998;8:360-369.

Aguirre GK, D'Esposito M. Experimental design for brain fMRI. In: Moonen CTW, Bandettini PA, editors. Functional MRI. Berlin: Springer, 2000:369-380.

Alarcon G, Guy CN, Binnie CD, Walker SR, Elwes RDC, Polkey CE. Intracerebral propagation of interictal activity in partial epilepsy: implications for source localisation. J Neurol Neurosurg Psych 1994;57:435-459.

Aldenkamp, AP. Effect of seizures and epileptiform discharges on cognitive function. Epilepsia 1997;38(Suppl. 1):52-55.

Allen PJ, Polizzi G, Krakow K, Fish DR, Lemieux L. Identification of EEG events in the MR scanner: the problem of pulse artifact and a method for its subtraction. Neuroimage 1998;8:229-239.

Allen PJ, Josephs O, Turner R. A method for removing imaging artifact from continuous EEG recorded during functional MRI. Neuroimage 2000;12:230-239.

Amadeo M, Shagass C. Brief latency click-evoked potentials during waking and sleep in man. Psychophysiol 1973;10:244-250.

Amaral DG, Price JL, Pitkanen A, Carmichael ST. In: The amygdala: Neurobiological Aspects of Emotion, Memory, and Mental Dysfunction. Aggleton JP, editor. New York: Wiley, 1992:1-66.

Annegers JF, Rocca WA, Hauser WA. Causes of epilepsy: contributions of the Rochester epidemiology project. Mayo Clin Proc 1996;71:570-575.

Armony JL, LeDoux JE. In: The new cognitive neurosciences. Gazzaniga MS, editor. Cambridge, Massachussetts: The MIT press, 2000:1067-1079.

Ashburner J, Friston KJ. Multimodal image coregistration and partitioning – a unified framework. Neuroimage 1997;6:209-217.

Ashburner J, Friston, KJ. Nonlinear spatial normalization using basis functions. Hum Brain Mapp 1999;7:254-266.

Ashburner J, Friston KJ. Image registration. In: Moonen CTW, Bandettini PA, editors. Functional MRI. Berlin: Springer, 2000: 285-299.

Ashburner J, Friston KJ. Voxel-based morphometry-the methods. Neuroimage 2000;11:805-821.

Ashburner J, Neelin P, Collins DL, Evans AC, Friston KJ. Incorporating prior knowledge into image registration. Neuroimage 1997;6:344-352.

Awad IA, Rosenfeld J, Ahl J, Hahn JF, Lüders H. Intractable epilepsy and structural lesions of the brain: mapping, resection strategies, and seizure outcome. Epilepsia 1991;32:179-186.

Bandettini PA, Wong EC, Hinks RS, Tikofsky RS, Hyde JS. Time course EPI of human brain function during task activation. Magn Reson Med 25;1992:390.

Bartenstein PA, Duncan JS, Prevett MC, Cunningham VJ, Fish DR, Jones AK, Luthra SK, Sawle GV, Brooks DJ. Investigation of the opioid system in absence seizures with positron emission tomography. J Neurol Neurosurg Psychiatry 1993;56:1295-1302.

Basser PJ, Pierpaoli C. Microstructural and physiological features of tissues elucidated by quantitative-diffusion-tensor MRI. J Magn Reson B 1996;111:209-219.

Bastos AC, Comeau RM, Andermann F, Melanson D, Cendes F, Dubeau F et al. Diagnosis of subtle focal dysplastic lesion: curvilinear reformatting from three-dimensional magnetic resonance imaging. Ann Neurol 1999;46:88-94.

Bastuji H, Garcia Larrea L, Bertrand O, Mauguiere F. BAEP latency changes during nocturnal sleep are not correlated with sleep states but with body temperature variations. Electroencephalogr Clin Neurophysiol 1988;70:9-15.

Bastuji H, Garcia Larrea L, Franc C, Mauguiere F. Brain processing of stimulus deviance during slow-wave and paradoxical sleep: a study of human auditory evoked responses using the oddball paradigm. J. Clin Neurophysiol 1995;12:155-167.

Bellgowan PSF, Binder JR, Swanson SJ, Hammeke TA, Springer JA, Frost JA, Mueller WM, Morris GL. Lateralization of seizure focus predicts activation of the left medial temporal lobe during semantic information encoding: an fMRI study. Neurology 51;1998:479-484.

Bergen D, Bleck T, Ramsey R, Clasen R, Ristanovic R, Smith M, Whisler WW. Magnetic resonance imaging as a sensitive and specific predictor of neoplasms removed for intractable epilepsy. Epilepsia 30;1989:318-321.

Berger H. Über das Electrekephalogramm des Menschen. Arch Psychiat Nervenkrankh 1929;87:527-570.

Berkovic SF, Andermann F, Olivier A, Ethier R, Melanson D, Robitaille Y, Kuzniecky R, Peters T, Feindel W. Hippocampal sclerosis in temporal lobe epilepsy demonstrated by magnetic resonance imaging. Ann Neurol 1991;29:175-182.

Berkovic SF, Newton MR, Chiron C, Dulac O. Single photon emission tomography. In: Engel J Jr, editor. Surgical Treatment of the Epilepsies. 2nd ed. New York: Raven Press, 1993:233–243.

Berkovic SF, Newton MR. Single photon emission tomography. In: Engel J Jr, Pedley TA, editors. Epilepsy. A comprehensive textbook. Philadelphia: Lippincott-Raven, 1998: Chapter 82.

Berlad I, Pratt H. P300 in response to the subject's own name. Electroenceph Clin Neurophysiol 1995;96:472-474.

Biersack HJ, Reichmann K, Winkler C, Stefan H, Kuhnen K, Bulau P, Penin H, Tyrell DA, Neirinckx RD, Gruner KR. 99mTc-labelled hexamethylpropyleneamine oxime photon emission scans in epilepsy. Lancet 1985;2(8469-84970):1436–1437.

Binder JR, Rao SM, Hammeke TA, Frost TA, Bandettini PA, Jesmanowicz A, Hyde JS. Lateralizes human brain language systems demonstrated by task subtraction functional magnetic resonance imaging. Arch Neurology 52;1995:593-601.

Binder JR, Swanson SJ, Hammeke TA, Morris GL, Mueller WM, Fischer M, Benbabis S, Frost JA, Rao SM, Haughton VM. Determination of language dominance using functional MRI: a comparison with the Wada test. Neurology 46;1996:978-894.

Binder JR, Frost JA, Hammeke TA, Cox RW, Rao SM, Prieto T. Human brain language areas identified by functional imaging J Neuroscience 1997;17:353-362.

Binnie CD. Seizures, EEG discharges and cognition. In: Trimble MR, Reynolds EH, editors. Epilepsy, behaviour and cognitive function. New York: Wiley & Sons, 1987: 45-51.

Bonmassar G, Anami K, Ives J, Belliveau JW. Visual evoked potential (VEP) measured by simultaneous 64-channel EEG and 3T fMRI. Neuroreport 1999;10:1893-1897.

Bookheimer S, Dapretto M, Cohen M, Wang J, Small G. Functional MRI of the hippocampus during short term memory tasks: parametric responses to task difficulty and stimulus novelty. Neuroimage 4;1996:531.

Brain R. The physiological basis of consciousness. Brain 1958;81:426-455.

Brown BH, Johnson SG, Betts RP, Henry L. Burns thresholds to radio frequency leakage currents from surgical diathermy equipment. J Med Eng Technol 1977;1:277-281.

Brown TR, Goldstein B, Little J. Severe burns resulting from magnetic resonance imaging with cardiopulmonary monitoring. Risks and relevant safety precautions. Am J Phys Med Rehabil 1993;72:166-167.

Brualla J, Romero MF, Serrano M, Valdizan JR. Auditory event-related potentials to semantic priming during sleep. Electroencephalogr Clin Neurophysiol 1998;108:283-290.

Buchwald JS, Hinman C, Norman RJ, Huang CM, Brown KA. Middle- and long-latency auditory evoked responses recorded from the vertex of normal and chronically lesioned cats. Brain Res 1981;205:91-109.

Buchwald JS. Generators. In: Bases of auditory brainstem evoked responses. Grune and Stratton, editors. New York, 1983:157-195.

Bullmore E, Brammer M, Williams SCR. Statistical methods of estimation and inference for functional MR image analysis. Mag Res Med 1996;35:261-277.

Burton SA, Harsh JR, Badia P. Cognititve activity in sleep and responsiveness to external stimuli. Sleep 1988;11:61-68.

Carskadon MA, Dement WC. Normal human sleep: an overview. In: Principles and practice of sleep Medicine. Kryger, Roth, Dement, editors. Philadelphia: Saunders, 1994:6-25.

Cascino GD, Hirschhorn KA, Jack CR, Sharbrough FW. Gadolinium-DTPA-enhanced magnetic resonance imaging in intractable partial epilepsy. Neurology 1989;39:1115-1118.

Cascino GD, Jack CR, Parisi JE, Sharbrough FW, Hirschhorn KA, Meyer FB, Marsh WR, O'Brien PC. Magnetic resonance imaging-based volume studies in temporal lobe epilepsy: pathological correlations. Ann Neurol 1991;30:31-36.

Cascino GD. Commentary: how has neuroimaging improved patient care? Epilepsia 1994;35(Suppl. 6):S103-107.

Celesia GC, Puletti F. Auditory cortical areas of man. Neurology 1969;19:211-220.

Cendes F, Andermann F, Dubeau F, Matthews PM, Arnold DL. Normalization of neuronal metabolic dysfunction after surgery for temporal lobe epilepsy - evidence from proton MR spectroscopic imaging. Neurology 1997;49:1525-1533.

Cendes F, Stanley JA, Dubeau F, Andermann F, Arnold DL. Proton magnetic resonance spectroscopic imaging for discrimination of absence and complex partial seizures. Ann Neurol 1997;41:74-81.

Chan S, Chin SS, Nordli DR, Goodman RR, DeLaPaz RL, Pedley TA. Prospective magnetic resonance imaging identification of focal cortical dysplasia, including the non-balloon cell subtype. Ann Neurol 1998;44:749-759.

Chee MW, Low S, Tan JS, Lim W, Wong J. Hippocampal volumetry with magnetic resonance imaging: a cost-effective validated solution. Epilepsia 1997;38:461-465.

Chen CN, Hoult DI. Biomedical Magnetic Resonance Technology. Bristol: Adam Hilger, 1989.

Chen W, Ogawa S. Principles of BOLD functional MRI. In: Moonen CTW, Bandettini PA, editors. Functional MRI. Springer: Berlin, 2000:103-113.

Cheon JE, Chang KH, Kim HD, Han MH, Hong SH, Seong SO Kim JO, Lee SG, Hwang YS, Kim HJ. MR of hippocampal sclerosis: comparison of qualitative and quantitative assessments. Am J Neuroradiol 1998;19:456-468.

Chiappa KH. Brainstem auditory evoked potentials in clinical neurology. Adv Neurol 1982;32:157-158.

Chinvarun Y, Newton MR, Berlangieri SU, McKay WJ, Berkovic SF. Extratemporal epilepsy: comparison of ictal SPECT and interictal FDG-PET. Epilepsia 1996;37(Suppl. 5):124.

Chu WJ, Hetherington HP, Kuzniecky RJ, Vaughan JT, Twieg DB, Faught RE, Gilliam FG, Hugg JW, Elgavish GA. Is the intracellular pH different from normal in the epileptic focus of patients with temporal lobe epilepsy? A 31P NMR study. Neurology 1996;47:756-760.

Cohen D, Cuffin BN, Yunokuchi K. MEG versus EEG localization test using implanted sources in the human brain. Ann Neurol 1990;28:811-817.

Cohen MS. Parametric analysis of fMRI data using linear systems methods. Neuroimage 1997;6:93-103.

Cohen MS, Goldman RI, Stern J, Engel JJr. Simultaneous EEG and fMRI made easy. Neuroimage 2001;13:S6.

Connelly A, Jackson GD, Duncan JS, King MD, Gadian DG. Magnetic resonance spectroscopy in temporal lobe epilepsy. Neurology 1994;44:1411-1417.

Constantinidis I. MRS Methodology. Adv Neurol 2000;83:235-246.

Cote KA, Campbell KB. P300 to high intensity stimuli during REM sleep. Clin Neurophysiol 1999;110:1345-1350.

Dale AM, Greve DN, Burock MA. Optimal stimulus sequences for event-related fMRI. Neuroimage 1999;9:S33.

Deiber MP, Ibanez V, Bastuji H, Fischer C, Mauguiere F. Changes of middle latency auditory evoked potentials during natural sleep in humans. Neurology 1989;39:806-813.

Detre JA, Sirven JI, Alsop DC, O'Connor MJ, French JA. Localization of subclinical ictal activity by functional magnetic resonance imaging: Correlation with invasive monitoring. Ann Neurol 1995;38:618-624.

Detre JA, Alsop DC, Aguirre GK, Sperling MR. Coupling of cortical and thalamic ictal activity in human partial epilepsy: demonstration by functional magnetic resonance imaging. Epilepsia 1996;37:657-661.

Disbrow, EA, Slutsky DA, Roberts TPL, Krubitzer LA. Functional MRI at 1.5 tesla: a comparison of the blood oxygenation level-dependent signal and electrophysiology. Proc Nat Acad Sci USA 2000;97:9718-9723.

Dodick DW, Cascino GD, Meyer FB. Vascular malformations and intractable epilepsy: outcome after surgical treatment. Mayo Clin Proc 1994;69:741–745.

Donchin E, Heffley E, Hillyard SA, Loveless N, Maltzman I, Ohman A, Rosler F, Ruchkin D, Siddle D. Cognition and event-related potentials. II. The orienting reflex and P300. Ann NY Acad Sci 1984;425:39-57.

Duckwiler GR, Levesque M, Wilson CL, Behnke E, Babb TL, Lufkin R. Imaging of MR-compatible intracerebral depth electrodes. Am J Neuroradiol 1990;11:353-354.

Duncan JS. Imaging and epilepsy. Brain 1997;120:339-377.

Duncan R, Patterson J, Hadley DM, Wyper DJ, McGeorge AP, Bone I. Tc99m HM-PAO single photon emission computed tomography in temporal lobe epilepsy. Acta Neurol Scand 1990;81:287–93.

Duncan R, Patterson J, Roberts R, Hadley DM, Bone I. Ictal/postictal SPECT in the presurgical localisation of complex partial seizures. J Neurol Neurosurg Psychiatry 1993;56:141–148.

Ebersole JS, Wade PB. Spike voltage topography identifies two types of fronto-temporal epileptic foci. Neurology 1991;41:1425-1433.

Ebersole JS. EEG and MEG dipole source modeling. In: Engel J Jr, Pedley TA, editors. Epilepsy. A comprehensive textbook. Philadelphia: Lippincott-Raven, 1998:919-935.

Emerson RG, Pedley TA. Electroencephalography and evoked potentials. In: Bradley WG, Daroff RB, Fenichel GM, Marsden CD, editors. Neurology in Clinical Practice. Boston: Butterworth Heinemann, 2000:473-496.

Engel J Jr, Kuhl DE, Phelps ME. Patterns of human local cerebral glucose metabolism during epileptic seizures. Science 1982;218:64–66.

Engel J Jr, Kuhl DE, Phelps ME, Rausch R, Nuwer M. Local cerebral metabolism during partial seizures. Neurology 1983;33:400–413.

Engel J Jr, Lubens P, Kuhl DE, Phelps ME. Local cerebral metabolic rate for glucose during petit mal absences. Ann Neurol 1985;17:121–128.

Engel J Jr, Ochs RF, Gloor P. Metabolic studies of generalized epilepsy. In: Avoli M, Gloor P, Kostopoulos G, Naguet R, editors. Generalized Epilepsy. Cambridge, MA: Birkhauser, 1990:387–396.

Engel J Jr, Kuhl DE, Phelps DE, Crandall PH. Comparative localization of epileptic foci in partial epilepsy by PCT and EEG. Ann Neurol 1982;12:529-537.

Engel J Jr, Kuhl DE, Phelps ME, Rausch R, Nuwer M. Local cerebral metabolism during partial seizures. Neurology 1983;33:400-413.

Engel J Jr, Pedley TA, editors. Epilepsy. A comprehensive textbook. Philadelphia: Lippincott-Raven, 1998, Vol. I, Chapter 79: 919-935.

Engel J Jr. Overview of functional neuroimaging in epilepsy. Advances in Neurology 2000;83:1-9.

Erwin R, Buchwald JS. Midlatency auditory evoked responses: differential effects of sleep in the human. Electroencephalogr Clin Neurophysiol 1986;165:383-392.

Evans AC, Collins DL, Mills SR, Brown ED, Kelly RL, Peters TM. 3d statistical neuroanatomical models from 305 MRI volumes. Nuclear science symposium and medical imaging conference, vols 1-3, IEEE Conference Record, Klaisner LA, editor. San Francisco, 1993:1813-1817.

Evans AC, Kamber M, Collins DL, Macdonald D. An MRI-based probabilistic atlas of neuroanatomy. In: Magnetic resonance scanning and epilepsy. Shorvon S, Fish D, Andermann F, Bydder GM, Stefan H, editors. New York: Plenum Press, 1994:263-274.

Falk D, Hildebolt C, Cheverud J, Kohn LA, Figiel G, Vannier M. Human cortical asymmetries determined with 3D MR technology. J Neurosci Methods 1991;39:185-191.

Felblinger J, Müri RM, Rösler KM, Jung B, Hess CW, Boesch C. EEG and visually evoked potential recordings in the MR environment. Proc Int Soc Magn Res in Medicine 1997;3:1653.

Fischer C, Bognar L, Turjman F, Lapras C. Auditory evoked potentials in a patient with a unilateral lesion of the inferior colliculus and medial geniculate body. Electroencephalogr Clin Neurophysiol 1995;96:261-267.

Fischler I, Jin YS, Boaz TL, Perry NW Jr, Childers DG. Brain potentials related to seeing one's own name. Brain Lang 1987;30:245-262.

Fish DR, Brooks DJ, Young IR, Bydder GM. Use of magnetic resonance imaging to identify changes in cerebral blood flow in epilepsia partialis continua. Magn Reson Med 1988;8:238-240.

Frey KA. Positron emission tomography. In: Siegel GJ, Agranoff BW, Albers RW, Molinoff PB, editors. Basic Neurochemistry: Molecular, Cellular, and Medical Aspects, 5th ed. New York: Raven Press, 1994:935–955.

Friston KJ. Statistical parametric maps in functional imaging: a general linear approach. Hum Brain Map 1995;2:189-210.

Friston KJ, Ashburner J, Frith CD, Poline JB, Heather JD, Frackowiak RSJ. Spatial registration and normalization of images. Hum Brain Map 1995;2:1-25.

Friston K, Ashburner J, Frith C, Poline JB, Heather J, Frackowiak RSJ. Spatial realignement and normalization of images. Hum Brain Map 1995;2:165-189.

Friston KJ, Holmes AP, Poline J-B, Grasby PJ, Williams SCR, Frackowiak RSJ, Turner R. Analysis of fMRI time-series revisited. Neuroimage 1995;2:45-53.

Friston KJ, Holmes AP, Worsley KJ, Poline JB, Frith CD, Frackowiak RSJ. Statistical parametric maps in functional imaging: A general linear approach. Hum Brain Map 1995:2:189-210.

Friston KJ, Josephs O, Ress G, Turner R. Nonlinear event-related responses in fMRI. Magn Reson Med 1998;39:41-52.

Friston K, Worsley KJ, Frackowiak RSJ, Mazziotta JC, Evans, AC. Assessing the significance of focal activations using their spatial extent. Hum Brain Map 1994;1:214-220.

Frith CD, Friston K, Liddle PF, Frackowiak RS. Willed action and the prefrontal cortex in man: a study with PET. Proc R Soc London B Biol Sci 1991;244:241-246.

Fuchs M, Wagner M, Köhler T, Wischmann HA. Linear and nonlinear current density reconstructions. J Clin Neurophysiol 1999;16:267-295.

Gadian DG. Nuclear magnetic resonance and its application to living systems. New York: Oxford University Press, 1982.

Gadian DG, Connelly A, Duncan JS, Cross JH, Kirkham FJ, Johnson CL, Vargha-Khadem F, Nevile BG, Jackson GD. 1H magnetic resonance spectroscopy in the investigation of intractable epilepsy. Acta Neurol Scand (Suppl.) 1994;152:116-121.

Gaillard WD, Bhatia S, Bookheimer SY, Fazilat S, Sato S, Theodore WH. FDG-PET and volumetric MRI in the evaluation of patients with partial epilepsy. Neurology 1995;45:123-126.

Garcia PA, Laxer KD, van der Grond J, Hugg JW, Matson GB, Weiner MW. Phosphorus magnetic resonance spectroscopic imaging in patients with frontal lobe epilepsy. Ann Neurol 1994;35:217-221.

Garcia PA, Laxer KD, van der Grond J, Hugg JW, Matson GB, Weiner MW. Proton magnetic resonance spectroscopic imaging in patients with frontal lobe epilepsy. Ann Neurol 1995;37:279-281.

Giard MH, Perrin F, Pernier J, Peronnet F. Several attention-related wave forms in auditory areas: a topographic study. Electroenceph Clin Neurophysiol 1988;69:371-384.

Gilliam F, Bowling S, Bilir E, Thomas J, Faught E, Morawetz R, Palmer C, Hugg J, Kuzniecky R. Association of combined MRI, interictal EEG, and ictal EEG results with outcome and pathology after temporal lobectomy. Epilepsia 1997;38:1315-1320.

Goldman RI, Stern JM, Engel J Jr, Cohen MS. Acquiring simultaneous EEG and functional MRI. Clinical Neurophysiology 2000;111:1974-1980.

Goldman R, Stern J, Engel J Jr, Cohen M. Tomographic mapping of alpha rhythm using simultaneous EEG/fMRI. Neuroimage 2001;13:S1291.

Haglund MM, Berger MS, Kunkel DD, Franck JE, Ghatan S, Ojemann GA. Changes in gamma-aminobutyric acid and somatostatin in epileptic cortex associated with low-grade gliomas. J Neurosurg 1992;77:209-216.

Hajek M, Antonini A, Leenders KL, Wieser HG. Epilepsia partialis continua studied with PET. Epilepsy Res 1991;9:44–48.

Hajek M, Antonini A, Leenders KL, Wieser HG. Mesiobasal versus lateral temporal lobe epilepsy: metabolic differences in the temporal lobe shown by interictal 18F-FDG positron emission tomography. Neurology 1993;43:79–86.

Hajek M, Wieser HG, Khan N, Antonini A, Schrott PR, Maguire P, Beer HF, Leenders KL. Preoperative and postoperative glucose consumption in mesiobasal and lateral temporal lobe epilepsy. Neurology 1994;44:2125–2132.

Handforth A, Finch DM, Peters R, Tan AM, Treiman DM. Interictal spiking increases 2-deoxy[14C]glucose uptake and c-fos-like reactivity. Ann Neurol 1994;35:724–731.

Hannan AJ, Servotte S, Katsnelson A, Sisodiya S, Blakemore C, Squier M, Molnar Z. Characterization of nodular neuronal heterotopia in children. Brain 1999;122:219-238.

Hayes CE, Edelstein WA, Schenck JF, Mueller OM, Ash M. An efficient, highly homogeneous radiofrequency coil for whole-body NMR imaging at 1.5T. J Mag Res 1985;63:622-628.

Heinz ER, Heinz TR, Radtke R, Darwin R, Drayer BP, Fram E, Djang WT. Efficacy of MR vs CT in epilepsy. Am J Roentgenol 1989;152:347-352.

Henkes H, Hosten N, Cordes M, Neumann K, Hansen ML. Increased rCBF in gray matter heterotopias detected by SPECT using 99mTc hexamethyl-propyleneamine oxime. Neuroradiolgy 1991;33:310–312.

Hennig J, Janz C, Speck O, Ernst T. Functional spectroscopy of brain activation following a single light impulse: examinations of the mechanisms of fast initial response. International Journal of Imaging Systems and Technology 1995;6:203-208.

Henry TR, Chugani HT, Abou-Khalil BW, Theodore WH, Swartz BE. Positron emission tomography in presurgical evaluation of epilepsy. In: Engel J Jr, editor. Surgical Treatment of the Epilepsies, 2nd ed. New York: Raven Press, 1993:211–232.

Henry TR, Sutherling WW, Engel J Jr, Risinger MW, Levesque MF, Mazziotta JC, Phelps ME. Interictal cerebral metabolism in partial epilepsies of neocortical origin. Epilepsy Res 1991;10:174–182.

Henry TR, Sutherling WW, Engel J Jr, Risinger MW, Levesque MF. The role of positron emission tomography in presurgical evaluation of partial epilepsies of neocortical origin. In: Lüders H, editor. Epilepsy Surgery. New York: Raven Press, 1992:243–250.

Henry TR, Chugani HT. Positron emission tomography. In: Engel J Jr, Pedley TA, editors. Epilepsy. A comprehensive textbook. Philadelphia: Lippincott-Raven, 1998: Chapter 81.

Hertz-Pannier L, Gaillard WD, Mott SH, Cuenod CA, Bookheimer SY Weinstein S, Conry J, Papero PH, Schiff SJ, Le Bihan D, Theodore WH. Noninvasive assessment of language dominance in children and adolescents with functional MRI: a preliminary study. Neurology 1997;48:1003-1012.

Hill RA, Chiappa KH, Huang-Hellinger F, Jenkins BG. EEG during MR imaging: differentiation of movement artifact from paroxysmal cortical activity. Neurology 1995;45:1942-1943.

Hill RA, Chiappa KH, Huang-Hellinger F, Jenkins BG. Hemodynamic and metabolic aspects of photosensitive epilepsy revealed by functional magnetic resonance imaging and magnetic resonance spectroscopy. Epilepsia 1999;40:912-920.

Ho SS, Berkovic SF, McKay WJ, Kalnins RM, Bladin PF. Temporal lobe epilepsy subtypes: differential patterns of cerebral perfusion on ictal SPECT. Epilepsia 1996;37:788–795.

Ho SS, Berkovic SF, Newton MR, Austin MC, McKay WJ, Bladin PF. Parietal lobe epilepsy: clinical features and seizure localization by ictal SPECT. Neurology 1994;44:2277–2284.

Hoffmann A, Jäger L, Werhahn KJ, Jaschke M, Noachtar S, Reiser M. Electroencephalography during functional echo-planar imaging: detection of epileptic spikes using post-processing methods. Magnetic Resonance in Medicine 2000;44:791-798.

Hofman MBM, de Cock CC, van der Linden JC, van Rossum AC, Visser FC, Sprenger M, Westerhof N. Transesophageal cardiac pacing during magnetic resonance imaging: feasibility and safety considerations. Magn Reson Med 1996;35:413-422.

Holshouser BA, Hinshaw DB Jr, Shellock FG. Sedation, anaesthesia, and physiologic monitoring during MR imaging: evaluation of procedures and equipment. J Magn Reson Imaging 1993;3:553-558.

Horsley V. An address on the origin and seat of epileptic disturbance. Br Med J 1892;1:693–696.

Huang-Hellinger FR, Breiter HC, McCormack G, Cohen MS, Kwong KK, Sutton JP, Savoy RL, Weisskoff RM, Davis TL, Baker JR, Belliveau JW, Rosen BR. Simultaneous functional magnetic resonance imaging and electrophysiological recording. Hum Brain Map 1995;3:13-23.

Hugdahl K, Wester K, Asbjornsen A. Auditory neglect after right frontal lobe and right pulvinar thalamic lesions. Brain Lang 1991;41:465-73.

Hugg JW, Kuzniecky RI, Gilliam FG, Morawetz RB, Faught RE, Hetherington HP. Normalization of contralateral metabolic function following temporal lobectomy demonstrated by 1H magnetic resonance spectroscopic imaging. Ann Neurol 1996;40:236-239.

Hyder F, Phelps EA, Wiggins CJ, Labar KS, Blamire AM, Shulman RG. "Willed action": a functional MRI study of the human prefrontal cortex during a sensorimotor task. Proc Natl Acad Sci USA 1997;94:6989-6994.

International Electrotechnical Commission. IEC601-1: Safety of Medical Electrical Equipment, Part 1 General Requirements. International Electrotechnical Commission, Geneva, Switzerland, 1988.

Ives JR, Menon RS, Thomas CG, Butler J, Blume WT. Experience with recording 16-channels of EEG from a 4T system during fMRI sequences. Hum Brain Map 1997;5:S524.

Ives JR, Warach S, Schmitt F, Edelman RR, Schomer DL. Monitoring the patient's EEG during echo planar MRI. EEG Clin Neurophysiol 1993;87:417-420.

Jack CR Jr, Mullan BP, Sharbrough FW, Cascino GD, Hauser MF, Krecke KN, Luetmer PH, Trenerry MR, O'Brien PC, Parisi JE. Intractable nonlesional epilepsy of temporal lobe origin: lateralization by interictal SPECT versus MRI. Neurology 1994;44:829–836.

Jack CR Jr, Sharbrough FW, Cascino GD, Hirschhorn KA, O'Brien PC, Marsh WR. Magnetic resonance image-based hippocampal volumetry: correlation with outcome after temporal lobectomy. Ann Neurol 1992;31:138-146.

Jackson GD, Berkovic SF, Tress BM, Kalnins RM, Fabinyi GC, Bladin PF. Hippocampal sclerosis can be reliably detected by magnetic resonance imaging. Neurology 1990;40:1869-1875.

Jackson GD, Connelly A, Cross JH, Gordon I, Gardian DG. Functional magnetic resonance imaging of focal seizures. Neurology 1994a;44:850-856.

Jackson GD, Grunewald RA, Connelly A, Duncan JS. Quantitative MR relaxometry study of effects of vigabatrin on the brains of patients with epilepsy. Epilepsy Res 1994b;18:127-137.

Jasper HH. The ten-twenty electrode system of the International Federation. Electroenceph Clin Neurophysiol 1958;10:371-375.

Jewett DL, Williston JS. Auditory evoked far fields averaged from the scalp of humans. Brain 1971;94:681-696.

Jezzard P, Balaban RS. Correction for geometric distortion in echo-planar images from B0 field variations. Magn Reson Med 1995;34:65-73.

Jokeit H, Okujava M, Woermann FG. Memory fMRI lateralizes temporal lobe epilepsy. Neurology 2001;57:1786-1793.

Joseph PM, Atlas SW. Artifacts. In: Atlas SW, editor. Magnetic Resonance Imaging of the Brain and Spine (2nd ed.) Philadelphia: Lippincott-Raven, 1996:149-177.

Josephs O, Turner R, Friston K. Event-related fMRI. Hum Brain Map 1997;5:243-248.

Josephs O, Lemieux L, Krakow K, Friston K. Burst mode event-related fMRI Neuroimage 1999;9:S219.

Kaga K, Hink RF, Shinoda Y, Suzuki J. Evidence for a primary cortical origin of a middle latency auditory evoked potential in cat. Electroenceph Clin Neurophysiol 1980;50:254-266.

Kaiboriboon K, Lowe VJ, Chantarujikapong SI, Hogan RE. The usefulness of subtraction ictal SPECT coregistered to MRI in single- and dual-headed SPECT cameras in partial epilepsy. Epilepsia 2002;43:408-414.

Kendrick JF, Gibbs FA. Interrelations of mesial temporal and orbital frontal areas of man revealed by strychnine spikes. Arch Neurol Psych 1958;79:518-524.

Kleinschmidt A, Büchel C, Zeki S, Frackowiak RSJ. Human brain activity during spontaneously reversing perception of ambiguous pictures. Proc R Soc Lond B Biol Sci 1999;265:2427-2433.

Konings MK, Bakker CJG. Intolerable heating of intravascular guidewires by resonating RF waves. In: Workshop on new insights into safety and compatibility issues affecting in vivo MR. Washington: ISMRM: 1998.

Krakow K, Allen PJ, Lemieux L, Symms MR, Fish DR. Methodology: EEG-correlated fMRI. Adv Neurol 2001a;83:187-201.

Krakow K, Allen PJ, Symms MR, Lemieux L, Josephs O, Fish DR. EEG recording during fMRI experiments: image quality. Hum Brain Map 2000a;10:10-15.

Krakow K, Baxendale SA, Maguire EA, Krishnamoorthy ES, Lemieux L, Scott CA, Smith SJ. Fixation-off sensitivity as a model of continuous epileptiform discharges: electroencephalographic, neuropsychological and functional MRI findings. Epilepsy Research 2000b;42:1-6.

Krakow K, Messina D, Lemieux L, Duncan JS, Fish DR. Functional MRI activation of individual interictal epileptiform spikes. Neuroimage 2001b;13:502-505.

Krakow K, Lemieux L, Messina D, Scott CA, Symms MR, Duncan JS, Fish DR. Spatio-temporal imaging of focal interictal epileptiform activity using EEG-triggered functional MRI. Epileptic Disord 2001c;3:67-74.

Krakow K, Symms MR, Woermann FG, Allen PJ, Polizzi G, Fish DR. Reproducible localisation of interictal activation in epilepsy patients using spike-triggered fMRI. Neuroimage 1998;7:S288.

Krakow K, Wieshmann UC, Woermann FG, Symms MR, McLean MA, Lemieux L, Allen PJ, Barker GJ, Fish DR, Duncan JS. Multimodal MR imaging: functional, diffusion tensor, and chemical shift imaging in a patient with localization-related epilepsy. Epilepsia 1999a;40:1459-1462.

Krakow K ,Woermann FG, Symms MR, Allen PJ, Lemieux L, Barker GJ, Duncan JS, Fish DR. EEG-triggered functional MRI of interictal epileptiform activity in patients with partial seizures. Brain 1999b;122:1679-1688.

Krakow K, Woermann FG, Symms MR, Lemieux L, Barker GJ, Fish DR, Duncan JS. The time-course of the hemodynamic response is similar in interictal epileptiform discharges and brief visual stimuli. Proc Intl Soc Magn Reson Med 1999c;7:169.

Kreger KS, Giordano CR. Biopotential Adaptive filtering in an MR Environment. Abstracts SMRM 11th Annual Scientific Meeting. Vol. 1;1992:661.

Krings T, Chiappa KH, Cuffin BN, Buchbinder BR, Cosgrove GR. Accuracy of electroencephalographic dipole localization of epileptiform activities associated with focal brain lesions. Ann Neurol 1998;44:76-86.

Krings T, Topper R, Reinges MH, Foltys H, Spetzger U, Chiappa KH, Gilsbach JM, Thron A. Hemodynamic changes in simple partial epilepsy: a functional MRI study. Neurology 2000;54:524-527.

Kuzniecky RI, Bilir E, Gilliam F, Faught E, Palmer C, Morawetz R, Jackson G. Multimodality MRI in mesial temporal sclerosis: relative sensitivity and specificity. Neurology 1997;49:774-778.

Kuzniecky R, Cascino G, Palmini A, et al. Structural neuroimaging. In: Engel J Jr, editor. Surgical Treatment of the Epilepsies. New York: Raven Press, 1993:197.

Kuzniecky RI, Elgavish GA, Hetherington HP, Evanochko WT, Pohost GM. In vivo 31P nuclear magnetic resonance spectroscopy of human temporal lobe epilepsy. Neurology 1992;42:1586-1590.

Kuzniecky RI, Hetherington HP, Pan J, Hugg J, Palmer C, Gilliam F, Faught E, Morawetz R. Proton spectroscopic imaging at 4.1 tesla in patients with malformations of cortical development and epilepsy. Neurology 1997;48:1018-1024.

Kuzniecky RI, Jackson GD. Magnetic resonance in epilepsy. New York: Raven Press, 1995.

Kwong KK, Belliveau JW, Chesler DA, Goldberg IE, Weisskoff RM, Poncelet BP, Kennedy DN, Hoppel BE, Cohen MS, Turner R, Cheng H, Brady TJ, Rosen BR. Dynamic magnetic resonance imaging of human brain activity during primary sensory stimulation. Proc Natl Acad Sci USA 1992;89:5675-5679.

Lassen NA, Kanno I. The Metabolic and Hemodynamic Events Secondary to Functional Activation. Magn Reson Med 1997;38:521-523.

Laster DW, Penry JK, Moody DM, Ball MR, Witcofski RL, Riela AR. Chronic seizure disorders: contribution of MR imaging when CT is normal. Am J Neuroradiol 1985;6:177-180.

Latack JT, Abou-Khalil BW, Siegel GJ, Sackellares JC, Gabrielsen TO, Aisen AM. Patients with partial seizures: evaluation by MR, CT, and PET imaging. Radiology 1986;159:159-163.

Laudon MK, Webster JG, Frayne R, Grist TM. Minimizing Interference from Magnetic Resonance Imagers during Electrocardiography. IEEE trans on Biomedical Engineering 1998; 45:160-164.

Laureys S, Faymonville ME, Degueldre C, Fiore GD, Damas P, Lambermont B, Janssens N, Aerts J, Franck G, Luxen A, Moonen G, Lamy M, Maquet P. Auditory processing in vegetative state. Brain 2000;123:1589-1601.

LeDoux, J. The emotional brain. New York: Simon & Schuster, 1996.

Lee BC, Schmidt RE, Hatfield GA, Bourgeois B, Park TS. MRI of focal cortical dysplasia. Neuroradiology 1998;40:675-683.

Lee BI, Markand ON, Siddiqui AR, Park HM, Mock B, Wellman HH, Worth RM, Edwards MK. Single photon emission computed tomography (SPECT) brain imaging using N,N,N'-trimethyl-N'-(2 hydroxy-3-methyl-5-123I-iodobenzyl)-1,3-propanediamine 2 HCl (HIPDM): intractable complex partial seizures. Neurology 1986;36:1471-1476.

Lee BI, Markand ON, Wellman HN, Siddiqui AR, Mock B, Krepshaw J, Kung H. HIPDM single photon emission computed tomography brain imaging in partial onset secondarily generalized tonic-clonic seizures. Epilepsia 1987;28:305–311.

Lee BI, Markand ON, Wellman HN, et al. HIPDM-SPECT in patients with medically intractable complex partial seizures: ictal study. Arch Neurol 1988;45:397–412.

Lehericy S, Cohen L, Bazin B, Samson S, Giacomini E, Rougetet R, Hertz-Pannier L, Le Bihan D, Marsault C, Baulac M. Functional MR evaluation of temporal and frontal language dominance compared with the Wada test. Neurology 2000;54:1625-1633.

Leiderman DB, Balish M, Sato S, Kufta C, Reeves P, Gaillard WD, Theodore WH. Comparison of PET measurements of cerebral blood flow and glucose metabolism for the localization of human epileptic foci. Epilepsy Res 1992;13:153–157.

Lemieux L. A new method for the registration of EPI fMRI and gradient-echo T1-weighted volume data. Proc Intl Soc Magn Reson Med 2000:584.

Lemieux L, Allen PJ, Franconi F, Symms MR, Fish DR. Recording of EEG during fMRI experiments: Patient Safety. Mag Res Med 1997;38:943-952.

Lemieux L, Josephs O, Allen PJ, Fish, DR. Patient safety during EEG/fMRI experiments: extension to a high-performance scanner. Presented at the International Society for Magnetic Resonance in Medicine's Workshop on New Insights into Safety and Compatibility issues affecting in vivo MR; November 1-2, 1998; Washington D.C.

Lemieux L, Krakow K, Fish DR. Comparison of spike-triggered functional MRI BOLD activation and EEG dipole model localization. Neuroimage 2001b;14:780-787.

Lemieux L, Salek-Haddadi A, Josephs O, Allen PJ, Toms N, Scott C, Krakow K, Turner R, Fish DR. Event-related fMRI with simultaneous and continuous EEG. description of the method and initial case report. Neuroimage 2001a;14:780-787.

Lencz T, McCarthy G, Bronen RA, Scott TM, Inserni JA, Sass KJ, Novelly RA, Kim JH, Spencer DD. Quantitative MRI of the hippocampus in temporal lobe epilepsy: relationship to neuropathology and neuropsychological function. Ann Neurol 1992;31:629–637.

Li LM, Cendes F, Bastos AC, Andermann F, Dubeau F, Arnold DL. Neuronal metabolic dysfunction in patients with cortical developmental malformations: a proton magnetic resonance spectroscopic imaging study. Neurology 1998;50:755-759.

Liu AK, Belliveau JW, Dale AM. Spatiotemporal imaging of human brain activity using functional MRI constrained magnetoencephalography data: Monte Carlo simulations. Proc Natl Acad Sci USA 1998;95:8945-8950.

Llinás R, Pare D. Of dreaming and wakefulness. Neuroscience 1991;44:521-535.

Lorrain P, Corson DR. Electromagnetic Fields and Waves. San Francisco: W.H. Freeman and Company, 1970.

Lüders HO, editor. Epilepsy surgery. New York: Raven Press; 1992.

Lüders HO, Engel J Jr, Munari C. General principles. In: Engel J Jr, editor. Surgical treatment of the epilepsies. New York: Raven Press, 1993: 137-153.

Lufkin R, Jordan S, Lylyck P, Vinuela F. MR imaging with topographic EEG electrodes in place. Am J Neuroradiol 1988;9:953-954.

Lumer ED, Friston KJ, Rees G. Neural correlates of perceptual rivalry in the human brain. Science 1998;280:1930-1934.

Logothetis NK, Pauls J, Augath M, Trinath T, Oeltermann A. Neurophysiological investigation of the basis of the fMRI signal. Nature 2001;412:150-157.

Manno EM, Sperling MR, Ding X, Jaggi J, Alavi A, O'Connor MJ, Reivich M. Predictors of outcome after anterior temporal lobectomy: positron emission tomography. Neurology 1994;44:2331–2336.

Maquet P, Peters JM, Aerts J, Delfiore G, Dequeldre C, Luxen A, Franck G. Functional neuroanatomy of human rapid-eye-movement sleep and dreaming. Nature 1996;383,163-166.

Markand ON, Salanova V, Worth RM, Park HM, Wellman HH. Ictal brain imaging in presurgical evaluation of patients with medically intractable complex partial seizures. Acta Neurol Scand 1994;152(Suppl.):137–144.

Marks DA, Katz A, Hoffer P, Spencer SS. Localization of extratemporal epileptic foci during ictal single photon emission computed tomography. Ann Neurol 1992;31:250–255.

Maudgil DD, Free SL, Sisodiya SM, Lemieux L, Woermann FG, Fish DR, Shorvon SD. Identifying homologous anatomical landmarks on reconstructed magnetic resonance images of the human cerebral cortical surface. J Anat 1998;193:559-571.

Mazziotta JC, Pelizzari CC, Chen GT, Bookstein FL, Valentino D. Region of interest issues: the relationship between structure and function in the brain. J Cereb Blood Flow Metab 1991;11:A51-A56.

Mazziotta JC, Phelps ME, Plummer D, Kuhl DE. Quantitation in positron emission computed tomography: 5. Physical-anatomical effects. J Comput Assist Tomogr 1981;5:734–743.

McCarthy G, Blamire AM, Rothman DL, Gruetter R, Schulman RG. Echo-planar magnetic resonance imaging studies of frontal cortex activation during word generation in humans. Proc Natl Acad Sci USA 1993;90:4952-4959.

McDonald DG, Schicht WW, Frazier RE, Shallenberger HD, Edwards DJ. Studies of information processing in sleep. Psychophysiology 1975;12:624-629.

McGee T, Kraus N, Littman T, Nicol T. Contributions of medial geniculate body subdivisions to the middle latency response. Hear Res 1992;61:147-154.

McLean MA, Parker GJM, Barker GJ. Automated production of quantitative metabolite maps from short echo time 1H-CSI of the brain. Proc 6th ISMRM 1998: 626.

Mendel MI, Kupperman GL. Early components of the averaged electroencephalic response to constant level clicks during Rapid Eye Movement sleep. Audiology 1974;13:23-32.

Merlet I, Garcia-Larrea L, Ryvlin P, Isnard J, Sindou M, Mauguiere F. Topographical reliability of mesio-temporal sources of interictal spikes in temporal lobe epilepsy. Electroencephalogr Clin Neurophysiol 1998;107:206-212.

Merlet I, Gotman J. Reliability of dipole models of epileptic spikes. Clin Neurophysiol 1999;110:1013-1028.

Michel CM, Grave de Peralta R, Lantz G. Andino SG, Spinelli L, Blanke O, Landis T, Seeck M. Spatio-temporal EEG analysis and distributed source estimation in presurgical epilepsy evaluation. J Clin Neurophysiol 1999;16:239-266.

Moran NF, Lemieux L, Maudgill DD, Kitchen ND, Fish DR, Shorvon SD. Analysis of temporal lobe resections in MR images. Epilepsia 1999;40:1077-1084.

Morris J, Ohman A, Dolan RJ. Conscious and unconscious emotional learning in the human amygdala. Nature 1998;393:467-470.

Mosher JC, Lewis PS, Leahy RM. Multiple dipole modelling and localization from spatio-temporal MEG data. IEEE Trans Biomed Eng 1992;39:541-557.

Nakasato N, Levesque MF, Barth DS, Baumgartner C, Rogers RL, Sutherling WW. Comparison of MEG, EEG, and EcoG source localization in neocortical partial epilepsy in humans. Electroenceph Clin Neurophysiol 1994;91:171-178.

National Radiological Protection Board. Restrictions on Exposure to Static and Time-varying Electromagnetic Fields. National Radiological Protection Board (UK), 1995.

National Radiological Protection Board. Statement on the Clinical Magnetic Resonance Diagnostic Procedures - Documents of the NRPB. National Radiological Protection Board (UK),vol. 2;1991.

Neumann-Haefelin T, Moseley ME, Albers GW. New magnetic resonance imaging methods for cerebrovascular disease: emerging clinical applications. Ann Neurol 2000;47:559-570.

Newton MR, Berkovic SF. Ictal SPECT. In: Pedley TA, Meldrum BS, editors. Recent Advances in Epilepsy 6. Edinburgh, Scotland: Churchill Livingstone, 1995:41–55.

Newton MR, Berkovic SF, Austin MC, Rowe CC, McKay WJ, Bladin PF. Postictal switch in blood flow distribution and temporal lobe seizures. J Neurol Neurosurg Psychiatry 1992;55:891–894.

Newton MR, Berkovic SF, Austin MC, Rowe CC, McKay WJ, Bladin PF. Ictal, postictal and interictal SPECT in the lateralization of temporal lobe epilepsy. Eur J Nucl Med 1994;21:1067–1071.

Newton MR, Berkovic SF, Austin MC, Rowe CC, McKay WJ, Bladin PF. SPECT in the localisation of extratemporal and temporal seizure foci. J Neurol Neurosurg Psychiatry 1995;59:26–30.

Nishihara K, Horiuchi S. Changes in sleep patterns of young women from late pregnancy to postpartum: relationships to their infants' movements. Percept Mot Skills 1998;87:1043-1056.

Nordby H, Hugdahl K, Stickgold R, Bronnick KS, Hobson JA. Event-related potentials (ERPs) to deviant auditory stimuli during sleep and waking. Neuroreport 1996;7:1082-1086.

Oswald I, Taylor AM, Treisman M. Discriminative responses to stimulation during human sleep. Brain 1960;80:440-453.

O'Brien TJ, So EL, Mullan BP, Hauser MF, Brinkmann BH, Bohnen NI, Hanson D, Cascino GD, Jack CR Jr, Sharbrough FW. Subtraction ictal SPECT co-registered to MRI improves clinical usefulness of SPECT in localizing the surgical seizure focus. Neurology 1998;50:445-454.

O'Brien TJ, So EL, Mullan BP, Hauser MF, Brinkmann BH, Jack CR Jr, Cascino GD, Meyer FB, Sharbrough FW. Subtraction SPECT co-registered to MRI improves postictal SPECT localization of seizure foci. Neurology 1999;52:137-146.

O'Brien TJ, So EL, Mullan BP, Cascino GD, Hauser MF, Brinkmann BH, Sharbrough FW, Meyer FB. Subtraction peri-ictal SPECT is predictive of extratemporal epilepsy surgery outcome. Neurology 2000;55:1668-1677.

Ochs RF, Gloor P, Tyler JL, Wolfson T, Worsley K, Andermann F, Diksic M, Meyer E, Evans A. Effect of generalized spike-and-wave discharge on glucose metabolism measured by positron emission tomography. Ann Neurol 1987;21:458–464.

Ogawa S, Tank DW, Menon R, Ellermann JM, Kim SG, Merkle H, Ugurbil K. Intrinsic signal changes accompanying sensory stimulation: functional brain mapping with magnetic resonance imaging. Proc Natl Acad Sci USA 1992;89:5951-5955.

Ormson MJ, Kispert DB, Sharbrough FW, Houser OW, Earnest F, Scheithauer BW, Laws ER Jr. Cryptic structural lesions in refractory partial epilepsy: MR imaging and CT studies. Radiology 1986;160:215-219.

Owen AM, Menon DK, Williams EJ, Minhas PS, Johnsrude IS, Scotts SK, et al. Functional imaging in persistent vegetative state (PVS). Neuroimage 1999;9:S581.

Palmini A, Gambardella A, Anderman F, Dubeau F, da Costa JC, Olivier A, Tampieri D, Gloor P, Quesney F, Andermann E et al. Intrinsic epileptogenicity of human dysplastic cortex as suggested by corticography and surgical results. Ann Neurol 1995;37:476-486.

Panayiotopoulos CP. Fixation off, scotosensitive, and other visual-related epilepsies. In: Zifkin BG, Andermann F, editors. Advances in Neurology, Vol. 75: Reflex epilepsies and reflex seizures. Philadelphia: Lippincott-Raven, 1998:139-157.

Perrin F, Garcia-Larrea L, Mauguiere F, Bastuji H. A differential brain response to the subject's own name persist during sleep. Clin Neurophysiol 1999;110,2153-2164.

Petersson KM, Elfgren C, Ingvar M. A dynamic role of the medial temporal lobe during retrieval of declarative memory in man. Neuroimage 1997;6:1-11.

Phelps ME. Positron emission tomography (PET) In: Mazziotta JC, Gilman S, editors. Clinical Brain Imaging: Principles and Applications. Philadelphia: F.A. Davis, 1992:71–107.

Phelps ME, Huang SC, Hoffman EJ, Selin C, Sokoloff L, Kuhl DE. Tomographic measurement of local cerebral glucose metabolic rate in humans with (F-18) 2-fluoro-2-deoxy-D-glucose: validation of method. Ann Neurol 1979;6:371–388.

Pilcher W, Silbergeld D, Berger M, Ojemann G. Intraoperative electrocorticography during tumour resection: impact on seizure outcome in patients with gangliogliomas. J Neurosurg 1993;78:891-902.

Plummer DL. Dispimage: a display and analyse tool for medical images. Revista di Neuroradiologica (Italy) 1992;5:489-495.

Portas CM, Krakow K, Allen P, Josephs O, Armony JL, Frith CD. Auditory processing across the sleep-wake cycle: simultaneous EEG and fMRI monitoring in humans. Neuron 2000;28:991-999.

Portas CM, Rees G, Howseman AM, Josephs O, Turner R, Frith CD. A specific role for the thalamus in mediating the interaction of attention and arousal in humans. J Neurosci 1998;18:8979-8989.

Portas CM, Strange BA, Friston KJ, Dolan RJ, Frith CD. How does the brain sustain a visual percept? Proc R Soc Lond B 2000;267:845-850.

Pratt H, Berlad I, Lavie P. 'Oddball' event-related potentials and information processing during REM and non REM sleep. Clin Neurophysiol 1999;110:53-61.

Prevett MC, Cunningham VJ, Brooks DJ, Fish DR, Duncan JS. Opiate receptors in idiopathic generalised epilepsy measured with [11C]diprenorphine and positron emission tomography. Epilepsy Res 1994;19:71-77.

Prevett MC, Lammertsma AA, Brooks DJ, Bartenstein PA, Patsalos PN, Fish DR, Duncan JS. Benzodiazepine-GABAA receptors in idiopathic generalized epilepsy measured with [11C]flumazenil and positron emission tomography. Epilepsia 1995;36:113-121.

Price CJ, Friston KJ. Scanning patients with tasks they can perform. Human Brain Map 1997;8:102-108.

Provencher SW. Estimation of metabolite concentrations from localized in vivo proton NMR spectra. Magn Res Med 1993;30:672-679.

Radtke RA, Hanson MW, Hoffman JM, Crain BJ, Walczak TS, Lewis DV, Beam C, Coleman RE, Friedman AH. Temporal lobe hypometabolism on PET: predictor of seizure control after temporal lobectomy. Neurology 1993;43:1088–1092.

Radtke RA, Hanson MW, Hoffman JM, et al. Positron emission tomography: comparison of clinical utility in temporal lobe and extratemporal epilepsy. J Epilepsy 1994;7:27–33.

Raichle ME. The metabolic requirements of functional activity in the human brain: a positron emission tomography study. Adv Exp Med Biol 1991;291:1–4.

Rechtschaffen A, Kales A. A manual standardized terminology, techniques and scoring system for sleep stages of human subjects. U.S. Department of Health, 1968.

Rechtschaffen A, Hauri P, Zeitlin M. Auditory awakenings thresholds in REM and nonREM sleep stages. Percept Motor Skills 1966;22:927-942.

Richardson MP, Friston KJ, Sisodiya SM, Koepp MJ, Ashburner J, Free SL, Brooks DJ, Duncan JS. Cortical grey matter and benzodiazepine receptors in malformations of cortical development. A voxel-based comparison of structural and functional imaging data. Brain 1997;120:1961-1973.

Richter W, Ugurbil K, Georgopoulos A, Kim SG. Time-resolved fMRI of mental rotation. Neuroreport 1997;8:3697-3702.

Romanski LM, Clugnet MC, Bordi F, LeDoux JE. Somatosensory and auditory convergence in the lateral nucleus of the amygdala. Behav Neurosci 1993;107:444-450.

Rosen BR, Buckner RL, Dale AM. Event-related functional MRI: past, present, and future. Proc Natl Acad Sci USA 1998;95:773-780.

Rosenow F, Lüders H. Presurgical evaluation of epilepsy. Brain 2001;124:1683-1700.

Roth BJ, Pascual Leone A, Cohen LG, Hallett M. The heating of metal electrodes during rapid-rate magnetic stimulation: a possible safety hazard. EEG Clin Neurophysiol 1992;85:116-123.

Roth M, Shaw J, Green J. The form, voltage distribution and physiological significance of the K-complex. Electroenceph Clin Neurophysiol 1956;8:385-402.

Roth BJ, Ko D, von Albertini-Carletti IR, Scaffidi D, Sato S. Dipole localization in patients with epilepsy using the realistically shaped head model. Electroencephalogr Clin Neurophysiol 1997;102:171-178.

Rowe CC, Berkovic SF, Austin MC, McKay WJ, Bladin PF. Patterns of postictal cerebral blood flow in temporal lobe epilepsy: qualitative and quantitative analysis. Neurology 1991;41:1096–1103.

Rugland AL. "Subclinical" epileptogenic activity. In: Sillanpää M, Dam M, Blennow G, editors. Paediatric epilepsy. Petersfield: Wrightson Biomedical Publishing, 1990: 217-224.

Salek-Haddadi A, Merschhemke M, Lemieux L, Fish DR. Simultaneous EEG-correlated ictal fMRI. Neuroimage 2002;16:32-40.

Savic I, Widen L, Thorell JO, Blomqvist G, Ericson K, Roland P. Cortical benzodiazepine receptor binding in patients with generalized and partial epilepsy. Epilepsia 1990;31:724-730.

Savic I, Pauli S, Thorell JO, Blomqvist G. In vivo demonstration of altered benzodiazepine receptor density in patients with generalised epilepsy. J Neurol Neurosurg Psychiatry 1994;57:797-804.

Schaefer DJ. Bioeffects of MRI and Patient Safety. In: Bronskill MJ, Sprawls P, editors. The Physics of MRI - 1992 AAPM Summer School Proceedings. Woodbury, New York: AAPM, 1993.

Schoner W, Meencke HJ, Felix R. Temporal-lobe epilepsy: comparison of CT and MR imaging. Am J Roentgenol 1987;149:1231-1239.

Seeck M, Lazeyras F, Michel CM, Blanke O, Gericke CA, Ives J, Delavelle J, Golay X, Haenggeli CA, de Tribolte N, Landis T. Non-invasive epileptic focus localization using EEG-triggered functional MRI and electromagnetic tomography. EEG Clin Neurophys 1998;106:508-512.

Semah F, Picot MC, Adam C, Broglin D, Arzimanoglou A, Bazin B, Cavalcanti D, Baulac M. Is the underlying cause of epilepsy a major prognostic factor for recurrence? Neurology 1998;51:1256-1262.

Shellock FG, Kanal E. Magnetic resonance: bioeffects, safety, and patient management. Philadelphia: Lippincott-Raven, 1996.

Shellock FG, Slimp GL. Severe burn of the finger caused by using a pulse oximeter during MR imaging [letter]. Am J Roentgenol 1989;153:1105.

Shin WC, Hong SB, Tae WS, Kim SE. Ictal hyperperfusion patterns according to the progression of temporal lobe seizures. Neurology 2002;58:373-380.

Sijbers J, Michiels I, Verhoye M, Van Audekerke J, Van der Linden A, Van Dyck D.

Restoration of MR-induced artifacts in simultaneously recorded MR/EEG data. Magn Reson Imaging 1999;17:1383-1391.

Sisodiya SM. Surgery for malformations of cortical development causing epilepsy. Brain 2000;123:1075-10921.

Sisodiya SM, Free SL, Fish DR, Shorvon SD. Increasing the yield from volumetric MRI in patients with epilepsy. Magn Reson Imaging 1995a;13:1147-1152.

Sisodiya SM, Free SL, Stevens JM, Fish DR, Shorvon SD. Widespread cerebral structural changes in patients with cortical dysgenesis and epilepsy. Brain 1995b;118:1039-1050.

Sisodiya SM, Stevens JM, Fish DR, Free SL, Shorvon SD. The demonstration of gyral abnormalities in patients with cryptogenic partial epilepsy using three-dimensional MRI. Arch Neurol 1996;53:28-34.

Smallwood RH, Barker AT, Brydon J, Pay DA, Dowd WJO. Hospital Physicists' Association Topic Group Report 37 - Safe Design and Construction of Electromedical Equipment. The Institute of Physical Sciences in Medicine, UK, 1983.

Song AW, Popp CA, Mao J, Dixon WT. FMRI: Methodology – Acquisition and Processing. Advances in Neurology 2000;83:177-185.

Spencer SS. MRI and epilepsy surgery. Neurology 1995;45:1248-1250.

Spencer SS, McCarthy G, Spencer DD. Diagnosis of medial temporal lobe seizure onset: relative specificity and sensitivity of quantitative MRI. Neurology 1993;43:2117-2124.

Sperling MR, Gur RC, Alavi A, Gur RE, Resnick S, O'Connor MJ, Reivich M. Subcortical metabolic alterations in partial epilepsy. Epilepsia 1990;31:145–155.

Stanley JA, Cendes F, Dubeau F, Andermann F, Arnold DL. Proton magnetic resonance spectroscopic imaging in patients with extratemporal epilepsy. Epilepsia 1998;39:267-273.

Stefan H, Bauer J, Feistel H, Schulemann H, Neubauer U, Wenzel B, Wolf F, Neundorfer B, Huk WJ. Regional cerebral blood flow during focal seizures of temporal and frontocentral onset. Ann Neurol 1990;27:162–166.

Steriade M, Hobson J. Neuronal activity during the sleep-waking cycle. Prog Neurobiol 1976;6:155-376.

Steriade M, Oakson G, Kitsikis A. Firing rates and patterns of output and nonoutput cells in cortical areas 5 and 7 of cat during the sleep-waking cycle. Exp Neurology 1978;60:443-468.

Stern CE, Corkin S, Gonzalez RG, Guimaraes AR, Baker JR, Jennings PJ, Carr CA, Suguira RM, Vadantham V, Rosen BR. The hippocampal formation participates in novel picture encoding: evidence from functional magnetic resonance imaging. Proc Natl Acad Sci USA 1996:93:8660-8665.

Strupp J. Stimulate: A GUI based fMRI Analysis Software Package. Neuroimage 1996;3:S607.

Studholme C, Todd Constable R, Duncan JS. Accurate alignment of functional EPI data to anatomical MRI using a physics-based distortion model. IEEE Trans Med Imaging 2000;19:1115-1127.

Swartz BE, Halgren E, Delgado-Escueta AV, Mandelkern M, Feldstein P, Maldonado H, Ropchan J, Blahd W, Walsh GO, Quinones N et al. Multidisciplinary analysis of patients with extratemporal complex partial seizures. I. Intertest agreement. Epilepsy Res 1990;5:61–73.

Swartz BE, Halgren E, Delgado-Escueta AV, Mandelkern F, Gee M, Quinones N, Blahd WH, Repchan J. Neuroimaging in patients with seizures of probable frontal lobe origin. Epilepsia 1989;30:547–558.

Swartz BE, Theodore WH, Sanabria E, Fisher RS. Positron emission and single photon emission computed tomographic studies in the frontal lobe with emphasis on the relationship to seizure foci. In: Chauvel P, Delgado-Escueta AV, Halgren E, Bancaud J, editors. Frontal Lobe Seizures and Epilepsies. New York: Raven Press, 1992a:487–497.

Swartz BE, Tomiyasu U, Delgado-Escueta AV, Mandelkern M, Khonsari A. Neuroimaging in temporal lobe epilepsy: test sensitivity and relationships to pathology and post-surgical outcome. Epilepsia 1992b;33:624–634.

Symms MR, Allen PJ, Woermann FG, Polizzi G, Krakow K, Barker GJ, Fish DR, Duncan JS. Reproducible localisation of interictal epileptiform discharges using EEG correlated fMRI. Proceedings of the International Society for Magnetic Resonance in Medicine, Sydney, 1998: 168.

Talairach J, Tournoux P. Co-planar stereotactic atlas of the human brain. Stuttgart: Thieme, 1988.

Tenforde TS, Gaffey CT, Moyer BR, Budinger TF. Cardiovascular alterations in Macaca monkeys exposed to stationary magnetic fields: experimental observations and theoretical analysis. Bioelectromagnetics 1983;4:1-9.

Theodore WH, Brooks R, Margolin R, Patronas N, Sato S, Porter RJ, Mansi L, Bairamian D, DiChiro G. Positron emission tomography in generalized seizures. Neurology 1985;35:684–690.

Theodore WH, Holmes MD, Dorwart RH, Porter RJ, Di Chiro G, Sato S, Rose D. Complex partial seizures: cerebral structure and cerebral function. Epilepsia 1986;27:576–582.

Theodore WH, Sato S, Kufta C, Balish MB, Bromfield EB, Leiderman D. Temporal lobectomy for uncontrolled seizures: the role of positron emission tomography. Ann Neurol 1992;32:789–794.

Theodore WH. Positron emission tomography in the evaluation of epilepsy. In: Cascino GD, Jack CR, editors. Neuroimaging in Epilepsy. Boston: Butterworth Heinemann, 1996: 165–175.

Turner R, Howseman A, Rees G.E, Josephs O, Friston KJ. Functional magnetic resonance imaging of the human brain: data acquisition and analysis. Exp Brain Res 1998;123:5-12.

Van der Grond J, Gerson JR, Laxer KD, Hugg JW, Matson GB, Weiner MW. Regional distribution of interictal 31P metabolic changes in patients with temporal lobe epilepsy. Epilepsia 1998;39:527-536.

von Smekal A, Seelos KC, Kuper CR, Reiser M. Patient monitoring and safety during MRI examinations. Eur Radiol 1995;5:302-305.

Valenti MP, Froelich S, Armspach JP, Chenard MP, Dietemann JL, Kerhli P, Marescaux C, Hirsch E, Namer IJ. Contribution of SISCOM imaging in the presurgical evaluation of temporal lobe epilepsy related to dysembryoplastic neuroepithelial tumors. Epilepsia 2002;43:270-276.

Van Paesschen W, Connelly A, King MD, Jackson GD, Duncan JS. The spectrum of hippocampal sclerosis: a quantitative magnetic resonance imaging study. Ann Neurol 1997;41:41-51.

Van Paesschen W, Sisodiya S, Connelly A, Duncan JS, Free SL, Raymond AA, Grunewald RA, Revesz T, Shorvon SD, Fish DR, Stevens JM, Scaravilli F, Harkness WFJ, Jackson GD. Quantitative hippocampal MRI and intractable temporal lobe epilepsy. Neurology 1995;45:2233-2240.

Voss U, Harsh J. Information processing and copying style during the wake/sleep transition. J Sleep Res 1998;7:225-232.

Wagner M, Fuchs M, Kohlhoff H. Automatic generation of the 10/20 electrode system. Brain Topogr 1996;8:409.

Wagner M, Fuchs M, Wischmann HA, Ottenberg K, Dössel O. Cortex segmentation from 3D MR images for MEG reconstructions. In: Baumgartner C et al., editors. Biomagnetism: fundamental research and clinical applications. Amsterdam: Elsevier Science IOS Press, 1995: 433-438.

Warach S, Ives JR, Schlaug G, Patel MR, Darby DG, Thangaraj V, Edelman RR, Schomer DL. EEG-triggered echo-planar functional MRI in epilepsy. Neurology 1996;47:89-93.

Warach S, Levin JM, Schomer DL, Holman BL, Edelman RR. Hyperperfusion of ictal seizure focus demonstrated by MR perfusion imaging. AJNR 1994;15:965-968

Watson C, Cendes F, Fuerst D, Dubeau F, Williamson B, Evans A, Andermann F. Specificity of volumetric magnetic resonance imaging in detecting hippocampal sclerosis. Arch Neurol 1997;54:67-73.

Wesenten NJ, Badia P. The P300 component in sleep. Physiol Behav 1998;44:215-220.

Whalen PJ, Rauch SL, Etcoff NL, McInerney SC, Lee MB, Jenike MA. Masked presentations of emotional facial expressions modulate amygdala activity without explicit knowledge. J Neurosci 1998;18:411-418.

Wieshmann UC, Symms MR, Shorvon SD. Diffusion changes in status epilepticus. Lancet 1997;350:493-494.

Wieshmann UC, Krakow K, Symms MR, Parker GJ, Clark CA, Barker GJ, Shorvon SD. Combined functional magnetic resonance imaging and diffusion tensor imaging demonstrate widespread modified organisation in malformation of cortical development. J Neurol Neurosurg Psychiatry 2001;70:521-523.

Woermann FG, Barker GJ, Birnie KD, Meencke HJ, Duncan JS. Regional changes in hippocampal T2 relaxation and volume: a quantitative magnetic resonance imaging study of hippocampal sclerosis. J Neurol Neurosurg Psychiatry 1998;65:656-664.

Woermann FG, Free SL, Koepp MJ, Asburner J, Duncan JS, Voxel-by-voxel comparison of automatically segmented cerebral gray matter – a rater-independent comparison of structural MRI in patients with epilepsy. Neuroimage 1999;10:373-384.

Woermann FG, McLean MA, Bartlett PA, Barker GJ, Duncan JS. Quantitave short echo time proton magnetic resonance spectroscopic imaging study of malformations of cortical development causing epilepsy. Brain 2001;124:427-436.

Wolpaw JR. Single unit activity vs. amplitude of the epidural evoked potential in primary auditory cortex of awake cats. Electroenceph Clin Neurophysiol 1979;47:372-376.

Woods RP, Cherry SR, Mazziotta JC. Rapid Automated Algorithm for Aligning and Reslicing PET Images. J Comput Assist Tomogr 1992;16:620-633.

Zarahn E, Aguirre GK, D'Esposito M. A trial-based experimental design for fMRI. Neuroimage 1997;6:122-138.

Zentner J, Hufnagel A, Wolf HK, Ostertun B, Behrens E, Campos MG, Elger CE, Wiestler OD, Schramm J. Surgical treatment of temporal lobe epilepsy: clinical, radiological, and histopathological findings in 178 patients. J Neurol Neurosurg Psychiatry 1995;58:666-673.

List of publications

A list of publications included in this thesis is given in chapter 1.

1. Original publications

1. Vajkoczy P, Krakow K, Stodieck S, Pohlmann-Eden B, Schmiedeck P. Modified approach for the selective treatment of temporal lobe epilepsy: transsylvian-transcisternal mesial en-bloc resection.
Journal of Neurosurgery 1998; 88: 855-862.

2. Krakow K, Bühler K-E, Haltenhof H. Coping with refractory epilepsy.
Seizure 1999; 8: 111-115.

3. Krakow K, Haltenhof H, Bühler K-E. Coping with Parkinson's disease and refractory epilepsy. A comparative study.
J Nerv Ment Dis 1999; 187: 503-508.

4. Haltenhof H, Krakow K, Ulm G, Bühler K-E. Krankheitsverarbeitung beim Morbus Parkinson.
Nervenarzt 2000; 71: 275-281.

5. Schimpf J, Krakow K, Vehreschild N, Pohlmann-Eden B. Querschnittsmyelopathie als Komplikation einer intrathekalen Langzeitapplikation von Morphium bei chronischen Rückenschmerzen.
Anaesthesiol Intensivmed Notfallmed Schmerzther 1999; 34: 506-509.

6. Krakow K, Ries S, Daffertshofer M, Hennerici M. Simultaneous assessment of cerebral blood flow velocity and brain tissue oxygenation during orthostatic stress. European Neurology 2000; 43: 39-46.

7. Allen PJ, Polizzi G, Krakow K, Fish DR, Lemieux, L. Identification of EEG events in the MR scanner: the problem of pulse artifact and a method for its subtraction. Neuroimage 1998; 8: 229-239.

8. Lemieux L, Hagemann G, Krakow K, Woermann FG. Fast, accurate, and reproducible automatic segmentation of the brain in T1-weighted volume MRI data. Magn Reson Med 1999; 42: 127-135.

9. Lemieux L, Allen PJ, Krakow K, Symms MR, Fish DR. Methodological issues in EEG-correlated functional MRI experiments.
Int J Bioelectromagnetism 1999; 1: 87-95.

10. Krakow K, Allen PJ, Symms MR, Fish DR, Lemieux L. Imaging of interictal epileptiform discharges using spike-triggered fMRI.
Int J Bioelectromagnetism 1999; 1: 96-101.

11. Symms MR, Allen PJ, Woermann FG, Polizzi G, Krakow K, Barker GJ, Fish DR, Duncan JS. Reproducible localization of interictal epileptiform discharges using EEG-triggered fMRI.
Phys Med Biol 1999; 44: 161-166.

12. Krakow K, Woermann FG, Symms MR, Allen PJ, Lemieux L, Barker GJ, Duncan JS, Fish DR. EEG-triggered functional MRI of interictal epileptiform activity in patients with partial seizures.
Brain 1999; 122: 1679-1688.

13. Krakow K, Wieshmann UC, Woermann FG, Symms MR, McLean MA, Allen PJ, Barker GJ, Fish DR, Duncan JS. Multimodal MR imaging: functional, diffusion tensor, and chemical shift imaging in a patient with localization-related epilepsy.
Epilepsia 1999; 40: 1459-1462.

14. Krakow K, Allen PJ, Symms MR, Lemieux L, Josephs O, Fish DR. EEG recording during fMRI experiments: image quality.
Human Brain Mapping 2000; 10: 10-15.

15. Krakow K, Polizzi G, Riordan-Eva P, Holder G, MacLeod WN, Fish DR. Recovery of visual field constriction following discontinuation of vigabatrin.
Seizure 2000; 9: 287-290.

17. Krakow K, Baxendale SA, Maguire EA, Krishnamoorthy ES, Lemieux L, Scott CA, Smith SJ. Fixation-off sensitivity as a model of continuous epileptiform discharges: electroencephalographic, neuropsychological and functional MRI findings.
Epilepsy Research 2000; 42: 1-6.

18. Portas CM, Krakow K, Allen P, Josephs O, Armony JL, Frith CD: Auditory processing across the sleep-wake cycle: simultaneous EEG and fMRI monitoring in humans.
Neuron 2000; 28: 991-999.

19. Krakow K, Messina D, Lemieux L, Duncan JS, Fish DR. Functional MRI activation of individual interictal spikes.
Neuroimage 2001; 13: 502-505.

20. Krakow K, Lemieux L, Messina D, Scott CA, Symms MR, Duncan JS, Fish DR: Spatio-temporal imaging of focal interictal epileptiform activity using EEG-triggered functional MRI.
Epileptic Disord 2001; 3: 67-74.

21. Krakow K, Walker M, Otoul C, Sander JWAS. Long-term continuation of levetiracetam in patients with refractory epilepsy.
Neurology 2001; 56: 1772-1774.

22. Wieshmann UC, Krakow K, Symms MR, Parker GJ, Clark CA, Barker GJ, Shorvon SD. Combined functional magnetic resonance imaging and diffusion tensor imaging demonstrate widespread modified organisation in malformation of cortical development.
J Neurol Neurosurg Psychiatry 2001; 70: 521-523.

23. Lemieux L, Salek-Haddadi A, Josephs O, Allen P, Toms N, Scott C, Krakow K, Turner R, Fish DR. Event-related fMRI with simultaneous and continuous EEG: description of the method and initial case report.
Neuroimage 2001; 14: 780-787.

24. Lemieux L, Krakow K, Fish DR. Comparison of spike-triggered functional MRI BOLD activation and EEG dipole model localization.
Neuroimage 2001; 14: 1097-1104.

25. Weidauer S, Krakow K, Lanfermann H, Zanella FE. Reversible bilaterale kortikale MRT-Veränderung infolge einer Anfallsserie.
Nervenarzt 2001; 72: 958-962.

26. Weidauer S, Dettmann S, Krakow K, Lanfermann H. Diffusionsgewichtete MRT bei spinalen Infarkten. Darstellung von zwei Fällen und Literaturübersicht.
Nervenarzt 2002; 73: 999-1003

27. Hagemann G, Lemieux L, Free SL, Krakow K, Everitt AD, Kendall BE, Stevens JM, Shorvon SD. Cerebellar volumes in newly diagnosed and chronic epilepsy.
J Neurology 2002; 249: 1651-1658

28. Laufs H, Kleinschmidt A, Beyerle A, Eger E, Salek-Haddadi A, Preibisch C, Krakow K. EEG-correlated fMRI of human alpha activity:
Neuroimage 2003; 19: 1463-1476.

29. Laufs H, Krakow K, Sterzer P, Eger E, Beyerle A, Salek-Haddadi A, Kleinschmidt A. Electroencephalographic signatures of attentional and cognitive default modes in spontaneous brain activity fluctuations at rest.
Proc Natl Acad Sci U S A 2003; 100: 11053-11058.

2. Reviews, book-chapters, letters

1. Haltenhof H, Krakow K, Zöfel P, Ulm G. Depressivitä t und Krankheitsverarbeitung bei Patienten mit idiopathischem Parkinson-Syndrom. In: Huffmann, G., Braune, H.-J-., Henn, K.-H. (editors): Extrapyramidal-motorische Erkrankungen. Einhorn-Presse Verlag, Reinbeck 1994, 265-269

2. Krakow K, Pohlmann-Eden B. Epilepsien des höheren Lebensalters - Eine Literaturübersicht.
Epilepsie-Blätter 1997; 10: 54-61

3. Krakow K, Pohlmann-Eden B. Epilepsien und epileptische Anfälle im höheren Lebensalter.
Deutsche Medizinische Wochenschrift 1999; 124: 567-572

4. Hagemann G, Krakow K, Woermann FG. Funktionelle MR-Verfahren in der Epilepsie-Diagnostik.
Klinische Neurophysiologie 2000; 31: S49-S56

5. Krakow K, Allen PJ, Lemieux L, Fish DR. Methodology: EEG-correlated fMRI. Advances in Neurology 2000; 83: 187-201

6. Lemieux L, Salek-Haddadi A, Krakow K. The nature of MR signal changes [letter]. Radiology 2003; 226: 922-923

7. Krakow K: FMRI in the definition of eloquent cortical areas.
In: Handbook of Clinical Neurophysiology (Mauguiére F, Daube JR, editors); Volume: Presurgical assessment of the epilepsies with clinical neurophysiology und functional imaging (Rosenow F, Lüders HO, editors). Elsevier Science 2004, 317-332

8. Krakow K, Laufs H, Kleinschmidt. Multimodale Bildgebung.
In: Funktionelle Bildgebung des Gehirns in Psychiatrie und Psychotherapie. Walter H (editor). Stuttgart: Schattauer, Stuttgart, New York 2004, 180-191